THE VALIDATION OF THE VARIABLES (EVAPORATION AND SOIL WATER) IN HYDROMETEOROLOGICAL MODELS: PHASE II, APPLICATION OF COSMIC RAY PROBES FOR SOIL WATER MEASUREMENT

Report to the

Water Research Commission

by

CS Everson, MG Mengistu, T Vather

July 2017

Obtainable from

Water Research Commission

Private Bag X03

GEZINA, 0031

DISCLAIMER

This report has been reviewed by the Water Research Commission (WRC) and approved for publication. Approval does not signify that the contents necessarily reflect the views and policies of the WRC, nor does mention of trade names or commercial products constitute endorsement or recommendation for use.

EXECUTIVE SUMMARY

1.   Motivation

For many field and modelling applications, accurate soil water estimates are required, but these are often lacking. Modelled estimates of soil water are often used without proper validation and the verification of the results is questionable. In addition, remotely sensed products are becoming more widely used in hydrological modelling. However, remotely sensed soil water measurement cannot "see" below the soil surface and penetrate the aerial plant canopy layer. This still presents a major source of uncertainty in many hydrological applications where soil water forms the interface between the atmosphere and the vadose zone, and ultimately streamflow generation.

The vulnerability of South Africa to climate and environmental change is increasing as demands on resources continue to rise in conjunction with rapidly growing populations. Disaster management agencies have to adapt to the increasing number of natural disasters, which includes droughts and floods. In addition, water resources management, crop modelling, and irrigation scheduling all require accurate and spatially distributed daily estimates of soil water and total evaporation from catchment level to national scale. This will only be feasible through remote sensing technologies. It is therefore essential to further the development and integration of space-based technologies within already existing national disaster management plans.

In South Africa, total evaporation and soil water data has only become available recently when research by the University of KwaZulu-Natal's (UKZN) Satellite Applications and Hydrology Group (SAHG) developed a detailed spatial product for real-time estimates of soil water and total evaporation. These variables are now routinely calculated in real time and made available on the internet. The model has shown promise, but still requires further development. One of the major challenges facing providers of soil water products is validation.

One outcome of the project funded by the Water Research Commission (WRC), project K5/1683, which is run by UKZN researchers at SAHG, was on soil water estimation using an automated modelling system that produces countrywide estimates of the soil water state at three-hourly time steps on a 0.125° spatial grid over South Africa. The key focus of this product is to provide proof of concept for operational use by the South African Weather Service (SAWS) in their national Flash Flood Guidance system.

However, until the development of the cosmic ray probe (CRP), there has not been a suitable technology for measuring soil water at the appropriate scales to validate the models. The CRP is new technology that has not been used by researchers in southern Africa before. A cosmic array network could provide a powerful new addition to the flood forecasting ability of the SAWS.

The need to provide an independent validation of the Hydrologically Consistent Land Surface Model for Soil Moisture and Evapotranspiration (HylarsMet) model was recognised. As a result, another project (K5/2066) was initiated to provide a spatially explicit validation procedure for the 1 km grid of soil water and total evaporation produced by the SAHG at UKZN and other global climate models.

Measurements using the CRP at area scales of up to 34 ha have the potential to provide hydrometeorologists with an entirely new way of evaluating surface soil water at spatial scales never achieved with ground-based techniques. This new technology can be employed in water demand forecasting and promises to improve the utilisation of irrigation water especially in water scarce regions like South Africa. The probe can also be used for predictive weather and climate models by measuring soil water content (SWC). In addition to spatial estimates of total evaporation (micrometeorological and remote sensing techniques), spatially distributed field-based measurements of soil water were also used to verify the CRP estimates. The aim here was to assess how spatially determined soil water measurements compared with the point measurements of soil water, and soil water measured using the CRP.

The recent development of the CRP as part of a USA National Science Foundation and South African National Research Fund Research Infrastructure Support Programme (NRF RISP) project was therefore timely and provided a technology previously unobtainable, which fits perfectly with the spatial resolution of this project. The CRP uses cosmic ray neutrons to measure SWC over an area of tens of hectares (34 ha with a 660 m diameter). An objective of this project was to increase the research capacity in this domain in South Africa.

2.   Project objectives

This project is designed to build on the recent work in WRC projects, namely, K5/1683: *Soil water from satellites*, and K5/2066: *The validation of the variables (evaporation and soil moisture) in hydrometeorological models.* The aims of this project were to:

- Provide data for the continued support of soil water modelling of South Africa using a hydrologically consistent land surface model (follow-on project proposed from K5/1683).
- Provide accurate field and satellite estimates of total evaporation and soil water to calibrate hydrometeorological models.
- Evaluate the spatial variability of soil water at catchment scale.
- Test the suitability of the CRP for providing spatial estimates of soil water at the same scale as the remote sensing products from HylarsMet.

3.   Methods

3.1   Study Sites

Three different sites with contrasting land uses were selected for this study:

- Agricultural crops at Baynesfield (soybean and maize) near Pietermaritzburg.
- Natural grassland vegetation at Cathedral Peak in the KwaZulu-Natal Drakensberg.
- Commercial forestry at the Two Streams catchment, afforested with *Acacia mearnsii* (black wattle) in the KwaZulu-Natal midlands.

3.2   Micrometeorological Methods

Total evaporation was measured with an EC150 open path gas analyser and a 3D sonic anemometer eddy covariance system (Campbell Scientific Inc., Logan, Utah, USA) to measure fluxes of water vapour and carbon dioxide. The EC150 is an integrated in situ open path IRGA and sonic anemometer specifically designed for eddy covariance flux measurements. The system measures carbon dioxide flux, latent energy flux, barometric pressure, momentum flux, a computed sensible heat flux, nett radiation, a computed soil heat flux density, temperature, humidity, horizontal wind speed, and wind direction.

The surface renewal method was used to estimate total evaporation where full eddy covariance equipment was not available due to the high capital equipment costs, or to act as a backup to the eddy covariance derived estimates. Total evaporation was calculated using the surface renewal and eddy covariance techniques in the centre of the wattle stand. Two unshielded type-E (chromel/constantan) fine wire (76 μm diameter) thermocouples placed at heights of 19 m and 21 m above the ground surface were used to measure air temperatures, which was used to derive the sensible heat flux. Continuous data was recorded with a data logger (CR3000, Campbell Scientific Inc., Logan, Utah, USA) powered by two 70 Ah batteries and one 20 W solar panel. Data was saved on a 2 GB compact flash card, which is able to store up to six weeks of high frequency (10 Hz) data. Over the course of the measurements, the sensible heat flux was derived from two thermocouples using the surface renewal technique.

3.3 Soil Water

CS616 Campbell Scientific time domain reflectometry (TDR) probes were installed for profile volumetric soil water measurement. The CS616 probes were installed by excavating a pit to measure volumetric SWC at 0.05 m, 0.1 m, 0.15 m, 0.2 m and 0.3 m depths. The three CS616 probes were connected to a CR1000 data logger (Campbell Scientific Inc., Logan, Utah, USA). The measurements were sampled hourly and daily volumetric SWC measurements were computed and stored for further analysis.

3.4 Cosmic Ray Probes

Using CRPs is a new technique, which has the capability to provide data for large-scale studies, such as the calibration and validation of satellite-based soil water retrievals and land surface models (Villarreyes et al., 2013). The CRP can provide soil water estimates over hundreds of metres, which bridges the gap between point-scale and large-scale remote sensing measurements (Dutta and D'este, 2013). It measures background neutrons that are emitted from soil. These background neutrons occur naturally and are continuously produced due to collisions between terrestrial nuclei and cosmic ray hadrons (Desilets and Zreda, 2013).

The soil water is estimated by the concentration of neutrons above the soil surface. Dry soils are highly emissive, such that neutrons are more efficiently removed from the soil (Zreda et al., 2008). This results in more neutrons escaping to the surface of a dry soil, which would result in a higher concentration of neutrons above the soil surface (Franz et al., 2012).

When the CRP is placed in a static position a few metres above the ground, it has a radial footprint of 670 m in diameter at sea level (Zreda et al., 2008). The technique operates as the neutron fluxes are a great proxy for land surface water (Desilets et al., 2010). Along with the neutron count rate, the CRP also measures the internal temperature, relative humidity and external barometric pressure (Franz et al., 2013).

CRPs were installed on tripod masts in each of the three research catchments. Connected to the CRP data logger was an antenna used to send data via an iridium satellite data communication link to the Cosmic-ray Soil Moisture Observing System (COSMOS) server. Data from the CS616 soil water sensors and gravimetric samples were combined to calibrate the CRPs.

3.5 Remote Sensing

The surface energy balance system (SEBS) model was used for estimating total evaporation in the Integrated Land and Water Information System (ILWIS). High-resolution (30 × 30 m) satellite images (Landsat 8) were used to capture the heterogeneity of the land surface over the study sites. Meteorological data (solar radiation, air temperature, wind speed, relative humidity, and atmospheric pressure) from automatic weather stations at the specific sites were used to compute surface fluxes over the area of the satellite images.

Erdas imaging software was used for preprocessing Landsat images. The land surface's physical properties such as albedo, emissivity, temperature and vegetation coverage (NDVI) were determined from the spectral reflectance and radiance values of the Landsat bands. The Level 3 Advanced Microwave Scanning Radiometer (AMSR-2) soil moisture product at a 10 km spatial resolution was selected to be used in this study.

The Topographic Kinematic Approximation and Integration (PyTOPKAPI) soil water product was obtained from the SAHG. The data has a temporal resolution of three hours and a spatial resolution of ≈12 km. The data ranges from 2008 to present. The soil saturation index option was selected.

4. Results and discussion

4.1 First Validation Experiment

4.1.1 Validating the CRP soil water estimates

The CRP estimates were validated against in situ soil water datasets to test the suitability of the CRP to provide spatial estimates of soil water. A time series analysis was plotted to see how the CRP dataset compared with the in situ TDR soil water estimates. The volumetric SWC values at Baynesfield varied between 0.17 and 0.36 during the measurement period. Calibrated hourly CRP SWC calculated using the corrected neutron counts from two calibration periods showed that soil water values varied between 0.13 and 0.36 during the measurement period, which agreed with measured TDR values.

The CRP followed the same seasonal trend as the in situ soil water estimates at the Cathedral Peak Catchment VI site. The CRP correlated better with the in situ soil water dataset in wetter periods when the soil water values were higher (above 30%) than the drier periods. Overall, the CRP data correlated well with the in situ soil water dataset.

4.1.2 Validating the SEBS soil water estimates

In the first validation experiment, 15 relative evaporation maps were generated using the SEBS model in ILWIS 3.8.3. These maps were exported, opened and analysed in ArcGIS 9.3, where the relative evaporation of the area within Catchment VI was determined. The relative evaporation followed seasonal trends with the values being high in summer (wet period) and very low in winter (dry period). To estimate the actual soil water from the relative soil water, the saturated SWC was required. This was inferred from the porosity, which in turn was estimated using the bulk density.

The back-calculation of soil water from relative evaporation estimates the soil water in the root zone as this is where the evaporated water (soil evaporation and transpiration) is sourced from. The Su et al. (2003b) and Scott et al. (2003) methods were used for estimating soil water using the SEBS model relative evaporation values. The relative evaporation values were substituted in the equations, and the soil water at field capacity was 0.74. The estimated soil water was plotted against the corresponding CRP measurements. The methods proposed by Su et al. (2003b) and Scott et al. (2003) followed the same trend, but overestimated soil water in the wet periods and underestimated soil water in the dry periods. Both methods followed the expected seasonal trend. The Scott et al. (2003) method performed relatively better than the method proposed by Su et al. (2003b). The poor agreement with these methods and the CRP methods was mainly ascribed to vertical and horizontal scaling issues.

4.1.3 Validating the PyTOPKAPI (SAHG) soil water estimates

The SAHG soil water product is on a 12 × 12 km grid, which results in a pixel area of 144 km^2. To obtain a year-long dataset, 2920 images were downloaded and used to create 365 daily images. The SAHG dataset is continuous and has no gaps. The SAHG soil water was obtained in soil saturation index (SSI) and converted to soil water by using a representative porosity value. The SAHG soil water estimates followed the same seasonal trend as the CRP estimates with a close correlation between the two datasets in terms of general increases and decreases in SWC. The CRP had more day-to-day variation in soil water. The SAHG product had gradual changes in soil water and did not exhibit the same degree of temporal fluctuations observed in the CRP estimates. In general, the SAHG soil water product provided good estimates of soil water, which correlated well with the CRP measurements.

4.1.4   Validating AMSR-2 and soil moisture and ocean salinity soil water products

The AMSR-2 Level 3 soil water product is on a 10 km grid. Although this grid is relatively small in comparison to other remote sensing soil water products, it is still very large in comparison to the Catchment VI area of 0.68 km^2, whereas the pixel area is 100 km^2. Therefore, the pixel is 147 times larger than the study area. However, this is an improvement from validating remote sensing soil water products with in situ point measurements. The AMSR-2 soil water product underestimated soil water throughout the study period. The AMSR-2 soil water product followed the seasonal trend of the CRP estimates but fluctuated more in the wet periods with less fluctuation in the dry periods. Although, the AMSR-2 dataset underestimated the soil water at the site, it followed a similar trend in daily soil water fluctuations.

The soil moisture and ocean salinity (SMOS) Level 3 soil water product is on a 25 km grid. Although this grid is smaller than the Level 2 product (40 km), it is still very large in comparison to the catchment area. The pixel size was 920 times larger than the study area. The SMOS soil water estimates followed the same general trend as the CRP estimates. The SMOS dataset generally underestimated soil water for most of the study period. However, the SMOS product partly overestimated soil water during the wet period. The SMOS soil water estimates fluctuated most during the wet season. This fluctuation is less in the dry periods. This was due to greater fluxes in soil water in summer than winter.

4.2   Second Validation Experiment

The project team focused on the Baynesfield site for this experiment as the CRP, EC150 and large aperture scintillometry at Cathedral Peak was vandalised by thieves and the equipment was not available for this experiment.

4.2.1   Second validation of the SAHG soil water product

The CRP was used to validate the SAHG soil water product between 1 December 2015 and 16 January 2016. The CRP was plotted on a time series against the SAHG product. The CRP and the SAHG soil water estimates followed similar trends. The CRP daily estimates were more variable than the SAHG estimates, which did not fluctuate as much. Overall, the SAHG product estimated higher values of soil water throughout the period. A scatter graph of the CRP soil water estimates against the SAHG soil water estimates had an R^2 of 0.1371 and showed that the SAHG product overestimated soil water throughout the period, compared to the CRP estimates. The difference in soil water estimates were attributed to both the large vertical and horizontal scaling differences (the spatial scales were two orders of magnitude different, as the CRP has a measurement area of 0.34 km^2, while the SAHG product was 156 km^2).

To extend the validation period, a previous one-year period from March 2014 to March 2015 was selected. The first nine months (March 2014 to November 2014) of the time series analysis showed a close correlation between the CRP and SAHG soil water estimates. The last three months (December 2014 to February 2015) showed a poorer relationship in the fluctuations of the CRP soil water estimates. Discussions with the SAHG team indicated that this may have been due to an error in the PyTOPKAPI model, such as an error in input data. Considering these vertical and horizontal scaling differences, it was clear that the SAHG product still provided good estimates of the relative soil water conditions and confirmed its suitability for both flood forecasting and drought prediction.

4.2.2   Soil water back-calculated from SEBS

Landsat 8 images were used to estimate relative evaporation and evaporative fraction using the SEBS model. The SEBS model was run to obtain the evaporative fraction and relative evaporation fraction. The relative evaporation and the evaporative fraction values were then used in the equations developed by Su (2002) and Scott et al. (2003) to obtain estimates of soil water.

The daily evaporation estimates from the SEBS model during this period ranged from 2.5 mm·day^{-1} to 8 mm·day^{-1}. When these estimates were compared to the daily evaporation values estimated by the eddy covariance system, the SEBS daily soil water estimates were noticeably higher.

From 01 March 2014 to 01 March 2015, the relative evaporation and evaporative fractions were estimated using the SEBS model, which were used in the two equations to obtain soil water. These soil water estimates were then plotted against the CRP estimates from the same period.

The relative evaporation and evaporative fraction values followed a similar seasonal trend as the values were higher in the wetter periods and lower in the dry periods. The back-calculated soil water using both the Su and Scott methods resulted in the estimates following the general season trend. The back-calculation method of Scott et al. (2003) provided slightly better estimates of soil water than the method proposed by Su et al. (2003), when compared to the CRP soil water estimates.

5. Conclusion

Understanding the spatial and temporal variability of total evaporation and soil water at different scales is of great importance in many land surface disciplines such as hydrology. Soil water is a key hydrological variable as it impacts the water and energy balance at the land surface-atmosphere interface and is the main water source for natural vegetation and agriculture.

The CRP is a new and innovative in situ instrument capable of measuring soil water at an intermediate scale. The CRP, once properly calibrated, is suitable for providing spatial estimates of soil water. The CRP estimates were used to validate modelled soil water estimates. These included the SAHG soil water product and the back-calculation of soil water from relative evaporation estimates from the SEBS model.

There was good correlation between the SAHG and CRP datasets. Although the SAHG product performed well, there was still the presence of vertical and horizontal scaling issues due to differences in the measurement depth and the footprints of the two datasets. There was also the issue of the conversion of SSI to VWC, which required a representative porosity of the study area to be determined.

The back-calculation of soil water from relative evaporation and evaporative fraction, estimated using the SEBS model, looked like a promising technique. The spatial resolution was less than the catchment area and the measurement depth was representative of the root zone of the vegetation (0.50 m). Therefore, this product would have the least horizontal and vertical scaling issues when validated against the CRP. Although the back-calculation method results in soil water estimates on a 30 m spatial grid, the temporal resolution of the imagery used is 16 days, which is very impractical for continuous soil water measurements. The SEBS model performed poorly against the CRP validation data. It is recommended that further research is required into the measurement of soil water using remote sensing products.

6. Capacity building

The building of research capacity was achieved by registering students at the University of Pretoria and the UKZN (*Appendix 11.1*).

7. Data storage

See Appendix 11.2.

ACKNOWLEDGEMENTS

Page left blank intentionally

CONTENTS

LIST OF FIGURES

LIST OF TABLES

ABBREVIATIONS

UKZN	University of KwaZulu-Natal
SAHG	Satellite Applications and Hydrology Group
WRC	Water Research Commission
SAWS	South African Weather Service
FFG	Flash Flood Guidance
CRP	Cosmic Ray Probe
COSMOS	Cosmic-ray Soil Moisture Observing System
HylarsMet	Hydrologically Consistent Land Surface Model for Soil Moisture and Evapotranspiration
SWC	Soil Water Content
SEBAL	Surface Energy Balance Algorithm for Land
SEBS	Surface Energy Balance System
NRF RISP	National Research Fund Research Infrastructure Support Programme
TDR	Time Domain Reflectometry
cph	Counts per Hour
NDVI	Normalised Difference Vegetation Index
SMOS	Soil Moisture and Ocean Salinity
AMSR-E	Advanced Microwave Scanning Radiometer
ASCAT	Advanced Scatterometer
SMAP	Soil Moisture Active Passive
PyTOPKAPI	Topographic Kinematic Approximation and Integration
LAS	Large Aperture Scintillometer
LAS MkII (ET)	LAS MkII Evapotranspiration
ILWIS	Integrated land and Water Information System
BEC	Barcelona Expert Center
SSI	soil saturation index
SAEON	South African Environmental Observation Network
TOA	Top of Atmosphere
USGS	United States Geological Survey
SWIR	Short Wave Infrared
TIRS	Thermal Infrared Sensor
OLI	Operational Land Imager
ESUN	Sun Elevation

1. INTRODUCTION

The vulnerability of southern African countries such as South Africa to climate and environmental change is likely to increase as demands on resources continue to rise in conjunction with rapidly growing populations. Disaster management agencies will have to adapt to the increasing number of natural disasters, which includes droughts and floods. In addition, water resources management, crop modelling, and irrigation scheduling all require accurate spatially distributed daily estimates of soil water and total evaporation from catchment to national scale. This will only be feasible through remote sensing technologies. It is therefore essential to further the development and integration of space-based technologies within already existing national disaster management plans.

In South Africa, total evaporation and soil water data has only been available at isolated sites until recently when researchers at the University of KwaZulu-Natal (UKZN) developed a detailed spatial product of real-time estimates of soil water and total evaporation. These variables are now routinely calculated in real time and made available as up-to-date images on the Satellite Applications and Hydrology Group (SAHG) of the UKZN's website. The model has shown promise, but still requires further development as errors in the input data streams hamper the quality of the product (Pegram and Sinclair, pers. comm.).

Up-to-date estimates of soil water are of interest across a wide range of disciplines, including numerical weather prediction, agricultural applications and flood modelling. The current soil water state is a good indicator of flash flood potential on small catchments with a short response time, but this is not measured easily. There is significant global interest in estimating soil water from satellite platforms (e.g. Kerr et al., 2001; Njoku et al., 2003; Wagner et al., 1999). One of the major challenges facing providers of soil water products is validation. This is mainly due to the limited availability and coverage of in situ observation networks (Albergel et al., 2009). Several authors have pursued alternative techniques of validation, inter alia correlations between river flows and soil wetness (Scipal et al., 2005) and assimilation of remotely sensed soil water estimates into a water balance model (Crow, 2007). One outcome of the project funded by the Water Research Commission (WRC), namely K5/1683, which is run by UKZN researchers associated with this proposal was on soil water estimation using an automated modelling system that produces countrywide estimates of soil water state at a three-hourly time steps on a 0.125° spatial grid over South Africa. The key focus of this product is to provide a proof of concept for operational use by the South African Weather Service (SAWS) in their national Flash Flood Guidance (FFG) system, which will be an implementation of the system described by Ntelekos et al. (2006). There are numerous other fields (other than FFG) such as crop modelling and drought monitoring where soil water estimates could prove beneficial.

However, until the development of the cosmic ray probe (CRP), there has not been suitable technology that could measure soil water at the appropriate scales to validate the models. The CRP is an innovative technology that has not been used by researchers in southern Africa before. There are proposed plans for a global Cosmic-ray Soil Moisture Observing System (COSMOS) server network, so a South African network would fit nicely into that theme. A cosmic array network could provide a powerful new addition to the flood forecasting ability of the SAWS.

The need to provide an independent validation of the Hydrologically Consistent Land Surface Model for Soil Moisture and Evapotranspiration (HylarsMet) model was recognised and a project (K5/2066) was initiated to provide a spatially explicit validation procedure for the 1 km grid of soil water and total evaporation produced by the SAHG at UKZN and other global climate models. Automatically tracking the current soil water state is a core function that allows the South African government's FFG system to provide alerts based on current and predicted rainfall. In addition, the current South African FFG system uses a relatively crude total evaporation model. Therefore, the FFG system will be improved by validating total evaporation and soil water estimates with better temporal and spatial resolution.

Measurements using the CRP at area scales of up to 34 ha have the potential to provide hydrometeorologists with an entirely new way of evaluating surface soil water at spatial scales never achieved with ground-based techniques. This will provide water resource managers, engineers and agriculturalists with an invaluable but economical new tool to monitor the critical interface between the ground and atmosphere. This new technology can be employed in water demand forecasting and promises to improve the utilisation of irrigation water, especially in water scarce regions like South Africa. The probe can also be used for predictive weather and climate models by measuring soil water content (SWC).

The research team has developed the skills and has applied state-of-the-art equipment to address both the measurement of total evaporation using surface energy balance techniques, such as eddy covariance, surface renewal, large aperture and surface layer scintillometry, and soil water techniques such as time domain reflectometry (TDR), capacitance and neutron probe methods. The research team has also recently acquired new skills for measuring total evaporation at higher spatial resolutions (e.g. 30 × 30 m) using remote sensing technologies and surface energy balance models, for example, the surface energy balance algorithm for land (SEBAL) and the surface energy balance system (SEBS).

In addition to spatial estimates of total evaporation (micrometeorological and remote sensing techniques), spatially distributed field-based measurements of soil water have also been used to verify the CRP estimates. The aim here was to assess how spatially determined soil water measurements compared with the point measurements of soil water, and soil water measured using the CRP.

The recent development of the CRP as part of a USA National Science Foundation (NSF) and South Africa's National Research Fund Research Infrastructure Support Programme (NRF RISP) project was therefore timely and provided a technology previously unobtainable, which fits perfectly with the spatial resolution of the above project. The CRP uses cosmic ray neutrons to measure SWC over an area of tens of hectares (34 ha with a 660 m diameter). An objective of this project was to increase the research capacity in this domain in South Africa.

This project is designed to build on the recent work in WRC projects, namely, K5/1683: *Soil water from satellites*, and K5/2066: *The validation of the variables (evaporation and soil moisture) in hydrometeorological models.* The aims of this project were to:

- Provide data for the continued support of soil water modelling of South Africa using a hydrologically consistent land surface model (follow-on project proposed from K5/1683).
- Provide accurate field and satellite estimates of total evaporation and soil water for the calibration of Hydrometeorological models.
- Evaluate the spatial variability of soil water at catchment scale.
- Test the suitability of the CRP for providing spatial estimates of soil water at the same scale as the remote sensing products from HylarsMet.

2.   IN SITU METHODS OF TOTAL EVAPORATION AND SOIL WATER ESTIMATION

2.1   Total Evaporation

Estimating total evaporation, which includes evaporation from land and water surfaces, and transpiration by vegetation, is one of the most important processes when determining the exchange of energy and mass between the hydrosphere, atmosphere and biosphere (Sellers et al., 1996). Total evaporation varies regionally and seasonally according to weather and wind conditions (Hanson, 1991). Conventional micrometeorological methods such as eddy covariance (Meyers and Baldocchi, 2005), Bowen ratio (Fristchen and Simpson, 1989), scintillometry (De Bruin et al., 1995; Hill, 1992; Thiermann and Grassl, 1992), surface renewal (Paw U et al., 1995; Snyder et al., 1996), and lysimeters can be used to estimate total evaporation.

2.2   Eddy Covariance

The eddy covariance method provides a direct measure of the vertical turbulent flux of a scalar entity of interest F_s across the mean horizontal stream lines (Swinbank, 1951) providing that fast response sensors (≈10 Hz) for the wind vector and scalar entity of interest are available (Meyers and Baldocchi, 2005). For a sufficiently long averaging period over horizontally homogeneous surface, the flux is expressed as:

$$F_s = \rho_a \overline{w's'} \qquad (1)$$

where ρ_a is the density of air, W is the vertical wind speed and S is the concentration of the scalar of interest. The primes in Equation 1 indicate fluctuation from a temporal average, namely, $w' = w - \overline{w}$ and $s' = s - \overline{s}$); where the overbar represents a time average. The vertical wind component is responsible for the flux across a plane above a horizontal surface. Based on Equation 1, the sensible heat flux, H, can be expressed as:

$$H = \rho_a c_p \overline{w'T_s'} \qquad (2)$$

where c_p is the specific heat capacity of air, w' denotes the fluctuation from the mean of the vertical wind speed, and T_s' is the fluctuation of air temperature from the mean. The averaging period of the instantaneous fluctuations, of w' and s' should be long enough (30 to 60 minutes) to capture all the eddy motions contributing to the flux (Meyers and Baldocchi, 2005).

When properly applied, the eddy covariance technique can be used routinely for direct measurements of surface layer fluxes of momentum, heat, water vapour, and carbon dioxide between a surface and turbulent atmosphere (Finnigan et al., 2003; Massman, 2000; Massman and Lee, 2002; Savage et al., 1997). Like other micrometeorological methods, an adequate fetch is required for the eddy covariance method: a fetch-to-height ratio greater than 100 is usually considered adequate (Wieringa, 1993). The eddy covariance measurements of w' should ideally be at a height that allows small-sized eddies between the anemometer transducer to be sensed (Savage et al., 1995). If the sensor height is too close to the canopy, small-sized eddies may not be sensed, which results in a possible underestimation of the flux. Savage et al. (1995) suggested that measurements under unstable conditions above short turf grass surfaces, and at a height of 1 m above the plant canopy should be sufficient without needing corrections for spectral attenuation of the eddy structures from spatial averaging.

The eddy covariance method requires sensitive, expensive instruments to measure high frequency wind velocities and scalar quantities. Besides, eddy covariance data needs rigorous quality control and filtering, for example, anemometer tilt correction (coordinate rotation, planar fit), spike detection, and trend removal (Meyers and Baldocchi, 2005). Sensors must measure vertical wind speed, sonic

temperature and atmospheric humidity with sufficient frequency response to record the most rapid fluctuations important to the diffusion process (Drexler et al., 2004).

2.2.1 Surface renewal

The surface renewal method is a simple and relatively inexpensive technique based on the principle that an air parcel near the surface is renewed by an air parcel from above (Paw U et al., 1995). This process involves ramp-like structures (rapid increase and decrease of a scalar), which are the result of turbulent coherent structures known to exhibit ejections and sweeps under shear conditions (Gao et al., 1989; Paw U et al., 1992; Raupach et al., 1989). The theory of heat exchange between a surface and the atmosphere using the surface renewal method is described in detail in Paw U et al. (1995), Paw U et al. (2005) and Snyder et al. (1996).

The exchange of heat energy between a surface and the atmosphere is expressed as:

$$H = \alpha \rho_a c_p z \frac{a}{\tau} \qquad (3)$$

where α is a weighting factor; a is the amplitude of the air temperature ramps; and τ is the total ramping period. The amplitude (a) and the ramping period (τ) were deduced using analytical solutions of Van Atta (1977) for air temperature structure function:

$$S^n(r) = \frac{1}{m-j} \sum_{i=1+j}^{m} (T_i - T_{i-j})^n \qquad (4)$$

where n is the power of the function; m is the number of data points in the time interval measured at frequency f (Hz); j is the sample lag between data points corresponding to a time lag $r = j/f$; and T_i is the ith temperature sample. Time lags of 0.5 s and 1.0 s were used in this study. Second, third and fifth order of the air temperature structure parameter are required to solve for a and τ.

The sensible heat flux was finally estimated from Equation 3 using the measurement height (z) and a weighting factor (α) obtained by calibration using the eddy covariance method. The weighting factor (α) depends on the measurement height, canopy architecture and thermocouple size (Snyder et al., 1996; Spano et al., 1997, 2000). Once determined, the weighting factor is fairly stable and does not change from site to site, regardless of the weather conditions unless the surface roughness changes (Snyder et al., 1996; Spano et al., 2000; Paw U et al., 2005).

2.3 Soil Water

Although at first glance the term "soil water" appears simple, on closer inspection it is easy to confuse the different measures of SWC. In this report, we have followed the convention of using the term "soil water" rather than "soil moisture". There appears to be no clear reason for choosing either and we have opted for the term "soil water", which is used mostly by soil physicists rather than "soil moisture", which is used predominantly by the remote sensing community.

By definition, soil water is the amount of water held in a quantity of soil. When the amount is quantified, we use the term "soil water content" (SWC). There are two basic ways to define the amount of soil and, therefore, the water content (Cooper, 2015). Firstly, the volume (or mass) of water is expressed in relation to a known unit volume. This is the most useful way and the units are expressed as $m^3{\cdot}m^{-3}$. This is known as "volumetric water content" (θ). The second is the mass of water per unit of mass of dry soil ($kg{\cdot}kg^{-1}$). This is the "mass wetness" or w and is often term the "gravimetric water content". Volumetric water content is the most useful quantity since we require water volumes in a particular soil volume to calculate water budgets (Cooper, 2015). In addition, most SWC instruments (for example, TDR) are sensitive to, and measure the volumetric water content. In this report, the expression "water

content" is therefore used to mean "volumetric water content" with units m³·m⁻³. The general term "soil water" is used when units are omitted.

Ground-based soil water techniques are the conventional methods for estimating soil water. There are several ground-based techniques that have related an observed property, such as pressure, neutron count and mass, to soil water. In recent years, the use of the CRP to measure soil water has gradually attracted attention and has been implemented by few countries across the world. The next section provides an analysis of the conventional methods of soil water estimation, which will be followed by a detailed review of the CRP.

Ground-based soil water measurements have played a key role in a variety of large-scale applications and have been invaluable as calibration and validation data for satellite-based products, sensors and models (Gruber et al., 2013). There are several ground-based techniques including the gravimetric method, neutron scattering and TDR (Walker et al., 2004). The gravimetric method is an oven-drying technique, which has the advantages of being accurate, independent of soil type and easily calculated; however, it is a destructive technique that is time and labour consuming (Zazueta and Xin, 1994). The neutron-scattering method can measure soil profiles and the measurement is directly related to soil water; however, it is limited by its cost, radiation hazard, skills required and the time consumed (Zazueta and Xin, 1994). The TDR method is a common in situ method due to its accuracy and non-destructive procedure.

2.3.1 Time domain reflectometry

The TDR system transmits a very short rise time electromagnetic pulse along a coaxial system that includes a TDR probe for soil water measurements and samples. It digitises the resulting reflection waveform for analysis or storage. The elapsed travel time and pulse reflection amplitude contain information used by the on-board processor to determine soil volumetric water content, soil bulk electrical conductivity, rock mass deformation or user-specific time-domain measurements quickly and accurately.

TDR is a relatively new method for measuring soil water. The methodology was previously used in the telecommunications industry to identify discontinuities in cables. An electromagnetic wave is propagated down a cable and reflected, thus indicating discontinuities or breaks in the cable. Using time travel analysis, it is possible to determine the point of discontinuity or damage to the cable.

Development of TDR technique in the 1980s to measure volumetric SWC is presented in Topp et al. (2003). The time travel of a propagated signal is dependent on the velocity of the signal and the length of the waveguide or cable. The velocity of the electromagnetic wave is in turn dependent on the dielectric constant of the material surrounding the waveguide. This can be expressed as:

$$\Delta t = \frac{2L\sqrt{K_a}}{c}$$

(5)

where K_a is the apparent dielectric constant, c is the velocity of the electromagnetic signal in free space, L is the waveguide length, and Δt is the travel time.

The apparent probe length, which is the actual unit measured by TDR devices, can be defined as:

$$L_a = \frac{c\Delta t}{2}$$

(6)

In terms of dielectric constant (K_a), Equation 5 and Equation 6 can be simplified as the ratio of the apparent probe length to the real probe length.

$$\sqrt{K_a} = \frac{L_a}{L} \tag{7}$$

TDR can be used to estimate soil water because the dielectric constant of water relative to other soil constituents is high. Consequently, it is possible to develop a relationship between changes in dielectric constant and volumetric SWC (θ_v). The relationship between dielectric constant and volumetric water content has been described empirically by Topp et al. (1980) and Ledieu et al. (1986) using polynomial and linear equations. This empirical relationship was first described by Topp et al. (1980) as:

$$\theta_v = -5.3 \times 10^{-2} + 2.92 \times 10^{-2} K_a - 5.5 \times 10^{-4} K_a^2 + 4.3 \times 10^{-6} K_a^3 \tag{8}$$

and later developed further by Ledieu et al. (1986) as:

$$\theta_v = 0.1138\sqrt{K_a} - 0.1758 \tag{9}$$

These empirical relationships provide a good estimation of soil water in mineral soils where $\theta_v < 0.5$ covers the entire range of interest in most soils with an estimation error of 0.013 (Jones *et al*, 2002). Soils with $\theta_v > 0.5$ or with high organic or clay contents may require soil-specific calibration. An alternative is the dielectric mixing approach that uses dielectric constants and volume fractions for each soil constituent to derive a relationship describing the composite dielectric constant. This physically based approach was used by Roth et al. (1990) and Friedman (1998), but requires estimates of porosity for this technique.

The TDR method has number of advantages over other techniques used to measure volumetric soil water. The main advantages are (Jones et al., 2002):

- Superior accuracy (typically 1% to 2% volumetric water content).
- Calibration under normal conditions is minimal.
- TDR has excellent spatial and temporal resolution.
- Measurements are easily automated using loggers and multiplexers.
- Soil disturbance is minimal and there is no danger to hazardous exposure of radiation offered by other techniques such as neutron probes.

A critical limitation of the TDR system affecting the accuracy of volumetric SWC is the air gap effect. This occurs when there is a poor electrical contact between the probes and the soil. This problem can be created during installation. Patterson and Smith (1985) recommend using narrow pilot holes drilled into the soil to prevent gaps created by the insertion of the probes at an inconsistent angle. This can be particularly useful in hard soils where probe insertion may be difficult. This also reduces compaction of the soil when the probe is inserted, although the Campbell Scientific TDR Probe Instruction Manual states that the soil will experience rejuvenation of soil structure with time from wetting/drying cycles.

The volumetric SWC is assumed to be uniform around the vicinity of the probe, with the measurement being the average soil water of the material surrounding the probe. However, this may not be the case in reality and a study by Chan and Knight (1999) shows that signal noise may be created if soil water is not evenly distributed across the length of the probes.

2.3.2 Cosmic ray probe

The CRP method is a relatively new technique with the capability of providing data for large-scale studies, such as the calibration and validation of satellite-based soil water retrievals and land surface models (Villarreyes et al., 2013). The use of CRP for estimating soil water has been implemented by few countries across the world (Figure 1). It is capable of providing soil water estimates over hundreds of metres, which bridges the gap between point-scale and large-scale remote sensing measurements (Dutta and D'este, 2013). It measures the background neutrons that are emitted from the soil. These background neutrons are naturally occurring and continuously produced as a result of collisions between terrestrial nuclei and cosmic ray hadrons (Desilets and Zreda, 2013).

The intensity of the background neutrons are dependent on the occurrence of hydrogen-rich materials, such as water, due to hydrogen's neutron-scattering properties (Desilets and Zreda, 2013). The sensitivity of the CRP to the presence of water can mainly be attributed to the fairly large elastic scattering cross-section and low mass of the hydrogen nucleus (Desilets et al., 2010). Therefore, the presence of water within the soil pores plays an important and central role in moderating the concentration of cosmic ray neutrons above the soil surface (Desilets and Zreda, 2013).

The soil water is estimated by the concentration of neutrons above the soil surface. Dry soils are highly emissive, such that neutrons are more efficiently removed from soil (Zreda et al., 2008). This results in more neutrons escaping to the surface of a dry soil, which would result in a higher concentration of neutrons above the soil surface (Franz et al., 2012). The CRP system consists of two sensors. One measures the fast neutrons, which are attributed to the soil water, while the other sensor measures the slow neutrons, which are attributed to the water above the soil surface (biomass and snow).

The radial footprint of the CRP is dependent on the neutrons scattering in the air that can travel hundreds of metres from their source. Hence, the scattering properties of air significantly affect the diameter of the footprint (Jiao et al., 2014). The CRP can be used either in a fixed position or in a moving vehicle. The fixed position is used to obtain continuous monitoring of an area, while the roving method can be used for mapping large areas (Dutta and D'este, 2013).

Figure 1: Map of CRPs around the globe (http://cosmos.hwr.arizona.edu)

When the CRP is placed in a static position a few metres above the ground, it has a radial footprint of 670 m in diameter at sea level (Zreda et al., 2008). The footprint size is dependent on the atmospheric pressure and is inversely proportional to the density of air. The measurement depth is dependent on the SWC (Figure 2), such that a measurement depth of 0.72 m in dry soil and a depth of 0.12 m in wet soil are obtained (Zreda et al., 2008). The technique operates as the neutron fluxes are a great proxy for land surface water (Desilets et al., 2010). Along with the neutron count rate, CRP also measures the internal temperature, relative humidity and external barometric pressure (Franz et al., 2013).

There are two important procedures when obtaining SWC from measured neutron intensity. The first step is to correct the neutron-counting rate according to the barometric pressure, which is achieved by using Equation 10, which requires on-board pressure sensor data (Hydroinnova, 2013; Jiao et al., 2014):

$$N = N_{raw} \exp\big(\beta(P - P_o)\big) \qquad (10)$$

where N is the corrected pressure count rate, N_{raw} is the raw count rate, P is the barometric pressure over-counting interval, P_o is the reference barometric pressure at the site, and β is the barometric pressure coefficient (Hydroinnova, 2013; Jiao et al., 2014).
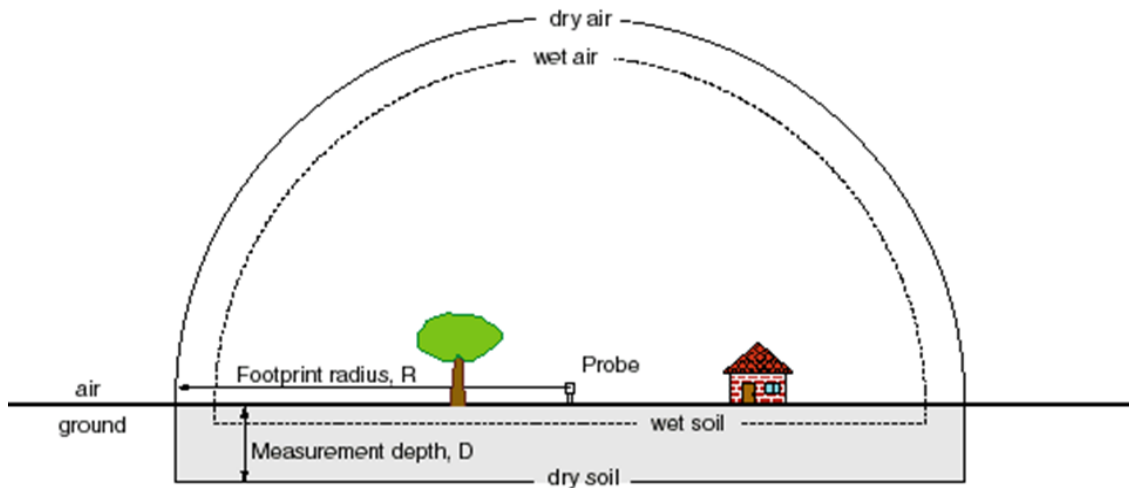
Figure 2: CRP measurement footprint and depth

The next step is to convert the corrected counting rate to a gravimetric water content, which is done using the baseline equation for a generic silicate soil (Hydroinnova, 2013):

$$\theta m = \frac{1}{a_1}\left(\frac{a_2}{\frac{N}{N_o} - a_3}\right) - a_4 \qquad (11)$$

where N_o is the count rate over dry soil conditions, and $a_1 = 0.079$, $a_2 = 0.640$, $a_3 = 0.370$ and $a_4 = 0.910$ are constants for all soils. N_o is determined through field calibration. The calibration does not need to be performed on dry soil (Hydroinnova, 2013; Jiao et al., 2014).

The CRP calibration procedure is performed using ground-based point measurements. It is recommended that a calibration procedure is carried out for both the dry season and the wet season (Dutta and D'este, 2013). The calibration procedure is carried out by taking eight sampling points at three rings (Figure 3), which radially expand away from the CRP. At each sampling point, three measurements are taken at different soil water depths (Dutta and D'este, 2013).
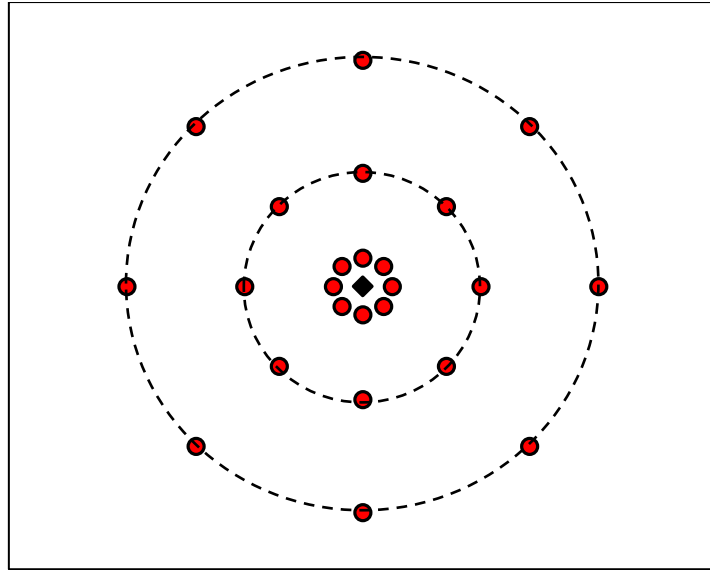
Figure 3: A diagram showing sampling points to calibrate CRP at three rings (25 m, 100 m, and 200 m away from the probe situated in the middle)

Desilets et al. (2010) found that by using a neutron particle transport model, they could establish a relationship between the water content in a homogeneous soil and the relative neutron counts. Neutron count rates from the probes need to be normalised to a reference solar activity level and atmospheric pressure. Correction factors need to be applied to account for solar activity (Zrede et al., 2012), geomagnetic latitude, atmospheric pressure (Desilets and Zreda, 2013), and atmospheric water vapour (Franz et al., 2012). Barring the water vapour correction factor, it must be noted that all other correction factors are automatically applied on the COSMOS website where neutron count readings are retrieved. The water vapour correction factor is determined through air densities, which in turn can be calculated from atmospheric measurements of air pressure, air temperature and relative humidity (Franz et al., 2012). The water vapour correction factor is site-specific and is applied to the neutron count. This is a result of all neutrons being affected by all sources of hydrogen. To detect soil water, atmospheric hydrogen needs to be excluded. The correct neutron count can be determined using Equation 12 as:

$$N = \frac{N' \times CP \times CWV}{CI \times CS} \begin{cases} CP = \exp\left(\dfrac{P_i - P_0}{130}\right) \\[2mm] CI = \dfrac{N_H^i(t)}{N_H^0} \\[2mm] CWV = 1 + 0.0054\left(\rho_v^i(T, P, RH) - \rho_v^0(T, P, RH)\right) \\[2mm] CS = f(x, y, z, t) \end{cases} \qquad (12)$$

Where N is the corrected neutron counts per hour (cph), N' is the raw moderated neutron counts (cph), CP is the pressure correction factor, CWV is the water vapour correction factor, CI is the high-energy intensity correction factor, and CS is the scaling factor for geomagnetic latitude. In CWV, ρ_v^i is the absolute humidity of the air (g/m³), ρ_v^0 is the reference absolute humidity of the air (g/m³), T is air temperature (°C), P is pressure (mb), and RH is relative humidity (%). In CS, x, y, z are location and elevation, and t is time.

$$es_0 = 611.2 \times \exp\left(\frac{17.67 \times T}{243.5 + T}\right) \qquad (13)$$

where es_0 is the saturated vapour pressure at surface (Pa), and T is air temperature (°C).
Note: 1 mb = 1 hPa =100 Pa, and $T(K) = T(°C) + 273.15$.

$$e_0 = \frac{RH}{100} \times es_0 \qquad (14)$$

where e_0 is actual vapour pressure at surface (Pa) and RH is the relative humidity (%).

$$\rho_v = \frac{e_0}{Rvap \times (T + 273.15)} \times 1000 \qquad (15)$$

$$R_{vap} = \frac{R}{0.001 M_{vap}}$$

where r_v is the absolute humidity of air (g/m³), $\phantom{R_{vap} = \frac{R}{0.001 M_{vap}}}$ is the gas constant for water vapour (J/K/kg), R is the universal gas constant (8.31 J/mol/K), M_{vap} is the molar mass of water vapour (18.015 g/mol or 0.018 kg/mol), and T is air temperature (°C).

The corrected volumetric SWC of a soil through calibration samples and various correction factors are then calculated as:

$$\left(\theta_p + \theta_{LW} + \theta_{SOC_{eq}}\right)\rho_{bd} = \frac{0.0808}{\dfrac{N}{N_0} - 0.372} - 0.115 \qquad (16)$$

where q_P is pore water content (g/g), q_{LW} is lattice water content (g/g), $q_{SOC_{eq}}$ is soil organic carbon water content (g/g), r_{bd} is dry soil bulk density (g/cm³), N is the corrected neutron counts (cph), and N_0 is an instrument-specific calibrated parameter that represents the count rate over dry silica soils (cph). The three coefficients were determined by Desilets et al. (2010) WRR from a semi-analytical solution of a neutron diffusion equation.

$$q_{SOC_{eq}} = \left(TC - \frac{12}{44} CO_2\right) \div 0.5556 \qquad (17)$$

where TC is the soil total carbon (g/g), CO_2 is the soil CO_2 (g/g), 12/44 is the stoichiometric ratio of carbon to CO_2, and 0.5556 is the stoichiometric ratio of H_2O to organic carbon (assuming organic carbon is cellulose: $C_6H_{10}O_5$).

The CRP has numerous operational advantages: the technique is passive, non-contact, insensitive to soil conditions, portable, easily automated, and it has minimal power requirements, a measurement depth of 12-72 cm, is less sensitive than remote sensing techniques to the interference by vegetation, and it does not contain a radioactive source (Zreda et al., 2008, Desilets and Zreda, 2013).

Applications are not limited to measuring soil water only as it can also be used to measure snow depth and biomass density (Hydroinnova, 2013). The potential applications make it appealing to scientists in various fields, such as agricultural and ecological monitoring, streamflow forecasting, climate science, drought- and flood forecasting, and slope stability (Desilets et al., 2010). It should be noted that the remote sensing discipline can benefit greatly from this innovative technology by using CRP measurements for both calibrating and validating sensors and data products, as it overcomes spatial limitations of conventional ground-based soil water estimates (Desilets et al., 2010).

3.   REMOTE SENSING OF TOTAL EVAPORATION AND SOIL WATER

3.1   Total Evaporation

Conventional micrometeorological methods estimate total evaporation based on point- or line-averaged measurements of components of the energy balance, which are only representative of local scales and cannot be extended to large areas because of land surface heterogeneity (French et al., 2005). Remote sensing based total evaporation models can provide representative measurements of several physical parameters from field (local), catchment to regional scale, and are better suited for estimating water use of different vegetation surfaces (Allen et al., 2007).

Research on the use of remotely sensed land surface temperature data to estimate total evaporation started towards the end of the 1970s (Jackson et al., 1977) and early 1980s (Carlson et al., 1981; Gurney and Camillo, 1984; Price, 1982; Seguin and Itier, 1983). Over the years, numerous remote sensing based models varying in complexity have been developed to estimate regional total evaporation. Surface energy balance models combine some empirical relationships and physical modules, and are based on a shortened energy balance for each pixel where total evaporation is estimated as a residual of the energy balance. Most current operational models (such as SEBAL, Mapping Evapotranspiration with Internalised Calibration [METRIC] and SEBS) use remote sensing directly to estimate input parameters and total evaporation. The SEBS model is used in this study to estimate total evaporation and soil water using satellite data.

3.1.1   SEBS model

The SEBS model consists of a set of tools to determine the land surface physical parameters such as albedo, emissivity, temperature, vegetation cover from spectral reflectance and radiance (Su et al., 1999). It is an extended model to determine the roughness length for heat transfer (Su et al., 2001) and a new method for determining the evaporative fraction on the basis of energy balance at limiting cases (Su, 2002).

The SEBS requires three sets of information or data. The first set of data consists of land surface albedo, emissivity, temperature, fractional vegetation coverage and leaf area index, and the height of the vegetation. If vegetation information is not available, the normalised difference vegetation index (NDVI) is used as a surrogate. This input data can be derived from remote sensing data in conjunction with other information about the surface of interest. The second set includes meteorological data such as air pressure, temperature, humidity and wind speed at a reference height. The reference height is the measurement height for point application and the height of the planetary boundary layer for regional application. This data set can include variables estimated by large-scale meteorological models. The third data set includes downward solar radiation and downward long-wave radiation, which can either be measured or estimated as model output or parameterization.

The SEBS also applies the surface energy balance equation to partition the available energy into sensible and latent heat flux density. The shortened energy balance equation is expressed as:

$$R_n = LE + H + G \qquad (18)$$

where R_n is the nett radiation (W·m^{-2}), LE is the latent heat flux (W·m^{-2}), H is the sensible heat flux (W·m^{-2}), and G is the soil heat flux (W·m^{-2}). The latent heat flux, which represents the energy required for evaporation, is computed as a residual of the energy balance:

$$LE = R_n - H - G \qquad (19)$$

The nett radiation, (R_n), can be computed using the expression described in Bastiaanssen et al. (1998) as:

$$R_n = (1-\alpha)R_{s\downarrow} + R_{l\downarrow} - R_{l\uparrow} - (1-\varepsilon)R_{l\downarrow}$$
$$= (1-\alpha)R_{s\downarrow} + \varepsilon' \sigma T_{air}^4 - \varepsilon \sigma T_s^4 - (1-\varepsilon)\varepsilon' \sigma T_{air}^4$$

(20)

where R_s is the incident solar radiation (W·m^{-2}), $R_{l\downarrow}$ and $R_{l\uparrow}$ are the incoming and outgoing long wave radiations respectively (W·m^{-2}), ε' is the apparent atmospheric emissivity (air emissivity), α is surface albedo, ε is the surface emissivity, σ is the Stefan-Boltzmann constant (5.67×10^{-8} W·m^{-2}K^{-4}), T_{air} is the air temperature (K), and T_s is the land surface temperature (K).

The equation to estimate soil heat flux, G, is parameterized as:

$$G = R_n \left[\Gamma_c + (1 - f_c)(\Gamma_s - \Gamma_c)\right]$$

(21)

where it is assumed that the ratio of soil heat flux to nett radiation Γ_c is 0.05 for full vegetation canopy by Monteith, cited in Su (2002), Γ_s is 0.315 for bare soil (Kustas and Daughtry, 1989), and f_c is the fractional canopy coverage used to separate non-vegetated, partially vegetated and densely vegetated land surfaces using NDVI.

SEBS uses the Monin–Obukhov similarity theory to estimate the sensible heat and latent heat fluxes. This theory relates surface fluxes to surface variables and variables in the atmospheric surface layer (Su et al., 2001). The aerodynamic (d and z_{om}) and thermal dynamic roughness parameters (z_{oh}) need to be known to estimate sensible heat flux. The aerodynamic parameters, d and z_{om} can be estimated from near surface wind speed and vegetation parameters (height and leaf area index). When wind speed and vegetation parameters are not available, the aerodynamic parameters can be related to vegetation indices derived from satellite data (Su, 2002).

The actual sensible heat flux (H) is constrained by the sensible heat flux at the wet limit, H_{wet}, and the sensible heat flux at the dry limit, H_{dry}, in SEBS like the S-SEBI model. Under the dry limit, the latent heat (evaporation) becomes zero due to the limitation of soil water and the sensible heat flux is at its maximum value. The dry limit is given as:

$$H_{dry} = R_n - G$$

(22)

$$LE_{dry} = R_n - G - H_{dry}$$

(23)

Under the wet limit, where evaporation takes place at potential rate, LE_{wet} (evaporation is limited only by the energy available under the given surface and atmospheric conditions), the sensible heat flux takes its minimum value, H_{wet}, namely:

$$H_{wet} = \left((R_n - G) - \frac{\rho C p (e_s - e)}{r_{ew} \gamma}\right) / \left(1 + \frac{\Delta}{\gamma}\right)$$

(24)

$$LE_{wet} = R_n - G - H_{wet}$$

(25)

where e is the actual measured vapour pressure, e_s is the saturation vapour pressure, γ is the psychrometric constant, Δ is the rate of change of saturation vapour pressure with temperature, and r_{ew} is the external resistance at the wet limit.

The relative evaporation (Λ_r) then can be given as:

$$\Lambda_r = \frac{LE}{LE_{wet}} = 1 - \frac{LE_{wet} - LE}{LE_{wet}} \qquad (26)$$

$$\Lambda_r = 1 - \frac{H - H_{wet}}{H_{dry} - H_{wet}} \qquad (27)$$

The evaporative fraction is then estimated as:

$$\Lambda = \frac{LE}{H + LE} = \frac{LE}{R_n - G} = \frac{\Lambda LE_{wet}}{R_n - G} \qquad (28)$$

The actual sensible heat and latent heat fluxes can be finally obtained by inverting Equation 28 as:

$$H = (1 - \Lambda)(R_n - G)$$
$$LE = (R_n - G) \qquad (29)$$

When the evaporative fraction is known, the daily evaporation (mm/day) can be determined as:

$$E_{daily} = 8.64 \times 10^7 \times \overline{\Lambda}(\frac{R_n - G}{\lambda \rho_w}) \qquad (30)$$

where $\overline{\Lambda}$ is the daily average evaporative fraction, and ρ_w is the density of water. Since the daily soil heat flux, *G*, is close to zero because the downward daytime and upward flux at night balance each other approximately, the daily evaporation is determined by assuming the daily evaporative fraction is approximately equal to the instantaneous value as:

$$E_{daily} = 8.64 \times 10^7 \times \frac{\overline{\Lambda} \overline{R_n}}{\lambda \rho_w} \qquad (31)$$

By summing up the corresponding daily evaporation for a certain period, the actual evaporation for a week, month, season, and year can be determined. However, errors will occur due to cloud effects. These effects can be removed by using time series processing or data assimilation procedures (Su et al., 2003a).

3.2   Soil Water

Soil water is an important hydrologic parameter linked to water availability, land surface evapotranspiration, runoff generation, ground water recharge, and irrigation scheduling (Scott et al., 2003). Spatial knowledge of land surface evapotranspiration and root zone soil water is of prime interest for environmental applications, such as optimising irrigation water use, irrigation system performance, crop water deficit, and drought mitigation strategies (Hafeez et al., 2007), and indicates where water is physically present in water sheds and river basins (Scott et al., 2003). The deviation between actual

and desirable values of soil water is critical for the water resources management decision-making process (Scott et al., 2003). Flood prediction, including information on the spatial extent of inundation, discharge, and timing of the flood peak, and duration of recession, is critically dependent on soil water data (Scott et al., 2003).

In situ soil water measurements are difficult due to the significant spatial variability. Therefore, it is necessary to investigate other soil water measurement methods at a larger scale. Remote sensing techniques can be used to assess spatial and temporal variation of soil water (Moran et al., 2002). Remote sensing is seen as a promising technique for soil water estimation as it overcomes the spatial and temporal heterogeneity of soil water (Zhao and Li, 2013). Additional advantages are its ability to monitor soil water in remote areas, usability and cost (Lakshmi, 2013; Mekonnen, 2009; Sabins, 2007). The major limitation to the implementation of remote sensing in critical hydrological application is its coarse resolution. The following subsections give an overview of remote sensing of soil water and models that use remotely sensed data as input to estimate soil water.

3.2.1 Overview of remote sensing soil water products

A few remote sensing soil water techniques have been researched and used. These techniques include the gamma radiation, thermal infrared, near infrared and microwave radiation techniques (Albergel et al., 2012). Each technique measures a different land surface quantity, uses a different range of the electromagnetic spectrum and has its own unique advantages and limitations (Mekonnen, 2009). From past research studies, it is evident that the microwave radiation technique, which consists of both active and passive methods, can be considered as the most promising technique for remote sensing of soil water. This is due to its advantages over the other techniques, such as its all-weather capability, large spatial coverage, temporal resolution, measurement depth and vegetative penetration, as well as the limitations of the other techniques (Guillem, 2010; Wagner, 2008; Wang and Qu, 2009).

Microwave radiation remote sensing observes the large contrast in the dielectric properties of soil particles and water. The dielectric constant increases as the soil water increases (Mekonnen, 2009; Wang and Qu, 2009). Remote sensing techniques do not measure the SWC directly, therefore mathematical models that describe the association between the measured signal and the subsequent soil water need to be derived (Wang and Qu, 2009).

Over the last few decades, active and passive microwave remote sensing has provided the unique ability to obtain estimates of soil water at a global scale (Brocca et al., 2013). The L-band range (1 GHz to 10 GHz) is preferably used, as higher frequencies are more affected by perturbation factors such as vegetation cover and atmospheric effects (Albergel et al., 2012). There have been many research studies on passive microwave remote sensing products over the last few decades. These products include soil moisture and ocean salinity (SMOS), advanced microwave scanning radiometer (AMSR-E), European remote sensing (ERS) ERS-1 and ERS-2, WindSat and advanced scatterometer (ASCAT) (Dorigo et al., 2011).

Remote sensing of soil water has progressed and product users have developed trust for remote sensing data as the sensors and their algorithms continually improve (Brocca et al., 2013). The launch of the SMOS satellite, which was the first satellite radiometer dedicated to measuring soil water over land, emphasized the increased need for measurements of soil water. This was further highlighted by the launch of the Soil Moisture Active Passive (SMAP) satellite in 2014 (Fang and Lakshmi, 2014; Jackson al., 2010; Lakshmi, 2013; Song et al., 2013). However, SMAP's radar stopped transmitting 7 July 2015 due to an anomaly to the power supply for the radar's high-power amplifier, which resulted in no further transmission of radar data.

Current remote sensing soil water products have a resolution of between 25 km^2 and 50 km^2. The vertical and horizontal scaling issues are the major issues in the calibration and validation procedure when using ground-based point measurements. The vertical scaling issues occur when remote sensing

surface soil water (top 10 cm) is calibrated and validated against ground-based soil water measurements (0 m to 2 m) (Jackson al., 2010). Therefore, the measurements are at different depths, which is a problem as soil water varies with depth. The horizontal scaling issues occur when a point measurement is used to validate a remote sensing area-averaged value. The assumption that the point is representative of a large area is considered incorrect due to the spatial variability of soil water (Gruber et al., 2013). Therefore, there needs to be a shift to area-averaged ground-based methods to validate and calibrate remote sensing data.

Currently, there are several satellite-based soil water products. The two most common products are AMSR-E and SMOS (Brocca et al., 2013). The AMSR-E is the lowest passive microwave radiometer in orbit (Zhang et al., 2011). The AMSR-E SIPS team processes Level-2 A data into Level-2B swath products and then into Level-3 daily, five-day, weekly, and monthly gridded products. It was the first satellite sensor to integrate soil water as a standard product. It has been in orbit abroad NASA's Aqua satellite since 2002 (Sahoo et al., 2008). The AMSR-E sensor measures the microwave radiation at six different frequency bands ranging from 6.9 GHz to 89.0 GHz using its 12 channels (Brocca et al., 2011). The observations are conducted by antenna beams, which scan the Earth's surface at a 55° intersection (Koike et al., 2004). The measurements are based on dual-polarization brightness temperature. The microwave radiation frequency range used determines the spatial resolution of the measurement (Zhang et al., 2011). Several algorithms have been developed by NASA, JAXA and other research groups, who have used different ancillary data, physical formulations and parameters (Brocca et al., 2011). The current AMSR-E soil water product has a spatial resolution of 25 km and represents the top few centimetres of the soil surface (Draper et al., 2009).

The SMOS satellite system is a passive microwave imaging L-band (1.4 GHz) radiometer with aperture synthesis (Albergel et al., 2012). Using the L-band frequency range results in an increased sensitivity to variations in soil water and a decrease in the susceptibility of atmospheric and vegetative attenuation (Mecklenburg et al., 2013). It was launched in 2009 and operates by measuring the phase difference of radiation from various incident angles, such that the Earth's surface is frequently viewed at different angles and polarizations (Fang and Lakshmi, 2014). The SMOS system is a Y-shaped instrument, which consists of 69 antennas. The antennas are equally spaced along three arms and view the surface of the Earth either through full or two polarized radiances to provide a full image (Gruhier et al., 2011). The SMOS soil water product has an average spatial resolution of 40 km; however, this varies from 30-50 km depending on the angle of incidence (Kerr et al., 2010). The entire globe is covered at least twice in three days (Qin et al., 2013).

3.2.2 PyTOPKAPI land surface model

The Topographic Kinematic Approximation and Integration (PyTOPKAPI) SAHG model is a physically based, rainfall-runoff model, which is used to examine the soil water dynamics at different scales, ranging from catchment to national scale (Sinclair and Pegram, 2013). The model is an open source operation of the TOPKAPI distributed hydrological model and has been successfully applied in several countries around the globe (Sinclair and Pegram, 2012).

The PyTOPKAPI model uses three sets of input data, which consists of meteorological, static and remote sensing data sets (Sinclair and Pegram, 2010). The meteorological input data includes the calculation of reference crop total evaporation and requires parameters, such as temperature, relative humidity, wind speed and solar radiation flux (Sinclair and Pegram, 2010). The static input data required are the digital elevation models, land cover and soil properties. The input remote sensing data required are the rainfall and NDVI products on a three-hour temporal scale. In addition, the solar radiation flux from the meteorological input data is a satellite-based product and can be considered as a remote sensing product (Sinclair and Pegram, 2012).

Since the model is used to estimate soil water, it uses several soil parameters including soil depth, residual and saturated soil water, slope, soil conductivity, channel flow and overland flow (Sinclair and

Pegram, 2013). The only input to the soil store as described in the PyTOPKAPI model is precipitation and subsequent infiltration, such that any water that is not partitioned as infiltration is subject to evaporation and surface runoff (Sinclair and Pegram, 2012). The precipitation is partitioned using the Green–Ampt infiltration algorithm. The model structure is set up so that the only way water can leave the soil store is through total evaporation or lateral flow (Sinclair and Pegram, 2012).

The benefits of using this model to estimate soil water are that three-hourly soil water estimates are obtained, which account for the temporal resolution of soil water to an extent. It has a spatial resolution of 1 km × 1 km, which is finer than current remote sensing soil water products.

3.2.3 Estimation of soil water using surface energy balance models

Remote sensing techniques based on different parts of the electromagnetic spectrum such as passive microwave, active microwave, visible, and thermal infrared can be used to estimate soil water as discussed in the previous sections. Microwave remote sensing of soil water has a good physical basis and operates under all weather conditions. The limitation of microwave methods is the shallow depth and that they cannot be used to estimate soil water in the root zone under lush green vegetation, such as in agriculture or in wetlands and other environmentally sensitive zones (Scott et al., 2003). The thermal infrared technique provides an integrated soil water value for the root zone. The advantages of thermal infrared method include good physical basis, which is applicable at a range of spatial and temporal scale, and being cost effective (Scott et al., 2003).

Applying the mass conservation principle and integrating with respect to depth and time increments (Su et al., 2003b):

$$\int_{z1}^{z2} \theta(z, t2)dz - \int_{z1}^{z2} \theta(z, t1)dz = Q(z1) - Q(z2) \tag{32}$$

where θ is the volumetric SWC, t is the time and z is the vertical distance. Applying Equation 32 with boundary conditions $Q(z1) = P_o + I_o - E$ at the soil surface and $Q(z2) = I_c$ at the bottom of the rooting zone. The change in SWC can be expressed as (Su et al., 2003b):

$$\Theta(t2) - \Theta(t1) = Po + Io + Ic - E \tag{33}$$

where Θ is the volumetric SWC in the rooting zone, P_o is the precipitation, I_o is the irrigation, I_c the capillary flux and E evaporation. The water balance is then considered at limiting cases. The wet limit is saturation, such that $\Theta(t1) = \Theta_{wet}$. At the dry limit $\Theta(t2) = \Theta_{dry}$, the evaporation is zero (Su et al., 2003b). From Equation 33:

$$\Theta_{wet} - \Theta_{dry} = Ic_{wet} - E_{wet} \tag{34}$$

For any time between the two boundary conditions:

$$\Theta - \Theta_{dry} = Ic_{wet} - E \tag{35}$$

Rearranging Equation 34 and Equation 35 (Su et al., 2003b):

$$\frac{\Theta - \Theta_{dry}}{\Theta_{wet} - \Theta_{dry}} = \frac{E - Ic}{E_{wet} - Ic_{wet}} \tag{36}$$

if it is assumed that the capillary flux is linked to the soil texture and is less than that of the uptake of root water ($I_c = I_{wet}$). By defining $R_\theta = \Theta/\Theta_{wet}$ as the relative SWC and using Equation 36 (Su et al., 2003b):

$$R_\theta = \frac{\Theta}{\Theta_{wet}} = \frac{\lambda E}{\lambda E_{wet}} \qquad (37)$$

This inverse relationship is often used in hydrological modelling and can be expressed as:

$$\frac{E_{actual}}{E_{potential}} = f\left(\frac{SM_{actual}}{SM_{field\ capacity}}\right) = relative\ soil\ water\ content \qquad (38)$$

Soil wetness is clearly evident in the surface energy balance by the magnitude of sensible heat and latent heat fluxes. If a soil is dry, sensible heat will be large and latent energy will be small. The contrary holds true for wet soil (the sum of sensible heat and latent energy does not change significantly with soil water). Measurements or estimates of sensible heat and latent energy can therefore be used to quantitatively express SWC. An empirical relationship between evaporative fraction (Λ) and volumetric SWC (θ) was developed by Bastiaanssen *et al*. (1998) using evaporative fraction data from SEBAL and in situ measured soil water data. Scott et al. (2003) modified this relationship by normalising soil water θ with saturated SWC θ_{sat}:

$$\theta/\theta_{sat} = \exp\{(\Lambda - 1.0)/0.421\} \qquad (39)$$

The value of relative SWC θ/θ_{sat} varies between 0 (oven dry) to 1 (full saturation) and is a standard relationship that can be applied to a wide range of soils. Scott et al. (2003) further validated the accuracy of the relationship using data collected from irrigated plains in Pakistan and Mexico. The value of Λ under non-advective conditions usually ranges between 0 and 1, which represents zero to maximum evapotranspiration. Since the evaporative fraction Λ can also be calculated over large areas using satellite imagery (e.g. Bastiaanssen et al*.,* 1998), the evaporative fraction is a suitable indicator for describing soil water conditions at the regional scale. It is possible to back-calculate Λ using actual data derived from this project.

4. MATERIALS AND METHODS

4.1 Site Description

Three different sites with contrasting land uses were selected for this study: agricultural crops at Baynesfield; natural vegetation at Cathedral Peak; and commercial forestry at Two Streams. The locations of these study sites in KwaZulu-Natal are shown in Figure 4.
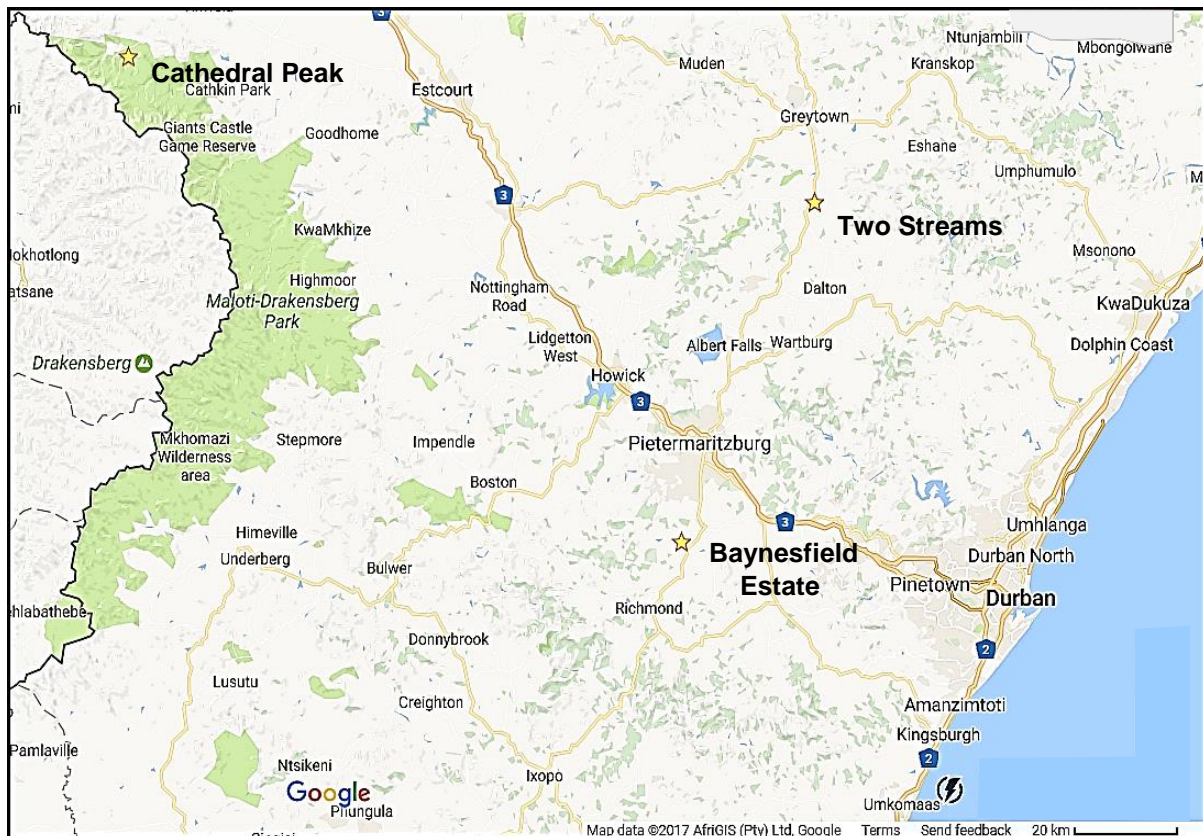
Figure 4: Location of the Baynesfield, Cathedral Peak and Two Streams study areas in KwaZulu-Natal

4.1.1 Baynesfield site

Baynesfield Estate was selected as a suitable site as the area is 3 × 3 km with a potential for a 1 km grid (WRC project K5/2066). The site has both homogeneous and heterogeneous areas with a good degree of sampling variability. The Baynesfield climate is classified as sub-humid with dry and cool winters and warm and rainy summers. The mean monthly air temperature ranges from a maximum of 21.1°C in January to a minimum of 13.3°C in June with a mean annual precipitation of 844 mm. The predominant wind direction is easterly. The research area has a variety of crops grown on a large-scale. The main crops grown at the study site are maize, soybean, sugarcane and avocados.

4.1.2 Catchment VI

The Cathedral Peak Research Catchment VI area is situated in the northern part of the Drakensberg mountain range foothills at latitude 29°00'S and longitude 29°15'E. It is at an altitude of between 1800 m and 2600 m. It forms part of the Cathedral Peak Forestry Research Station that is in the northern part of the crescent in a conserved area of the Natal Drakensberg Park. The Cathedral Peak Research Station is the main centre for hydrological research in the mountainous summer rainfall region of southern Africa. It was established in 1935 to examine the influences of various management practices on the vegetation and water yield of the local mountain catchments (Everson, 1985). The 15 research catchments (numbered I to XV) are situated at the head of three isolated Little Berg spurs at an altitude

of approximately 1890 m (Everson and Tainton, 1984). Each catchment receives a specific treatment (such as afforestation or protection from fire). The experiments in this study were carried out in Catchment VI, which is a grassland catchment receiving biennial spring burn treatment.

Catchment VI is in a summer rainfall region (wet and humid summers with dry and cold winters) with a mean annual precipitation of 1300 mm. Catchment VI is 0.677 km² (67.7 ha) and moderately dissected by streams. The terrain has a slope of 19%. The soils are residual and colluvial, acidic, highly leached and structureless, making them very friable, but well-suited to rapid infiltration (Everson et al., 1998).

4.1.3 Two Streams

The Two Streams catchment is situated 70 km from Pietermaritzburg near Seven Oaks on the Greytown road (Figure 4). The bioregion is "midlands mistbelt grassland". The area is generally hilly with rolling landscapes and a high percentage of arable land. It is dominated by forb-rich, tall, sour *Themeda triandra* grasslands of which only a few patches remain due to invasion of native *Aristida junciformis*. Soil forms are apedal and plinthic and are derived mainly from the Ecca Group with dolerite dykes and sills. Rainfall is primarily in summer with an annual rainfall ranging from 659 mm to 1139 mm. Rain is most commonly from summer thunderstorms or cold fronts. Mist can be heavy and frequent and might add significantly to precipitation (Everson et al., 2014).

4.2 Field Measurements

4.2.1 Baynesfield site

Figure 5 shows the position of the CRP, the TDR soil water profile site and the EC150 eddy covariance tower in relation to the maize field and the CRP footprint.
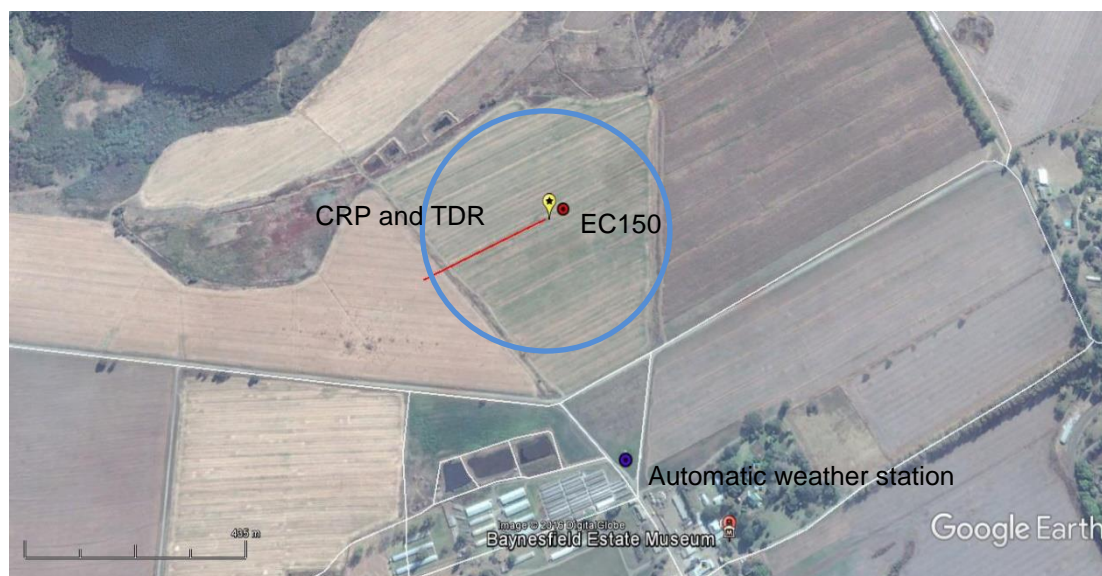
Figure 5: CRP, TDR, EC150 and automatic weather station in the maize field at Baynesfield

4.2.1.1 Total evaporation

An EC150 open path gas analyser and a 3D sonic anemometer (Campbell Scientific Inc., Logan, Utah, USA) were used as an eddy covariance system to measure fluxes of water vapour and carbon dioxide. The EC150 is an integrated in situ open path analyser and sonic anemometer specifically designed for eddy covariance flux measurements. The EC150 system consists of a CR3000 data logger, a CSAT3 three-dimensional sonic anemometer, an EC150 open path gas analyser, an HMP45C temperature and humidity probe, and energy balance sensors consisting of an NR-LITE nett radiometer, two soil heat flux plates, one soil temperature averaging probe, and one CS616 soil water reflectometer. The system measures carbon dioxide flux, latent energy flux, barometric pressure, momentum flux, a computed

sensible heat flux, nett radiation, a computed soil heat flux density, temperature, humidity, horizontal wind speed, and wind direction. The EC150 system was installed on a lattice mast 2.0 m above a maize canopy (Figure 6).

Figure 6: EC150 open path gas analyser and 3D sonic anemometer installed above the maize canopy at Baynesfield

4.2.1.2 Soil water

Three CS616 Campbell Scientific probes were installed for profile volumetric soil water measurement by excavating a 0.60 m deep pit to measure volumetric SWC at 0.1 m, 0.2 m and 0.4 m depths as shown in Figure 7. The three CS616 probes were connected to a CR10X data logger (Campbell Scientific Inc., Logan, Utah, USA). The measurements were sampled every hour with a Campbell CR10X. Hourly and daily volumetric SWC measurements were computed and stored for further analysis. These TDR soil water measurements were used to calibrate and validate the CRP estimates.
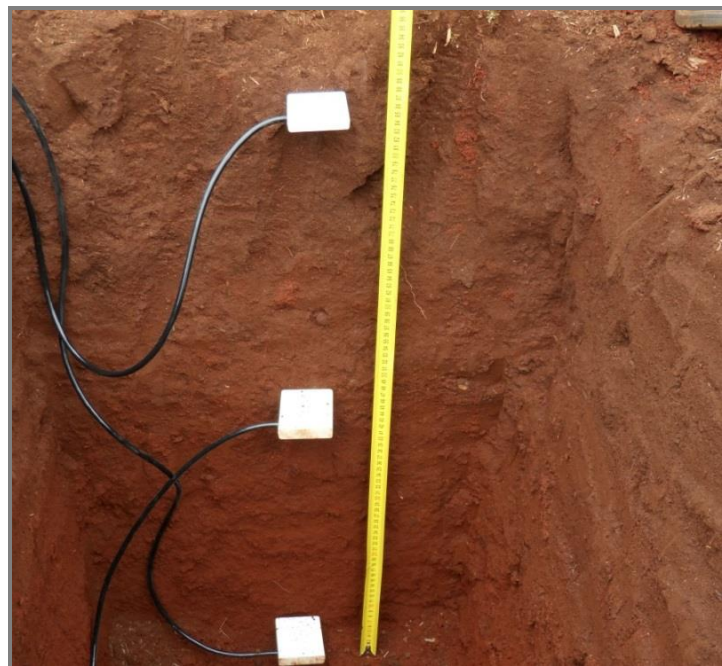
Figure 7: Three CS616 probes installed at 0.1 m, 0.2 m and 0.4 m below the soil surface

The CRP was installed on a tripod mast in the middle of the maize field in Baynesfield (Figure 8). This was done to allow for most of the soil under investigation to come from a homogenous field of the same crop. The logger enclosure and cosmic ray neutron sensors were placed on the mast. A bare sensor was used to pick up the fast cosmic ray neutrons scattered from the soil, while a mode sensor was used to identify the slow cosmic neutrons being scattered by the vegetation. Connected to the data logger was an antenna used to send data via an iridium satellite data communication link. Two CRPs were installed at Baynesfield to estimate soil water from both the soybean and maize sites.

Figure 8: A CRP installed in the middle of a maize field at Baynesfield

4.2.2   Cathedral Peak Catchment VI site

4.2.2.1   Total evaporation

At Cathedral Peak Catchment VI, total evaporation was estimated using the eddy covariance and large aperture scintillometry (LAS) methods (Figure 9). An EC150 system was installed as an eddy covariance system to measure fluxes of carbon dioxide and water vapour as shown in Figure 10. The EC150 system measures carbon dioxide flux, latent energy flux, barometric pressure, momentum flux, a computed sensible heat flux, nett radiation, a computed soil heat flux density, temperature, humidity, horizontal wind speed, and wind direction.
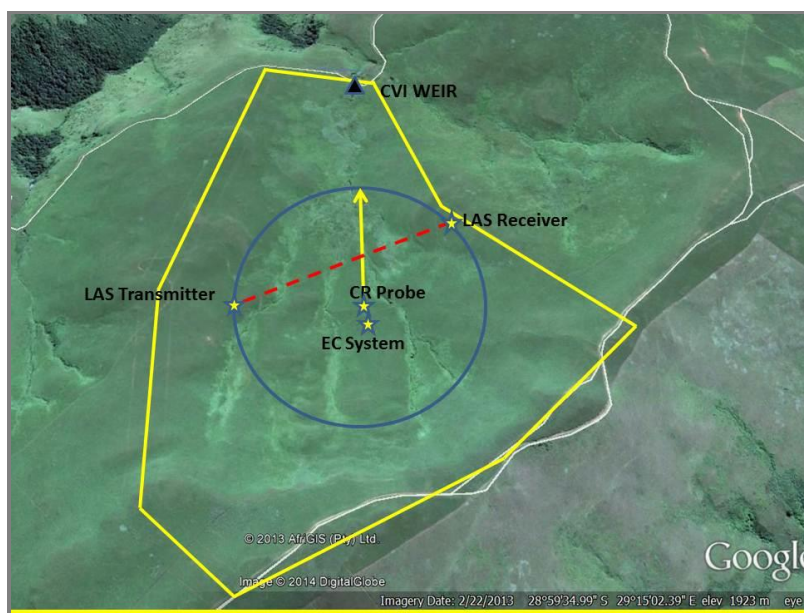
Figure 9: Eddy covariance (EC), LAS transmitter and receiver, and CRP in Cathedral Peak Catchment VI
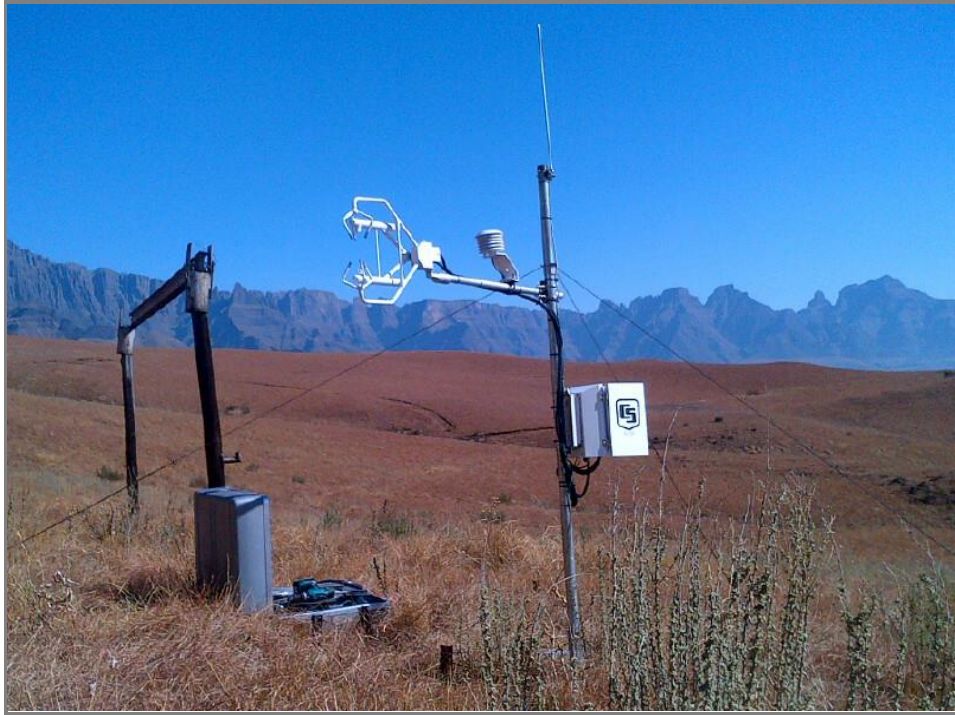
Figure 10: EC150 system installed at Cathedral Peak Catchment VI

A LAS MkII Evapotranspiration (ET) system was also installed at Catchment VI to estimate sensible and latent energy fluxes. The LAS MkII ET system is a complete solution for monitoring the energy balance within the boundary layer. The system comprises a LAS MkII scintillometer, nett radiation sensor, meteorological sensors and data acquisition. It has several telemetry and power supply options (Figure 11). It is specifically designed for field-scale observations of the path average energy fluxes using the scintillometry technique.
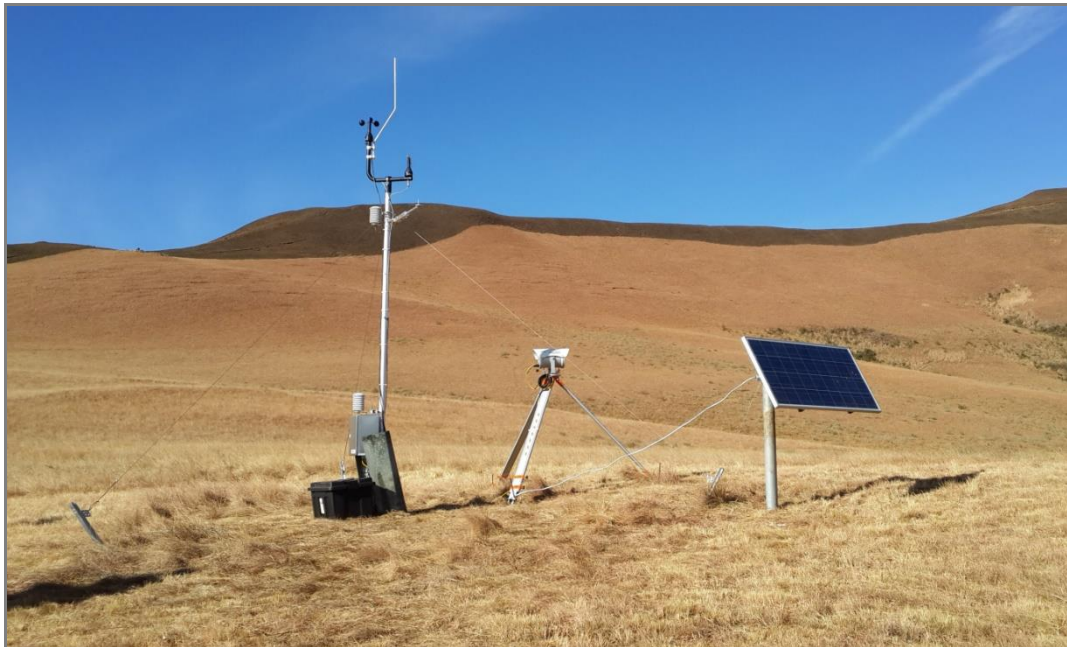
Figure 11: LAS MkII ET system installed in Catchment VI at Cathedral Peak

The LAS MkII ET system has been developed to provide area-representative surface fluxes of sensible heat and latent heat fluxes. A unique feature is the line of sight path-integrating capability of the large aperture scintillometer. This allows the user to measure area-averaged surface fluxes of sensible heat at scales from 100 m to 4.5 km over both homogenous and moderately heterogeneous areas. Since limited power is required, a simple solar-charged battery is sufficient in most cases. The LAS MkII receiver has an internal digital processing unit that automatically computes all relevant parameters, such as C_n^2 and sensible heat flux (Kipp & Zonen, 2014).

Real-time data is available on the display that shows the status of the experiment in seconds. The built-in data logger stores several months of measurements and results. A digital interface allows remote real-time display and full control over the instrument operational settings. Analogue outputs are also available, thus enabling connection of the instrument to virtually any data acquisition system. This allows for easy integration into new or existing measurement networks. The scintillometer on its own measures changes in refractive index of the atmosphere, C_n^2, but with the optional meteorological sensor kit it can calculate sensible heat flux.

4.2.2.2 Soil water

Four CS616 Campbell Scientific probes were installed for profile volumetric soil water measurement. The CS616 probes were installed by excavating a pit to measure volumetric SWC at 0.05 m, 0.1 m, 0.15 m, 0.2 m and 0.3 m depths. The three CS616 probes were connected to a CR1000 data logger (Campbell Scientific Inc., Logan, Utah, USA). The measurements were sampled every hour with a Campbell CR1000. Hourly and daily volumetric SWC measurements were computed and stored for further analysis.

A CRP was installed on a tripod mast in the middle of Catchment VI next to the EC150 eddy covariance system. The CRP was placed in the middle of the field and was connected to a solar panel used to charge the battery powering the system (Figure 12). Connected to the data logger was an antenna used to send data via an iridium satellite data communication link to the COSMOS server. Data from the CS616, CWS655A TDR sensors, EC-5 and 10HS Decagon devices soil water sensors, and gravimetric samples were combined to calibrate the CRP.

Figure 12: A CRP installed in the middle of Cathedral Peak Catchment VI

4.2.3 Two Streams catchment

The position of the CRP and the EC150 eddy covariance tower in the Two Streams Wattle plantation are shown in Figure 13.

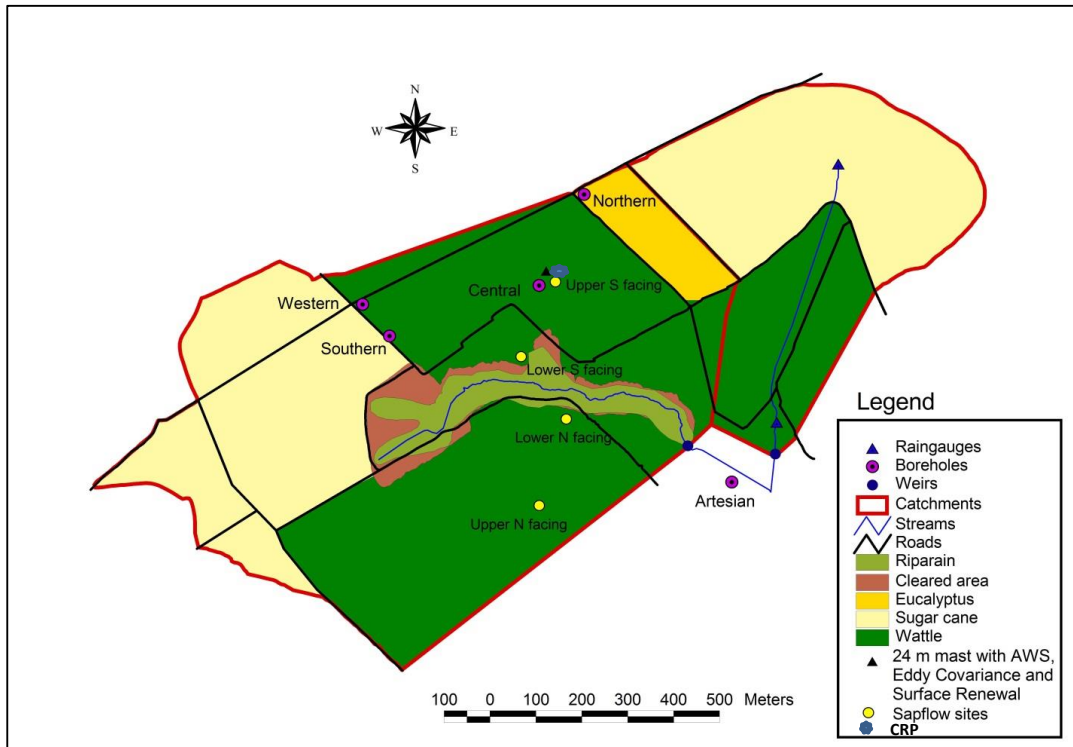**Figure 13: Position of the various monitoring locations in the Two Streams catchment**

4.2.3.1 Total evaporation

The surface renewal and eddy covariance methods were used to estimate total evaporation at the Two Streams catchment on an instrument mounted on a 24 m mast (Figure 14).

Figure 14: The surface renewal and automatic weather station sensors mounted on the 24 m mast at Two Streams

Sensible heat flux was calculated using the surface renewal and eddy covariance techniques in the centre of the wattle stand. Two unshielded type-E (chromel/constantan) fine wire (76 μm diameter) thermocouples placed at heights of 19 m and 21 m above ground surface were used to measure air temperatures. Continuous data was recorded with a data logger (CR3000, Campbell Scientific Inc., Logan, Utah, USA) powered by two 70 Ah batteries and one 20 W solar panel. Data was saved onto a 2 GB compact flash card able to store up to six weeks of high frequency (10 Hz) data. Over the course of the measurements, the sensible heat flux was derived from two thermocouples using the surface renewal technique.

4.2.3.2   Soil water

Six CS616 probes installed near the CRP in a pit to a depth of 2.4 m at 0.4 m intervals from the previous work at Two Streams (K5/2022) were used in this study to validate the data obtained from the CRP (Figure 15) and remote sensing estimates.

4.3   Satellite Estimates

The SEBS model is used for estimating total evaporation. It is available in the Integrated Land and Water Information System (ILWIS), which is a free open source software package.

High-resolution satellite images (Landsat 8) were used to capture the heterogeneity of the land surface over the study sites. These images provide high-resolution information (30 × 30 m) on the land surface temperature, land cover classification, albedo, and NDVI. Most of the images are for cloudless days where the fraction of cloud cover is not more than 5%. Meteorological data (solar radiation, air temperature, wind speed, relative humidity, and atmospheric pressure) from automatic weather stations at the specific sites were used to compute surface fluxes over the area of the satellite images.

Erdas Imaging software was used to preprocess the Landsat images. Erdas has several built-in standard options as well as convenient options for data exchange with ArcGIS. One of the strong features of Erdas is the model generator, which allows the user to set up a model with graphical interactions. SEBS uses a powerful open source geographical information system and remote sensing software, ILWIS, to preprocess satellite

Figure 15: A CRP installed in the middle of wattle trees at Two Streams Research Catchment

images. The land surface physical properties such as albedo, emissivity, temperature, and vegetation coverage (NDVI) were determined from the spectral reflectance and radiances of the Landsat bands. The images were converted to GeoTIFF format in Erdas before exporting to SEBS4ILWIS for surface flux computations.

The AMSR-2 soil water product was obtained from the Jaxa website: http://sharaku.eorc.jaxa.jp/. There is Level 2 and Level 3 soil water data available from the July 2012 to present. The Level 2 data is available on a 25 km spatial resolution grid, while the Level 3 data is available on both 10 km and 25 km spatial resolution grids. The Level 3 soil water product uses Level 1B brightness temperature and Level 2 soil water data and averages them spatially and temporally with respect to predefined lattice grid points on the Earth's surface.

The Level 3 AMSR-2 soil water product at a 10 km spatial resolution was selected to be used in this study. Once the Level 3 10 km soil water product has been selected, the data type needs to be chosen. The data type options include day and/or night and daily and/or monthly. For the purpose of this study,

the data type selected was day and night data at a daily time step. Next, the observation period needs to be specified before specifying the search area. The data format was then specified. There is an option to leave the data in its original format or convert it to HDF5, GeoTIFF of NetCDF. GeoTIFF was chosen as this data format is compatible with ArcGIS 9.3.

The Level 3 SMOS Barcelona Expert Center (BEC) 34 data was obtained from http://cp34-bec.cmima.csic.es/. This site is the SMOS BEC data distribution and visualisation service. There is a fairly short registration procedure before the data can be obtained. Once registered, the data can be accessed from the site's THREDDS service, which provides NetCDF data files. A user name and password, which are selected during the registration procedure, are required to gain access to the THREDDS service. The SMOS soil water products fall under the land category. The BEC land near real time (resolution 0.25° × 0.25°) was selected. As the other two options, it also had fine resolution soil water, which only covered the Iberian Peninsula. The selected option was a global dataset. There are numerous soil water products on different intervals. The one-day global soil water product was chosen. For each day there are two files, which are the ascending and descending orbits.

The PyTOPKAPI soil water product was obtained from the SAHG website: http://sahg.ukzn.ac.za/. The website is easy to use and site navigation was straightforward. The products are freely and readily available and there was no registration procedure required. The data has a temporal resolution of three hours and spatial resolution of ≈12 km. The data ranges from 2008 to present. The data was obtained by clicking on the *Download* tab on the SAHG homepage. There was an option to download either soil saturation index (SSI) or total evaporation. The SSI option was selected. The next page had the option to download the products in either ASCII or GeoTIFF file format. The ASCII file format was selected, as this format can be opened and processed in ArcGIS 9.3.

5. FIRST VALIDATION EXPERIMENT RESULTS

The project team has been busy monitoring and collecting total evaporation and soil water data. The EC150 eddy covariance system, LAS MkII ET system, surface renewal system, three CRPs, TDR probes and Decagon echoprobes have been installed at three different sites for estimating total evaporation and soil water. The project team is currently busy testing the CRP at the Two Streams Research Catchment.

The first validation experiment results included in this report are from ongoing field measurements of total evaporation and soil water, the calibration of the CRP and satellite estimates of total evaporation and soil water using the SEBS model, PyTOPKAPI soil moisture product (SAHG), AMSR-2 and SMOS soil moisture products.

5.1 Baynesfield Site

5.1.1 Total evaporation

Total evaporation over the maize canopy was estimated using the eddy covariance method. The distance to the leading edge of the maize field from the centre of the eddy covariance system was 300 m, which is the same as the CRP. Therefore, there were no fetch distance limitations. Energy flux measurements started on 9 December 2014 and stopped on 3 June 2015. Measurements were done from planting date to the end of the growing season of the maize canopy. The daily variations in total evaporation estimates (mm) over the maize canopy are shown in Figure 16. Daily total evaporation of the maize crop ranged from less than 0.5 mm to 5.4 mm. Total evaporation was higher for December 2014, January 2015 and February 2015 (Figure 16) due to the higher solar radiation and higher air temperatures experienced during these months. Total evaporation decreased in March 2015 (2 mm·day^{-1} on average) compared to January and February 2015. Average daily total evaporation estimates were close to 1 mm for April 2015, which decreased to less than 1 mm for most days in May 2015.
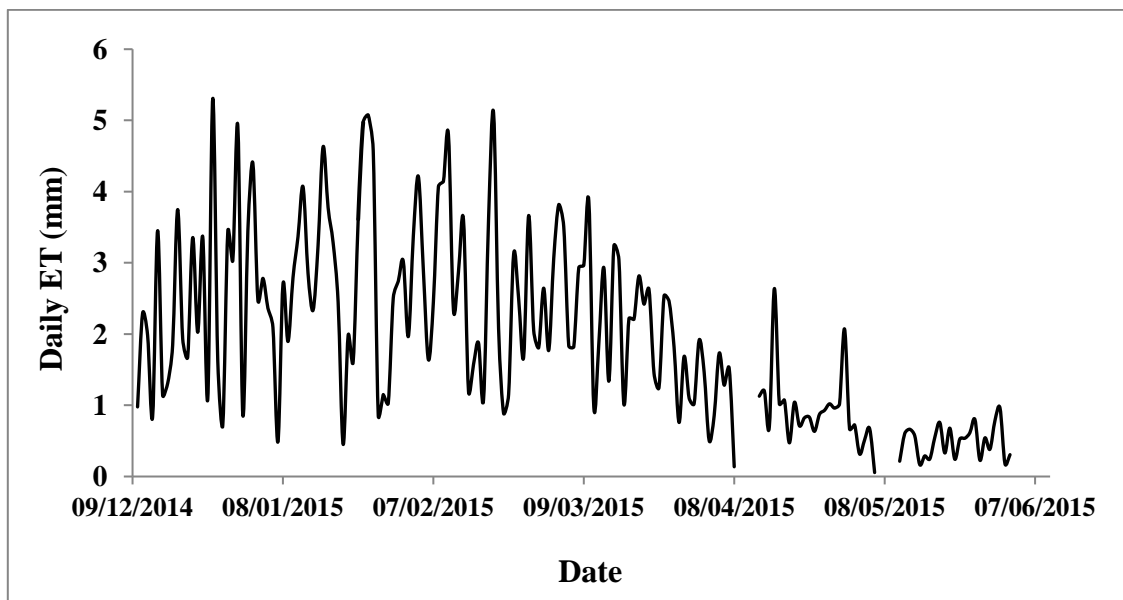
Figure 16: Total evaporation estimates (mm) above the maize canopy at the Baynesfield site

5.1.2 Soil water

The daily fractional volumetric SWC measurements using three CS616 probes installed at 0.1 m. 0.2 m, and 0.4 m depths are shown in Figure 17. Volumetric SWC values varied between 0.17 and 0.36 during the measurement period. Soil water increased with the increase in depth as shown in Figure 17. Soil water was the highest for the 0.4 m depth and lowest for the 0.1 m depth below soil surface.
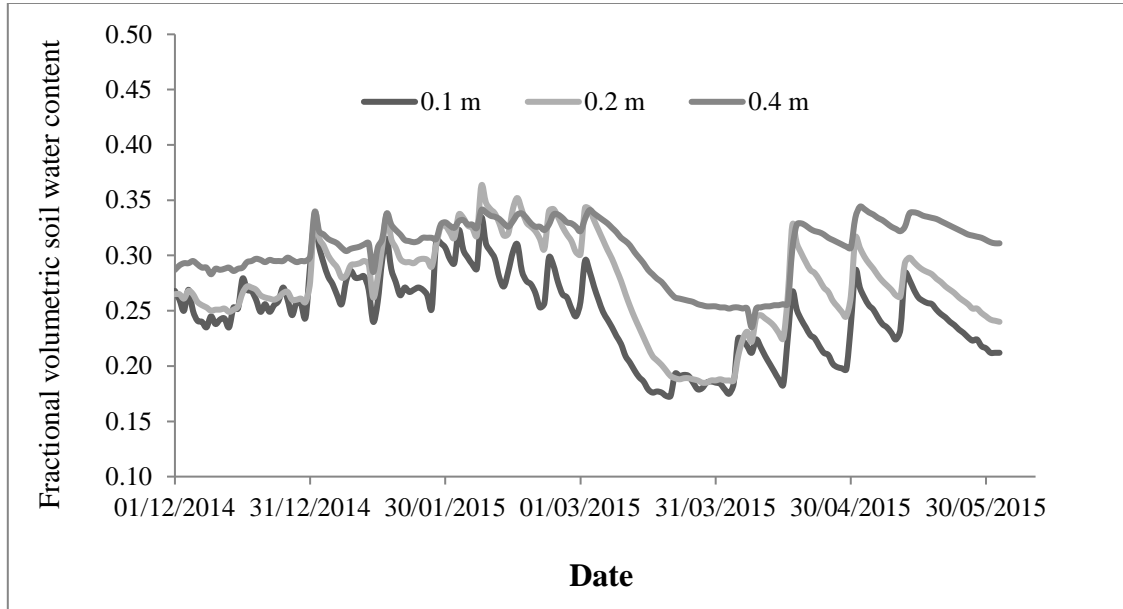
Figure 17: Fractional volumetric SWC measurements using three CS616 probes in the maize field at 0.1 m, 0.2 m and 0.4 m depths below the soil surface

Calibrated hourly CRP SWC values calculated using the corrected neutron counts from two calibration periods are presented in Figure 18. The CRP volumetric SWC values varied between 0.13 and 0.36 during the measurement period.

Figure 18: Calibrated hourly CRP SWC values calculated using the corrected neutron counts from two calibration periods at the Baynesfield site

5.2   Cathedral Peak Catchment VI Site

5.2.1   Total evaporation

Energy flux measurements at the Cathedral Peak Catchment VI started on 14 July 2014. The eddy covariance technique was used to estimate the total evaporation using the EC150 system as shown in Figure 10. Daily total evaporation at the catchment varied between 0.20 mm and 6.2 mm (Figure 19**Error! Reference source not found.**). Total evaporation was higher for December 2014, January 2015 and February 2015. Total evaporation was less than 1 mm for the winter months (June, July and August) of 2014 and 2015.

Figure 19: Total evaporation estimates (mm) above the natural grassland at the Cathedral Peak Catchment VI site

5.2.2   Soil water

Daily volumetric SWC measurements using five CS616 probes installed at 0.05 m, 0.1 m, 0.15 m, 0.2 m and 0.3 m depths are shown in Figure 20. Volumetric SWC values varied between 0.12 and 0.50 during the measurement period. Soil water at the 0.05 m depth fluctuated more than the other depths and was the lowest. Soil water was higher at the 0.1 m depth for most of the measurement days during the rainy season.

Figure 20: Fractional volumetric SWC measurements using five CS616 probes installed at 0.05 m, 0.1 m, 0.15 m, 0.2 m and 0.3 m depths at the Cathedral Peak Catchment VI site

Calibrated hourly CRP SWC values calculated using the corrected neutron counts from three calibration periods are presented in Figure 21. The CRP volumetric SWC values varied between 0.20 and 0.57 during the measurement period.
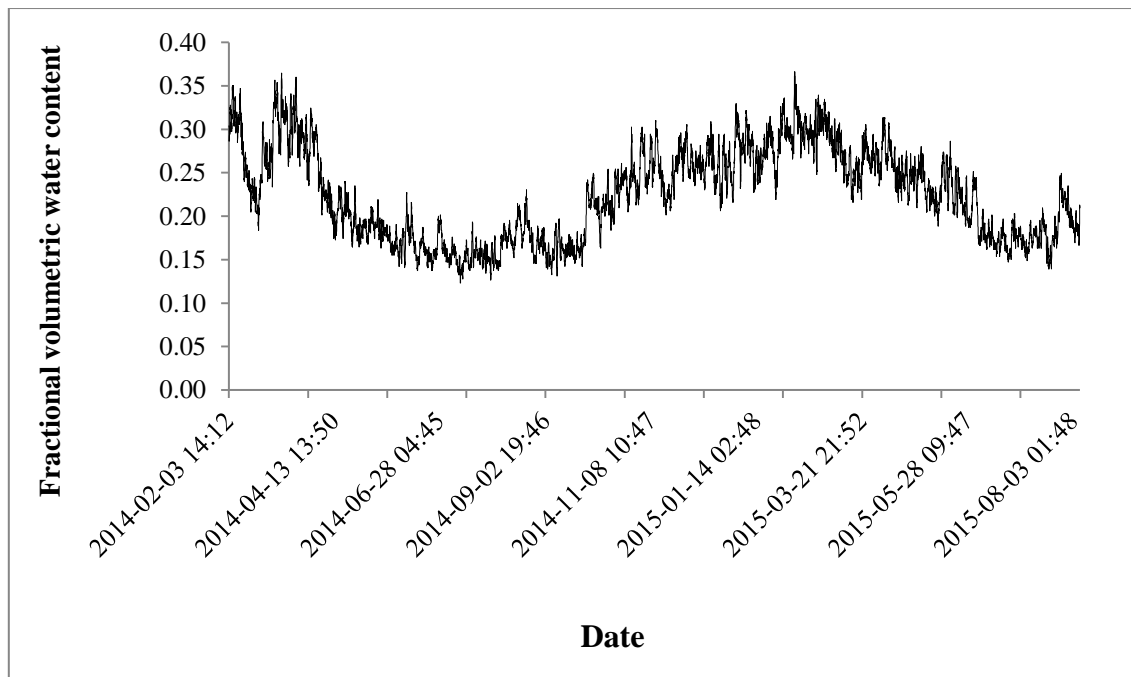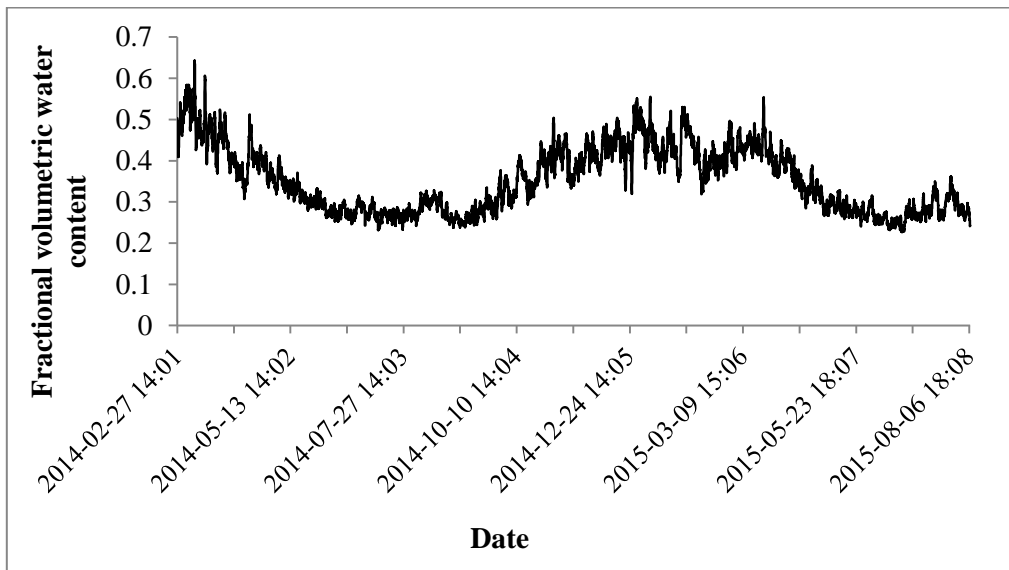

Figure 21: Calibrated hourly CRP SWCs calculated using the corrected neutron counts from three calibration periods at the Cathedral Peak Catchment VI site

5.3 Two Streams Catchment

5.3.1 Total evaporation

Energy flux measurements at the Two Streams catchment from 01 October 2014 is presented in Figure 22. The surface renewal technique was used for estimating total evaporation using two fine wire thermocouples. Daily total evaporation at the catchment varied between 0.20 mm and 7.0 mm. Total evaporation was higher for December 2014, January 2015 and February 2015. Total evaporation was less than 1 mm for June, July and August 2015.
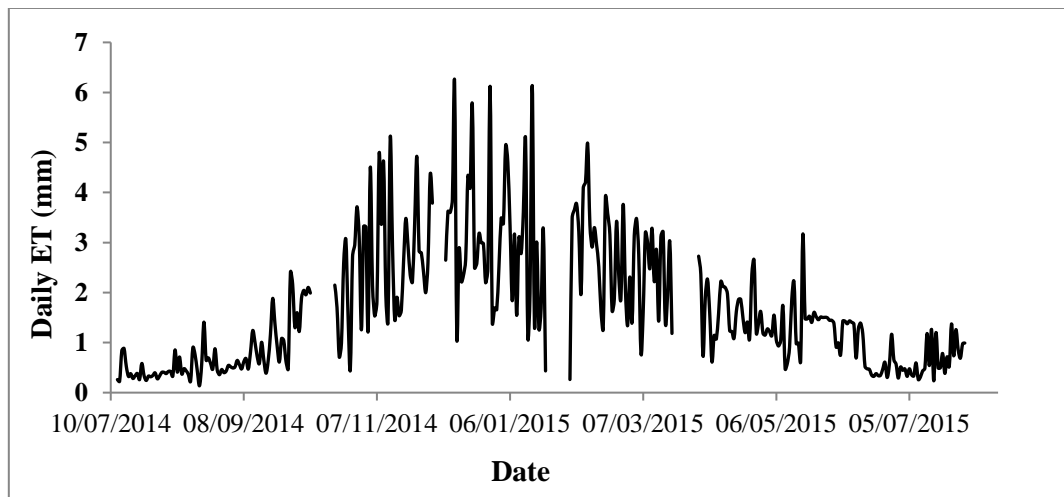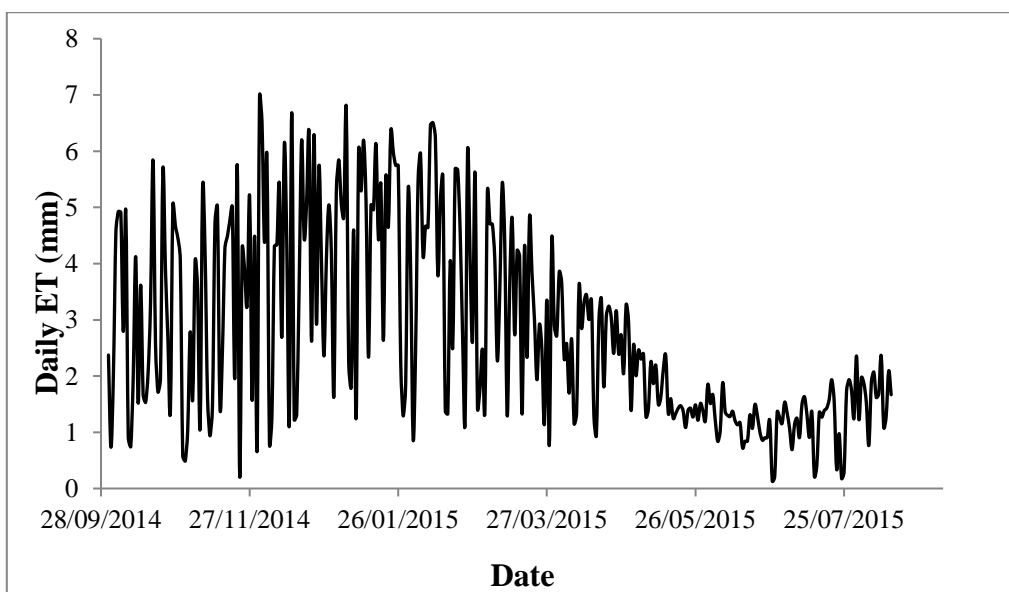

Figure 22: Daily total evaporation (mm) above the wattle stand at the Two Streams catchment estimated using the surface renewal method

5.3.2 Soil water

Daily volumetric SWC measurements using three CS616 probes installed at 0.08 m, 0.4 m and 0.8 m depths are shown in Figure 23. Volumetric SWC values varied between 0.10 and 0.30 during the measurement period. Soil water at the 0.08 m depth fluctuated more than the 0.4 m and 0.8 m measurements. Soil water was low at the 0.4 m depth for most measurement days during the rainy season as shown in Figure 23. The project team is busy testing and calibrating the CRP at the Two Streams catchment. Hourly CRP SWC values without the calibration corrections are presented in Figure 24. CRP volumetric SWC values varied between 0.15 and 0.25 during the measurement period.
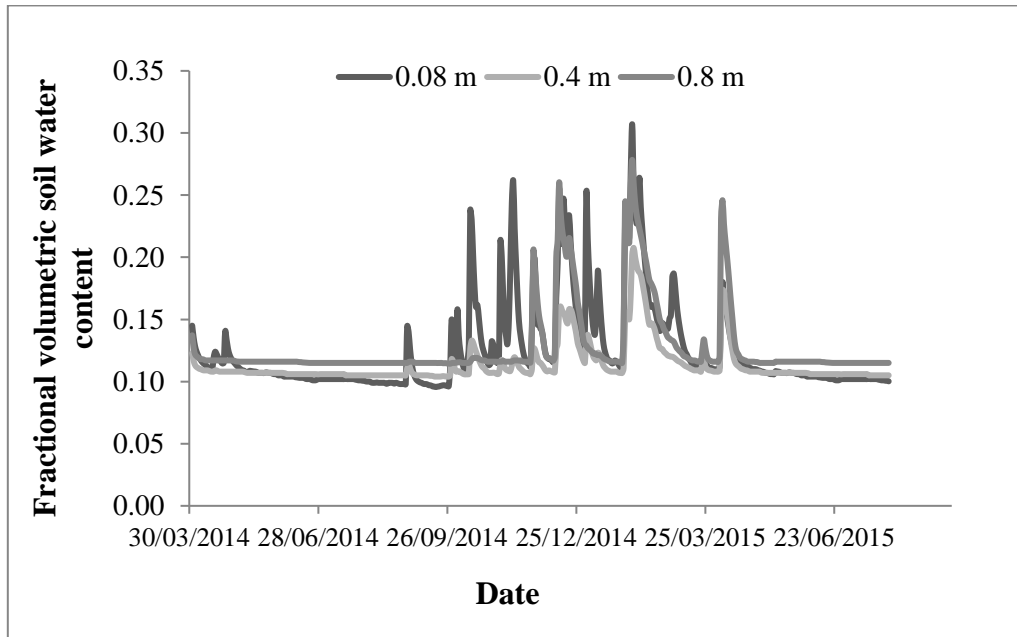
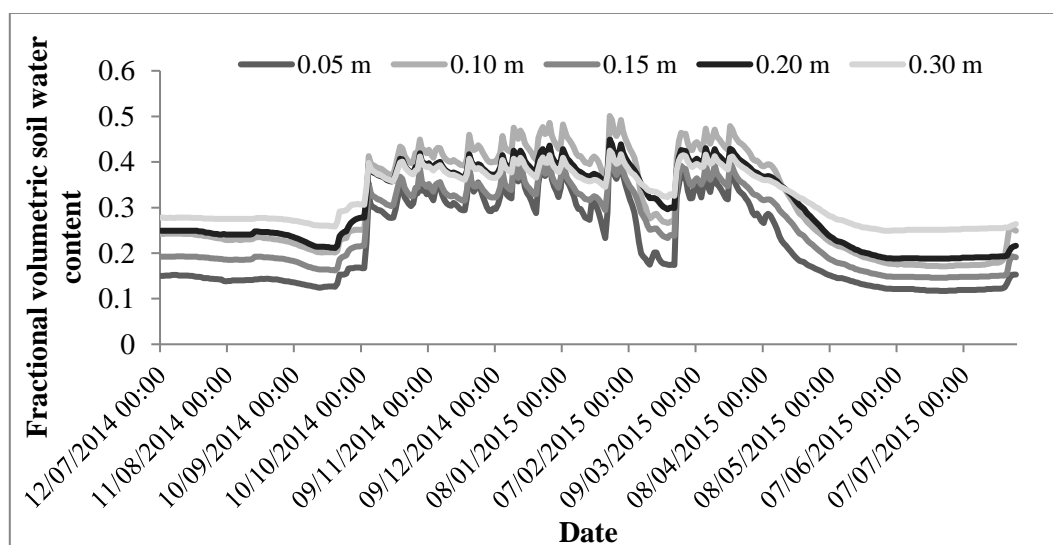**Figure 23: Fractional volumetric SWC measurements using three CS616 probes installed at 0.08 m, 0.4 m and 0.8 m depths at the Two Streams site**
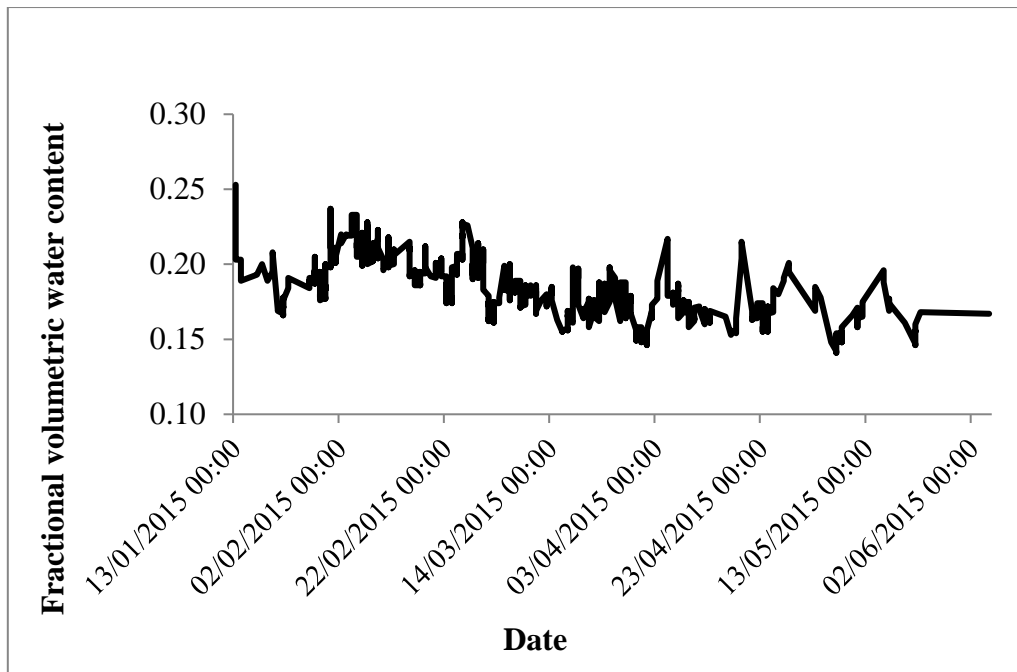
Figure 24: Hourly CRP SWC values without the calibration corrections at the Two Streams site

5.4   Satellite Images

Pre- and post-processing of the Landsat 8 images was done in ILWIS to create maps of the different surface fluxes using the SEBS model. The maps required in SEBS for total evaporation estimation are a land surface temperature map, an emissivity map, an albedo map, an NDVI map, and a vegetation cover map. Other maps required include a digital elevation map and a sun zenith angle map. A land use map with associated surface parameters is also required in SEBS. If land use and vegetation cover maps are not available, SEBS uses the NDVI map to estimate all surface parameters. Meteorological data from automatic weather stations at each specific site was used in SEBS to calculate fluxes.

Daily total evaporation maps for the Baynesfield area using Landsat 8 scenes (WRS path 168, WRS row 81) for 11 April 2015 and 13 May 2015 are shown in Figure 25 and Figure 26 respectively. The SEBS daily total evaporation estimates were higher for 11 April 2015 than for 13 May 2015.
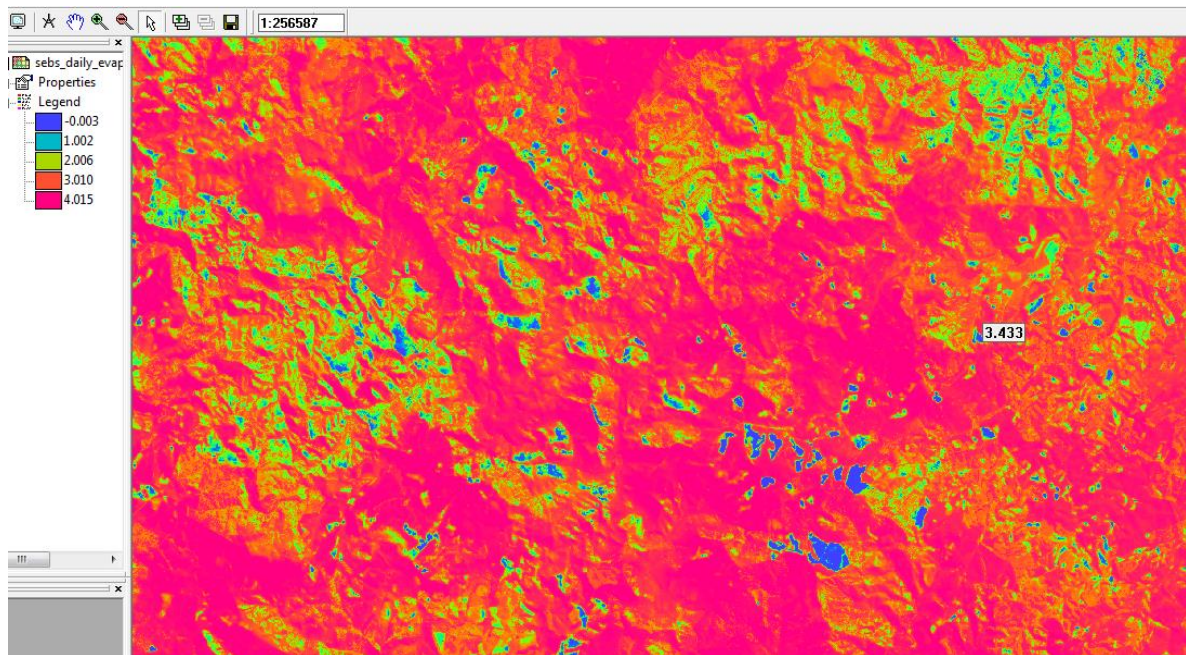
Figure 25: Daily total evaporation map for the Baynesfield site using Landsat 8 scene for 11 April 2015 (scale 1:256587); total evaporation at the site was 3.433 mm
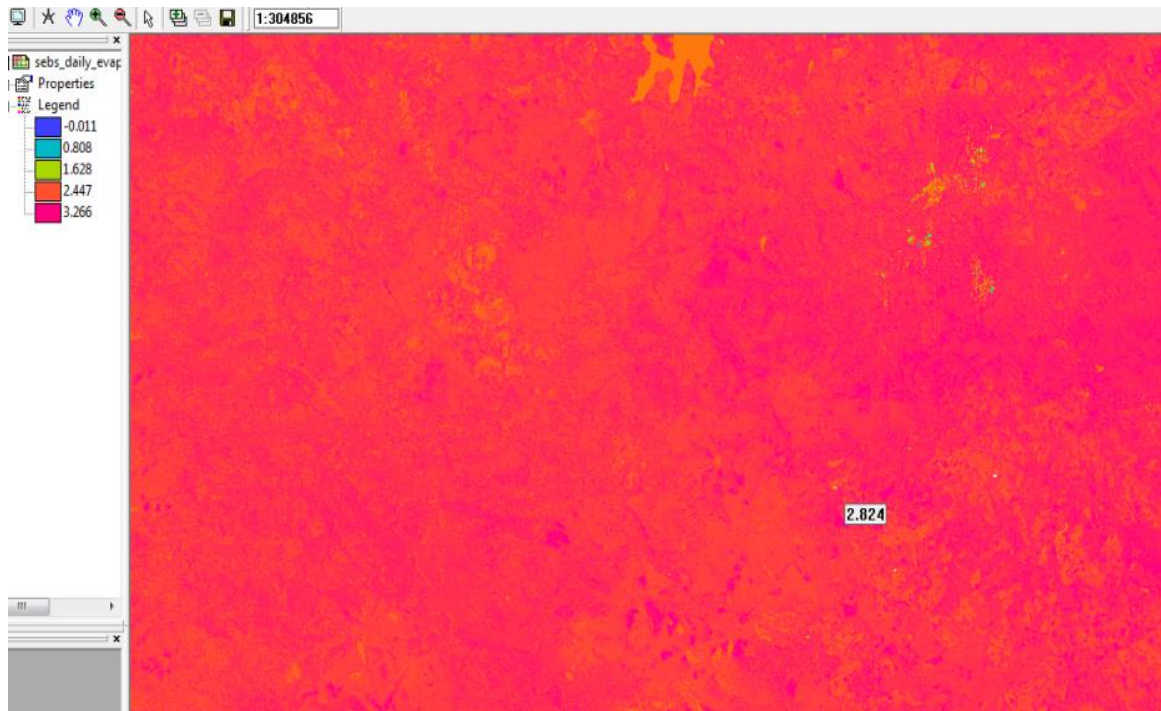
Figure 26: Daily total evaporation map for the Baynesfield site using Landsat 8 scene for 13 May 2015 (scale 1:304856); total evaporation at the site was 2.824 mm

The average relative soil water estimates using SEBS for the same days are presented in Figure 27 and Figure 28 for 11 April 2015 and 13 May 2015 respectively. The relative soil water was calculated using an empirical relationship (Equation 39) between evaporative fraction (Λ) and volumetric SWC (θ) following the Scott et al. (2003) method. The value of relative SWC (θ/θ_{sat}) varied between 0.09 (dry) and 1 (full saturation).
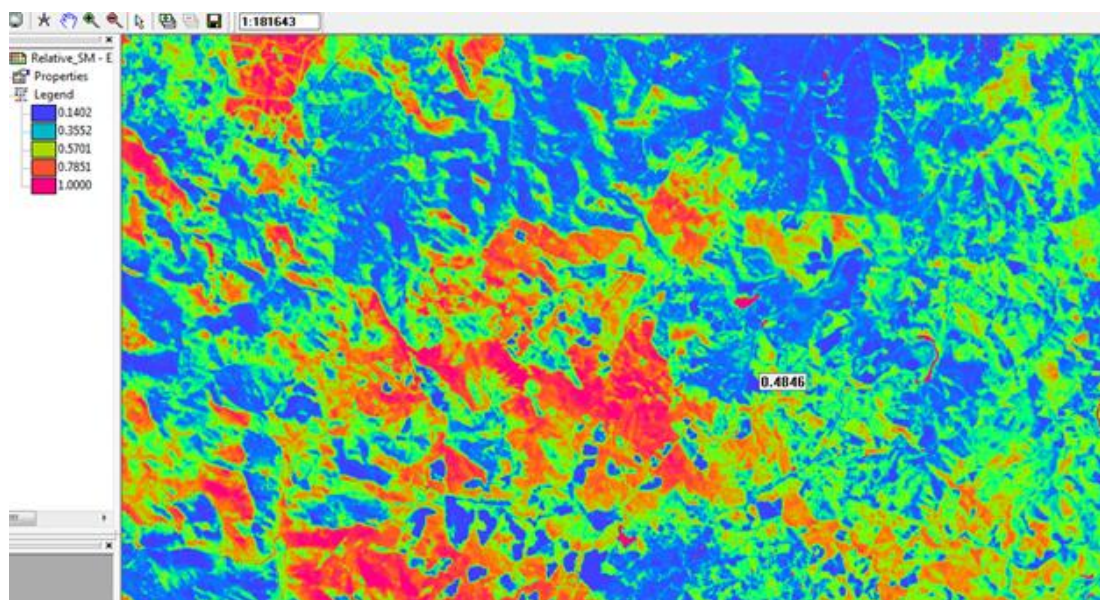
Figure 27: Relative soil water map (11 April 2015) for the Baynesfield site estimated using the Scott et al. (2003) equation (scale 1:181643); relative soil water = 0.4846

33
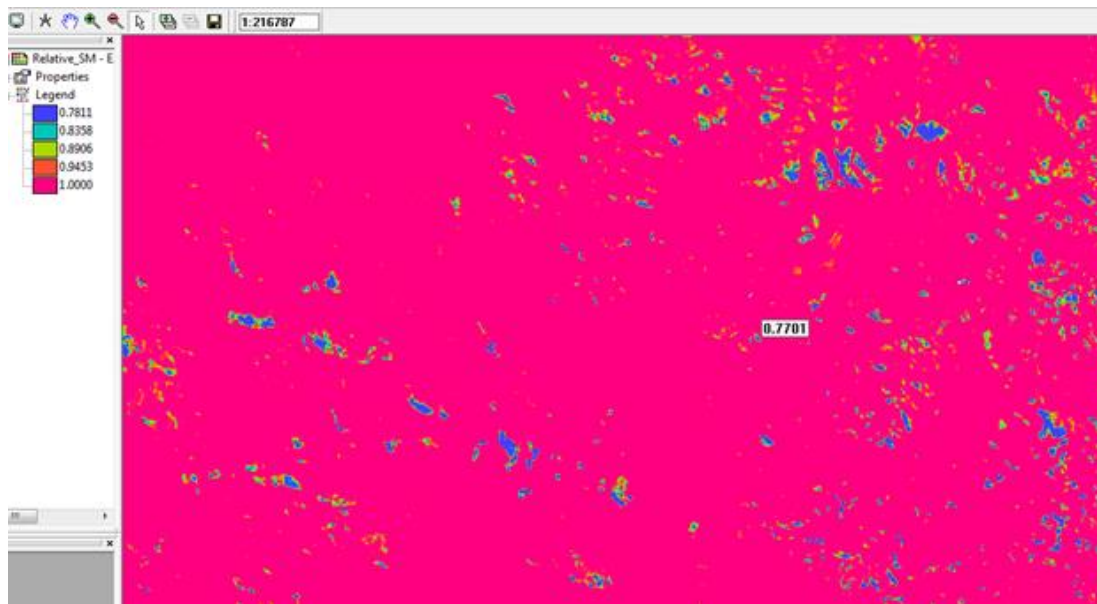
Figure 28: Relative soil water map (13 May 2015) for the Baynesfield site estimated using the Scott et al. (2003) equation (scale 1:216787); relative soil water = 0.7701

Daily total evaporation maps for the Cathedral Peak Catchment using Landsat 8 scenes for 30 March 2014 and 18 June 2014 are presented in Figure 29 and Figure 30. The SEBS daily total evaporation estimates were higher for the 30 March 2014 than the 18 June 2014 image.
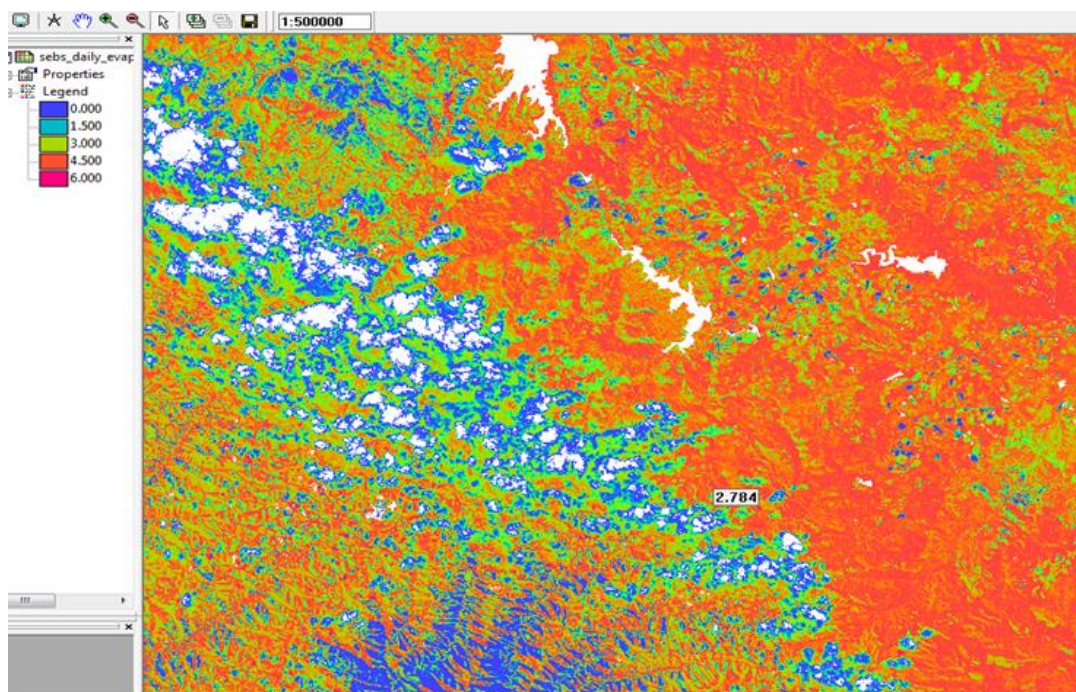
Figure 29: Daily total evaporation map for the Cathedral Peak Catchment VI site using Landsat 8 scene for 30 March 2014 (scale 1:500000); total evaporation = 2.784

34
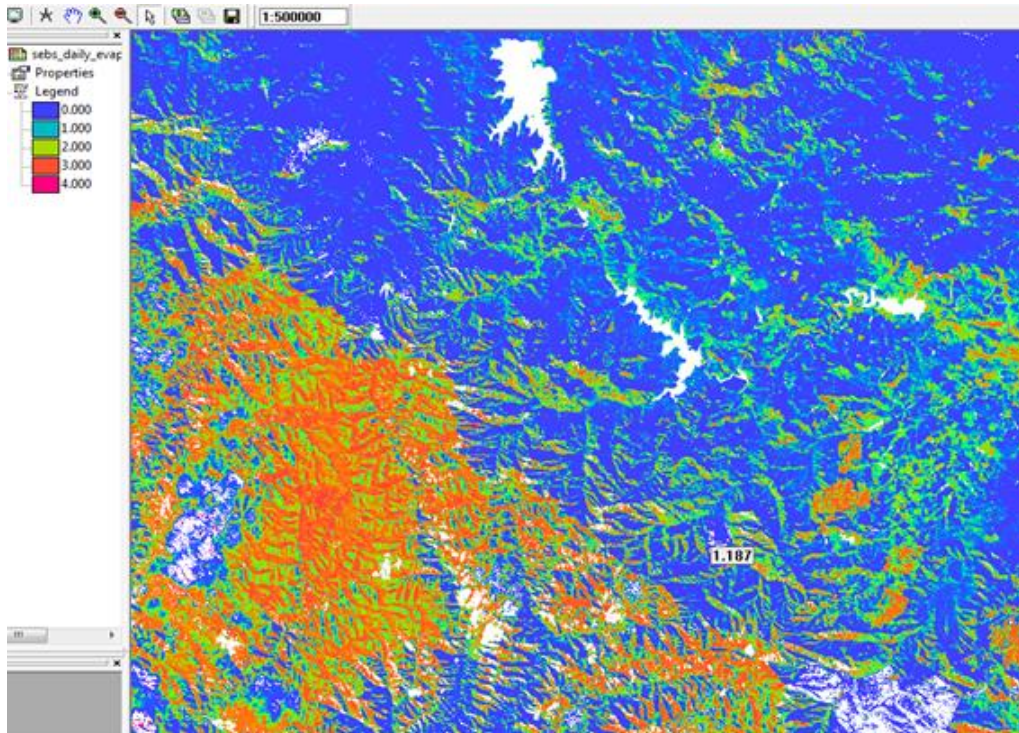
Figure 30: Daily total evaporation map for the Cathedral Peak Catchment VI site using Landsat 8 scene for 18 June 2014 (scale 1:500000); total evaporation = 1.187

The average relative soil water estimates using SEBS for the same days are presented in Figure 31 and Figure 32 for 30 March 2014 and 18 June 2014. The relative soil water was higher for 3 March 2014 (wet season) than 18 June 2014 (dry season).
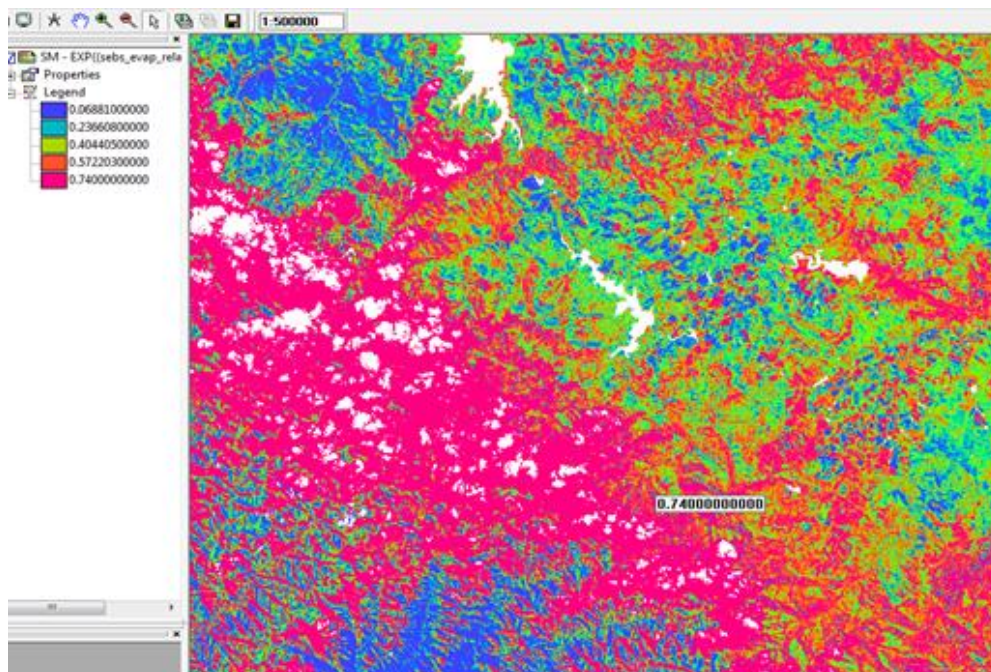
Figure 31: Relative soil water map (30 March 2014) for the Cathedral Peak Catchment VI site estimated using the Scott et al. (2003) equation (scale 1:500000); relative soil water = 0.740
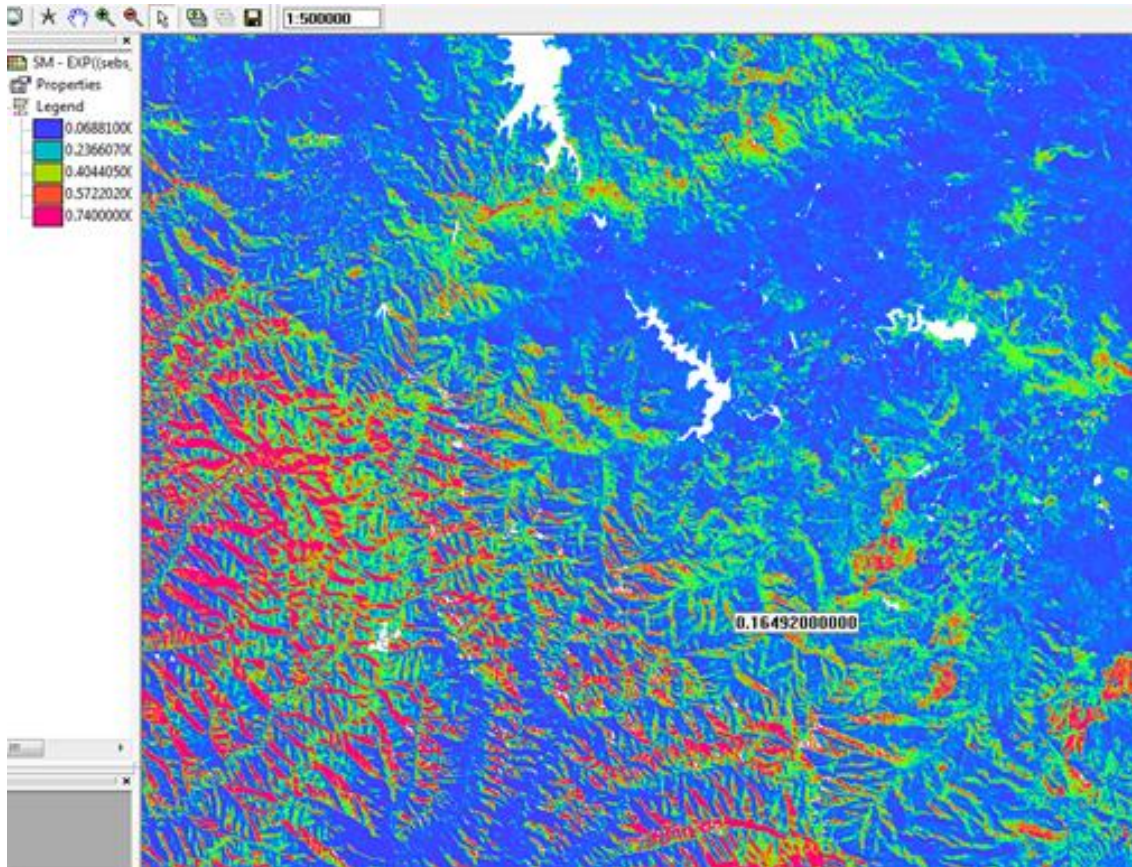
Figure 32: Relative soil water map (18 June 2014) for the Cathedral Peak Catchment VI site estimated using the Scott et al. (2003) equation (scale 1:500000). Relative soil water = 0.165

5.5 Validation of Soil Water at the Cathedral Peak Catchment VI Site

This section contains results on the validation of the CRP with a representative in situ soil water dataset, the validation of modelled soil water products (SAHG and SEBS) with CRP soil water estimates, and the validation of remote sensing soil water products (AMSR-2 and SMOS) with CRP soil water estimates. The validation will focus on comparing the spatial pattern, temporal development and regularity among the different data sources.

5.5.1 Validating the CRP soil water estimates

The CRP estimates are validated against in situ soil water dataset to test the suitability of the CRP to provide spatial estimates of soil water. A time series analysis was plotted to see how the CRP dataset compared with the in situ TDR soil water estimates as shown in Figure 33. The time period for which representative datasets were available (12 July to 28 February 2015) was used in the time series analysis. This period is adequate for the first validation experiment as it covers both the wet and dry periods.
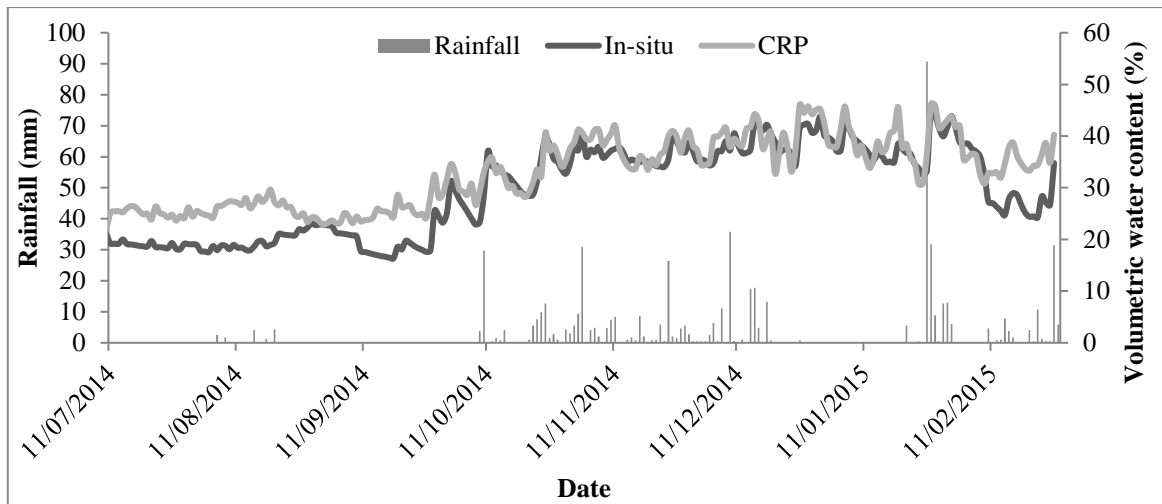
Figure 33: Daily in situ and CRP soil water estimates at the Cathedral Peak Catchment VI site along with rainfall

The CRP followed the same seasonal trend as the in situ soil water estimates. The CRP correlated better with the in situ soil water dataset in the wetter periods when the soil water values were higher (above 30%) than the drier periods. When the volumetric water content (soil water) was low, the CRP estimated higher soil water than the in situ dataset. The soil water fluctuations were dependent on the rainfall input and total evaporation rates, as in winter, there were smaller fluctuations due to little rainfall and lower total evaporation rates. In summer, the fluctuations in soil water were greater due to the higher rainfall received in the catchment and the higher total evaporation rates experienced during these months. The CRP estimates were generally slightly higher than the in situ dataset when the SWC was low. Overall, the CRP data correlated well with the in situ soil water dataset.

5.5.2 Validating the SEBS soil water estimates

In total, 15 relative evaporation maps were generated in ILWIS 3.8.3 using the SEBS model. These maps were exported, opened and analysed in ArcGIS 9.3, where the relative evaporation of the area within catchment six was determined. The relative evaporation results presented in Table 1 follow a seasonal trend. The values were high in summer (wet period) and very low in winter (dry period), with the intermediate values between the wet and dry periods (Figure 34). As shown in Figure 34, 30 March 2014 represents a day when the relative evaporation was very high (0.94717), whereas the relative evaporation was intermediate on 01 May (0.29912), and the relative evaporation was very low (0.0067) on 05 August. The total evaporation consists of water that evaporated from the land surface and water that transpired from vegetation. To estimate the actual soil water from the relative soil water, the saturated SWC is required. The saturated SWC can be inferred from the porosity, which in turn is estimated using the bulk density.

Table 1: Relative evaporation calculated using SEBS for the Cathedral Peak Catchment VI site

Date	Relative Evaporation
14-Mar-14	0.73396
30-Mar-14	0.94717
15-Apr-14	0.87145
1-May-14	0.29912
17-May-14	Cloud
2-Jun-14	0.00000
18-Jun-14	0.00143
4-Jul-14	0.02200
20-Jul-14	0.00902

Date	Relative Evaporation
5-Aug-14	0.00067
21-Aug-14	Cloud
6-Sep-14	0.00000
22-Sep-14	0.00000
8-Oct-14	0.00000
24-Oct-14	0.11804
9-Nov-14	0.93836
25-Nov-14	Cloud
11-Dec-14	0.85773
27-Dec-14	Sensor Error
12-Jan-15	Sensor Error
28-Jan-15	Sensor Error
13-Feb-15	Sensor Error
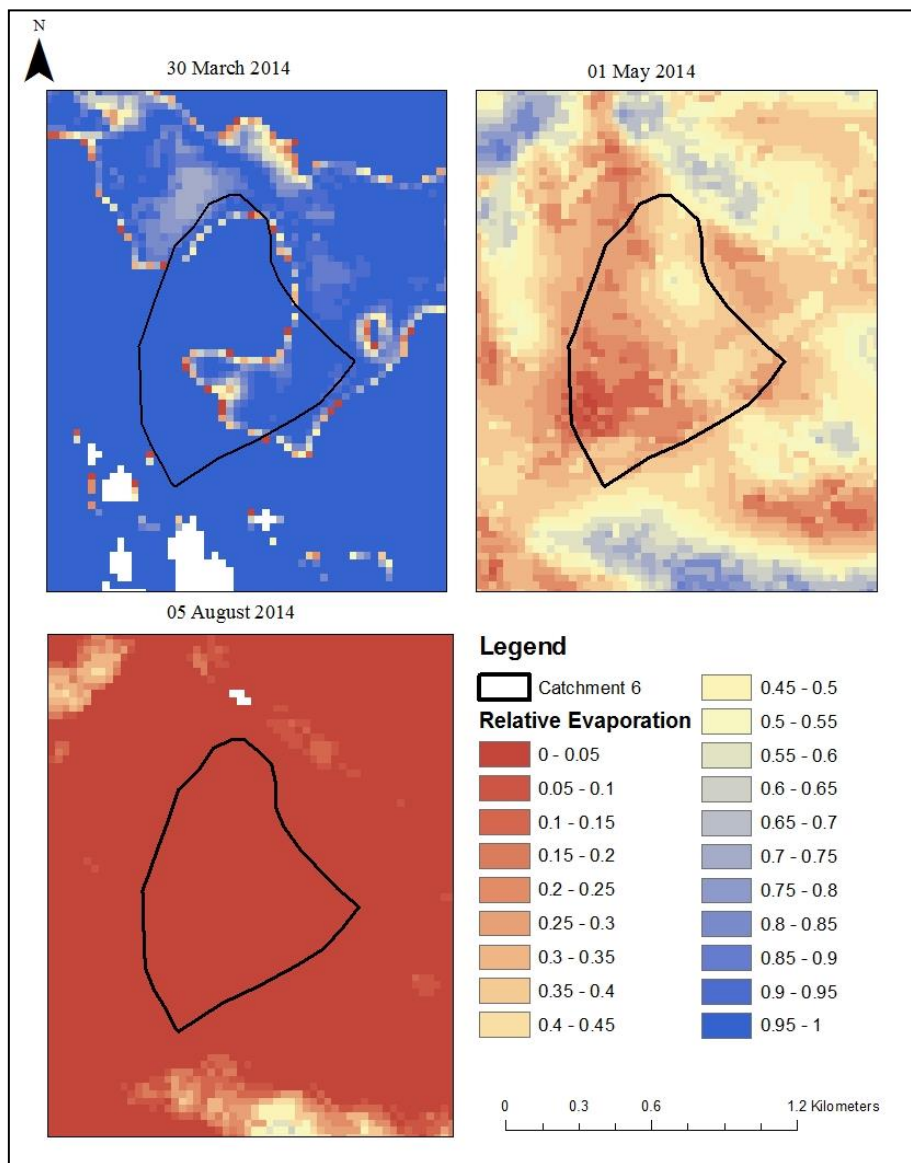
Figure 34: A range of different relative evaporation images for the Cathedral Peak Catchment VI site using the SEBS model

The back-calculation of soil water from relative evaporation estimates the soil water in the root zone, as this is where evaporated water (soil evaporation and transpiration) is sourced from. The rooting zone of the grassland vegetation is 0.5 m. Therefore, the average bulk density of the soil from 0 m to 0.5 m is required to obtain the porosity of the rooting zone.

The bulk density was obtained from prior data Everson et al. *(*1998) and measured values (Table 2).

Table 2: Bulk density values

Soil depth (m)	Mean bulk density (g/cm³)
0.05	0.525
0.10	0.597
0.15	0.656
0.20	0.800
0.50	0.861
Average	0.688

The bulk density was estimated to be 0.688 g/cm³; therefore, the porosity was calculated to be 0.74 using Equation 40.

$$Porosity = 1 - \frac{Pb}{Ps} \tag{40}$$

where *Pb* is the bulk density and *Ps* is the particle density. The bulk density was determined to be 0.688 g/cm³ and a generic value of 2.65 g/cm³ was used for the particle density (Hillel, 2008). This porosity would be used as the saturated SWC in the rooting zone.

The Su et al. (2003b) (Equation 38) and Scott et al. (2003) methods (Equation 39) were used for estimating soil water using the SEBS model relative evaporation values. The relative evaporation values were substituted into the equations and the soil water at field capacity was 0.74. The estimated soil water was plotted against the corresponding CRP measurements, which were changed to match the 16-day time step. The results of the back-calculated soil water from the two equations, using the relative evaporation derived from the SEBS model, are presented in Figure 35.
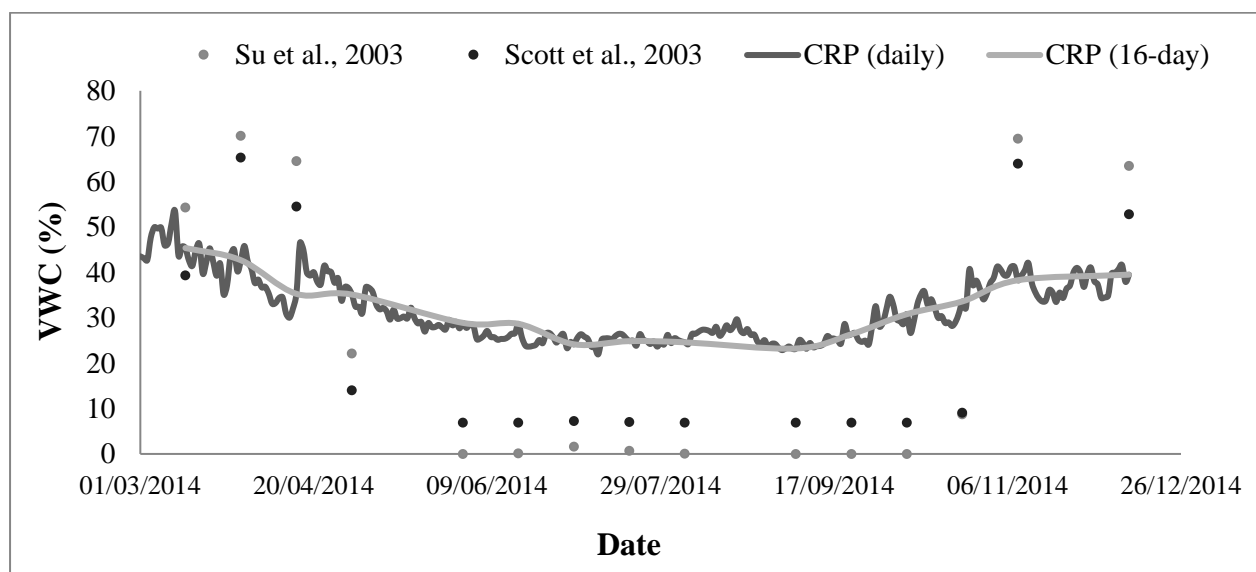
Figure 35: Time series of CRP and soil water back-calculated from the SEBS model for the Cathedral Peak Catchment VI site

The methods proposed by Su et al. (2003b) and Scott et al. (2003) followed the same trend, but overestimated soil water in the wet periods and underestimated soil water in the dry period. Both methods followed a seasonal trend. Scott et al. (2003) performed relatively better than the method proposed by Su et al. (2003b).

5.5.3   Validating the PyTOPKAPI (SAHG) soil water estimates

The SAHG soil water product is on a 12 × 12 km grid, which results in a pixel area of 144 km^2. To obtain a year-long dataset, 2920 images were downloaded and used to create 365 daily images. The SAHG dataset is continuous and has no gaps. The SAHG soil water was obtained in SSI and converted to soil water by using a representative porosity value. A graph of the SAHG and CRP soil water estimates are presented in Figure 36.

The SAHG soil water estimates followed the same seasonal trend as the CRP estimates. As shown in Figure 36, there is close correlation between the two datasets in terms of general increases and decreases in SWC. The CRP had more day-to-day variation in soil water. The SAHG product had gradual changes in soil water and did not exhibit the same degree of temporal fluctuations observed in the CRP estimates. In general, the SAHG soil water product provided good estimates of soil water, which correlated well with the CRP measurements. The SAHG soil water product measures the SSI (%) in the A and B soil horizons. The SSI was obtained as an average of a depth of one metre.
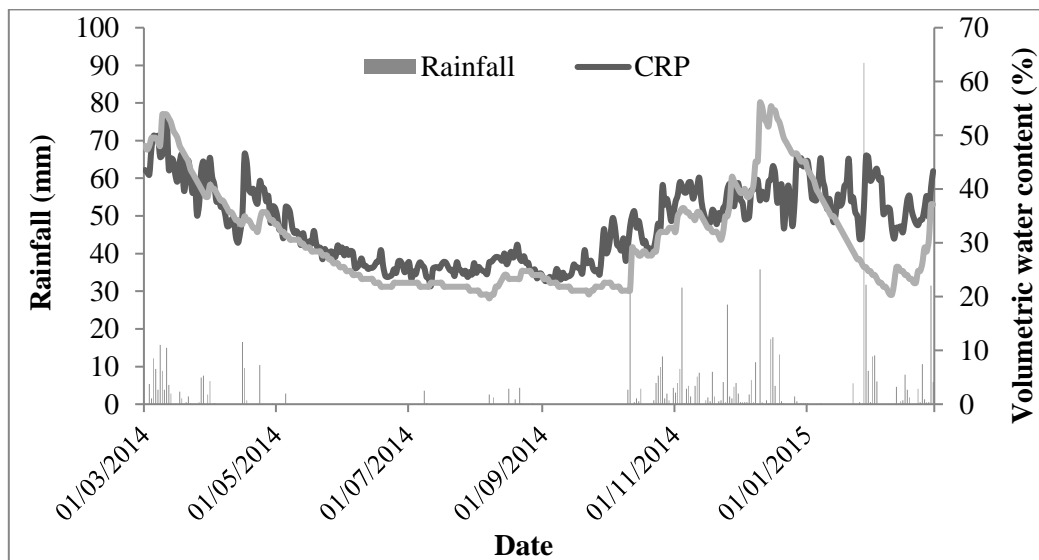
Figure 36: Time series analysis of SAHG and CRP soil water estimates for the Cathedral Peak Catchment VI site

5.5.4   Validating AMSR-2 and SMOS soil water products

The AMSR-2 Level 3 soil water product is on a 10 km grid. Although this grid is relatively small compared to other remote sensing soil water products, it is still very large compared to the catchment area. The catchment area is 0.68 km^2, whereas the pixel area is 100 km^2. Therefore, the pixel is 147 times larger than the study area. However, this is an improvement from validating remote sensing soil water products with in situ point measurements. A time series analysis graph was plotted to see the characteristics of the AMSR-2, CRP and rainfall data over time as shown in Figure 37.

The AMSR-2 soil water product underestimated soil water throughout the study period (Figure 37). The AMSR-2 soil water product followed the seasonal trend of the CRP estimates. The AMSR-2 dataset fluctuated more in the wet periods with less fluctuation in the dry periods. Although, the AMSR-2 dataset underestimated the soil water at the site, it followed a similar trend in daily soil water fluctuations.
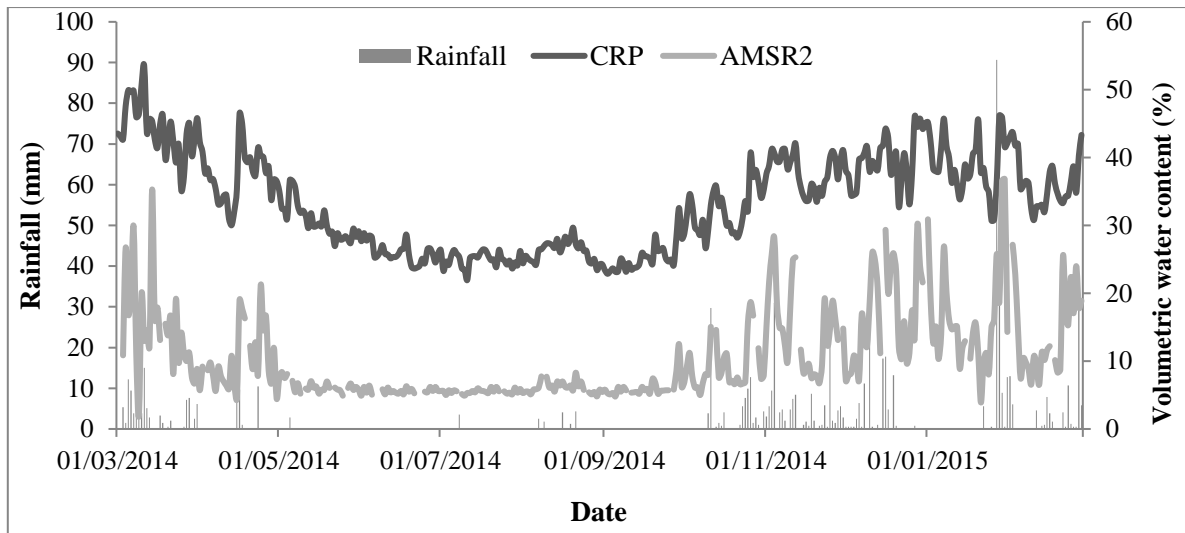
Figure 37: Time series analysis of CRP and AMSR-2 soil water estimates for the Cathedral Peak Catchment VI site

The SMOS Level 3 soil water product is on a 25 km grid. Although this grid is smaller than the Level 2 product (40 km), it is still very large compared to the catchment area. The catchment area is 0.68 km^2, while the pixel area is 625 km^2. Therefore, the pixel is 920 times larger than the study area. The SMOS soil water product is a daily product; however, the satellite coverage does not scan the entire Earth's surface in one day. The dataset had numerous gaps for the study area.

A graph of the daily CRP and SMOS datasets were plotted against time (Figure 38). The SMOS soil water estimates followed the same general trend as the CRP estimates. The SMOS dataset generally underestimated soil water for most of the study period. However, the SMOS product partly over-estimated soil water during the wet period. The SMOS soil water estimates fluctuated most during the wet season. This fluctuation is less in the dry periods. This is due to greater fluxes in soil water in summer than winter.
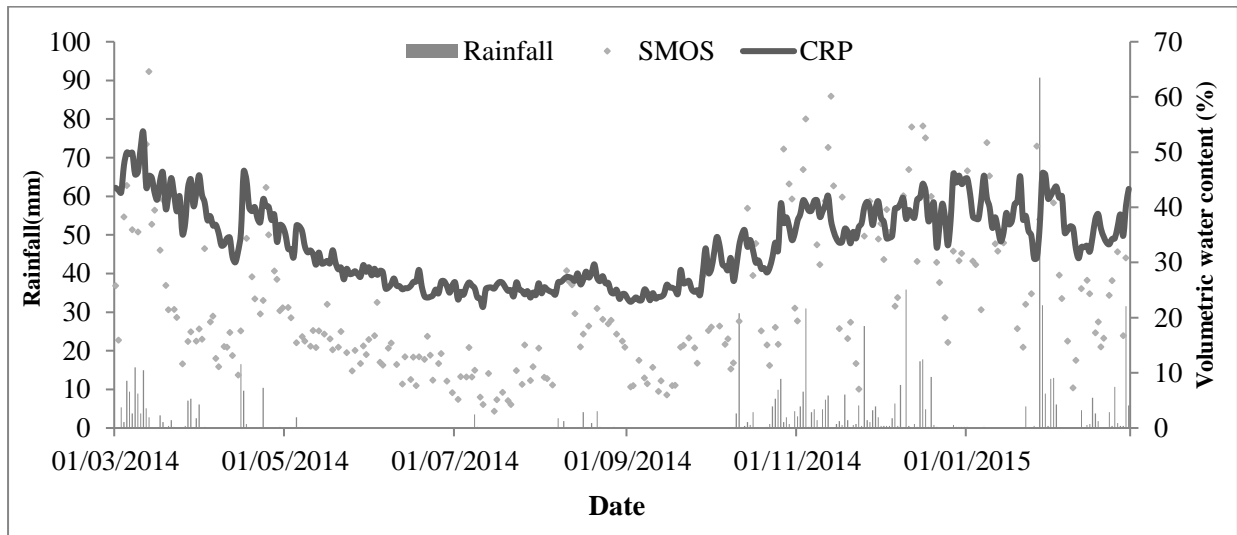
Figure 38: Time series analysis of CRP and SMOS soil water estimates for the Cathedral Peak Catchment VI site

41

6. SECOND VALIDATION EXPERIMENT

The project team re-established the Baynesfield site and continued with CRP measurements at Two Streams for the second validation. The CRP, EC150 and LAS at Cathedral Peak were vandalised by thieves, therefore, the equipment was not available for this experiment. The damage to the equipment was approximately R1.0 million.

6.1 Baynesfield Site

In December, the project team installed an EC150 system on a 6 m mast to measure total evaporation in a newly planted maize field (Figure 39).

Figure 39: The newly installed EC150 in a recently planted maize field at Baynesfield

During this exercise, the opportunity was taken to train Kent Lawrence and Siphiwe Mfeka from the South African Environmental Observation Network (SAEON) in the EC150 technique (Figure 40).

Figure 40: Kent Lawrence receiving instruction from Michael Mengistu on the EC150

The CRP and CS616 soil water probes were repaired due to damage from cattle chewing the detector and power cables (Figure 41). The hourly time series of soil water using the CRP at Baynesfield from February 2014 to 6 January 2016 illustrates the extent of this season's summer drought when compared to the 2014/15 period (Figure 42). For example, between October and November 2014, values were mostly >15% but in 2016, values were generally <15%.

Figure 41: The CRP and CS616 soil water probes at Baynesfield
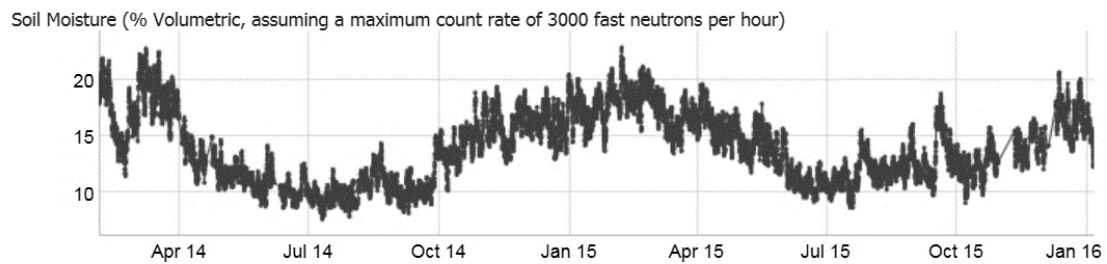
Figure 42: The hourly time series data of soil water for the CRP from February 2014 to January 2016 as shown on the COSMOS website

6.2 Calibrating the CRP (Second Validation)

The calibrated CRP hourly soil water estimates are shown in Figure 43. The dataset for this period (second validation) covers nearly two months as the eddy covariance was set up on 10 December 2015 due to late planting because of the drought. The CRP failed to function after 16 January 2016.
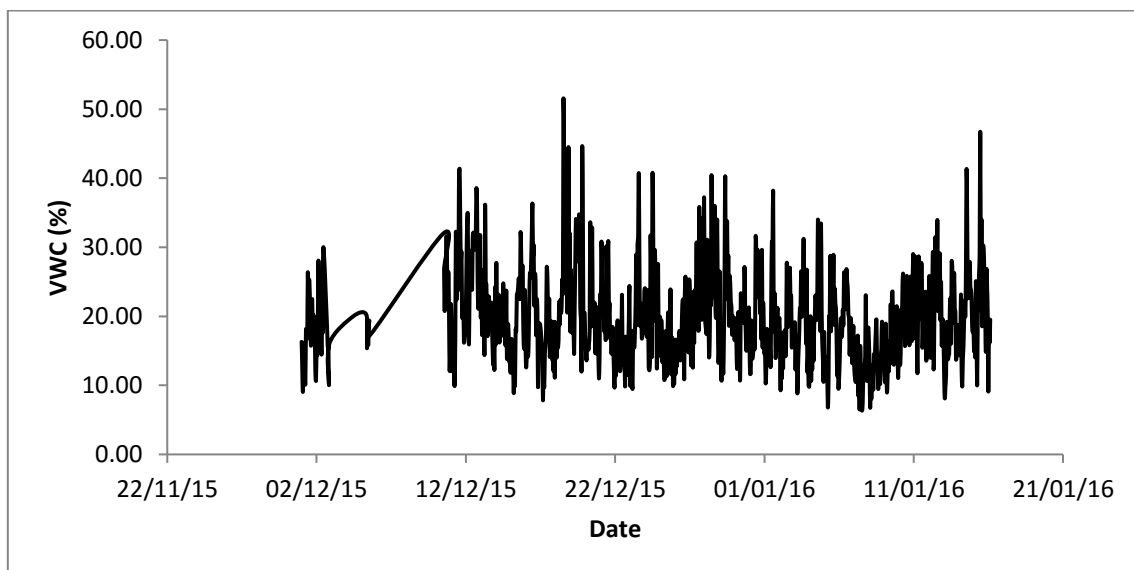
Figure 43: Hourly CRP soil water estimates

The calibration curve (Figure 44) was generated for this period by plotting the neutron counts against the subsequent soil water values. Thus, soil water estimates could be estimated using the exponential curve equation for a neutron (count/hour) value at this site.
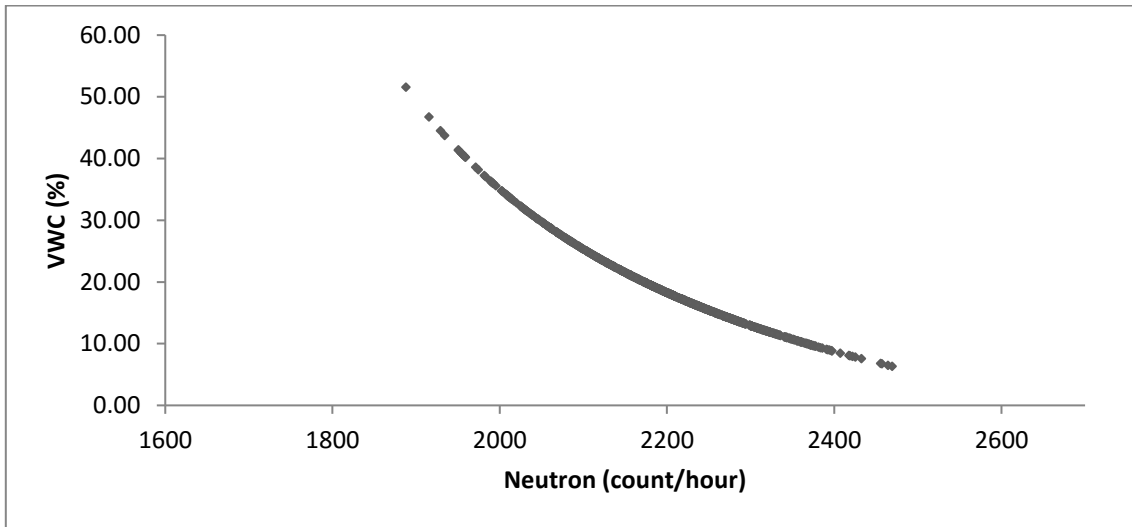
Figure 44: Calibration curve

It is worth noting that the calibration was based on a two-point calibration, with both calibrations days occurring in the same season. Ideally, the calibration days should be in contrasting seasons when a two-point calibration is used to account for the changes in the wet (summer) and the dry (winter) periods. Additionally, the various calibration factors were conducted, except for the biomass calibration factor, as the biomass data was not available.

The daily soil water estimates obtained from the CRP were generated as seen in Figure 45. The change in time step from hourly to daily soil water smooths the data, as the neutron counts, which vary within an hour are averaged.
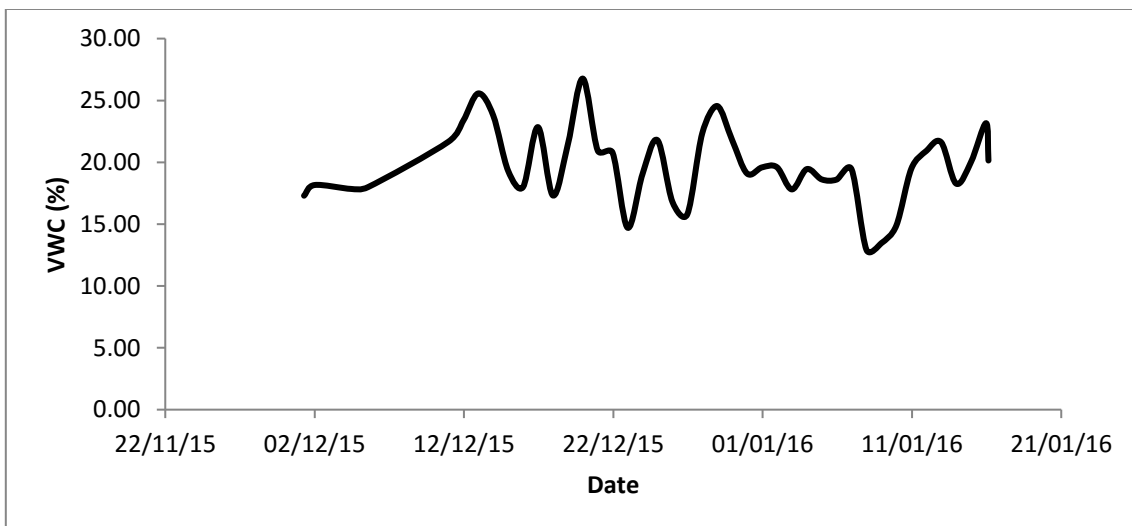
Figure 45: Daily CRP soil water estimates

6.3 Second Validation of The SAHG Soil Water Product

The SAHG soil water product output of the PyTOPKAPI model is described in Section 2.2.2. The CRP was used to validate the SAHG soil water product. The CRP dataset available was the period from the 1 December 2015 to 16 January 2016. The SAHG product used was the same product from the first deliverable, which was a three-hourly product that was averaged to obtain a daily soil water estimates.

The CRP was plotted on a time series against the SAHG product and rainfall data was also used as rainfall is the primary input to soil water. As seen in Figure 46, the CRP and the SAHG soil water estimates follow a similar trend. The CRP daily estimates varied more than the SAHG estimates, which did not fluctuate as much. Overall, the SAHG product estimated higher values of soil water throughout the measurement period.
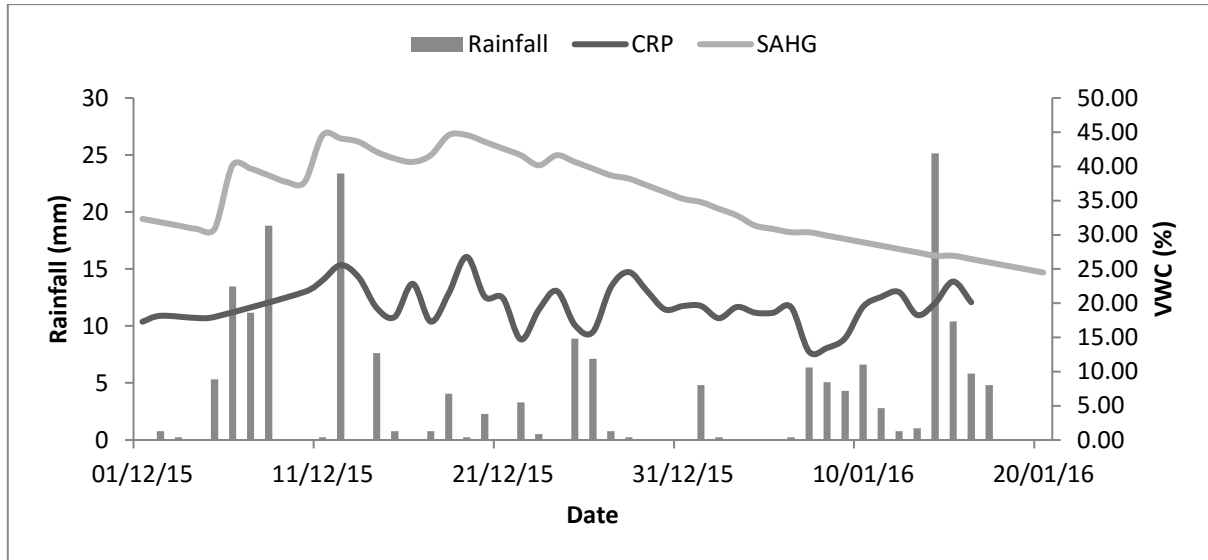
Figure 46: CRP estimates against SAHG estimates

A scatter graph of the CRP soil water estimates (x-axis) against the SAHG soil water estimates (y-axis) was plotted (Figure 47). The graph had an R^2 of 0.1371 and an intercept of 21.3, which indicated that the SAHG product overestimated soil water throughout the period, compared to the CRP estimates.
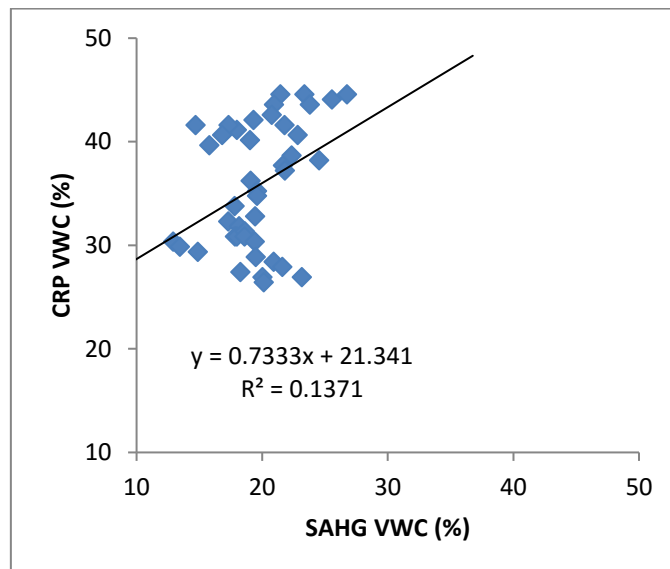
Figure 47: Scatter graph of CRP against SAHG

The difference in soil water estimates can be due to the following: The spatial scales are two orders of magnitude different, as the CRP has a measurement area of roughly 0.34 km², while the SAHG product is on a 12.5 × 12.5 km spatial grid, which results in a measurement area of 156 km². Therefore, the area of the SAHG product not covered by the CRP footprint is neglected, but still present in the SAHG soil water value. The measurement depth is also a factor in the difference, as the CRP measures between an effective depth of 0.1 m and 0.7 m depending on the soil water status, while the SAHG product is given as an SSI, which provides an average over the top two soil horizons.

To extend the validation period, a previous one-year period from March 2014 to March 2015 was selected. The calibrated CRP soil water estimates were plotted against the SAHG soil water product. Both soil water estimates followed a similar trend as both estimated higher soil water values in the wet periods and lower soil water values in the dry periods (Figure 48).
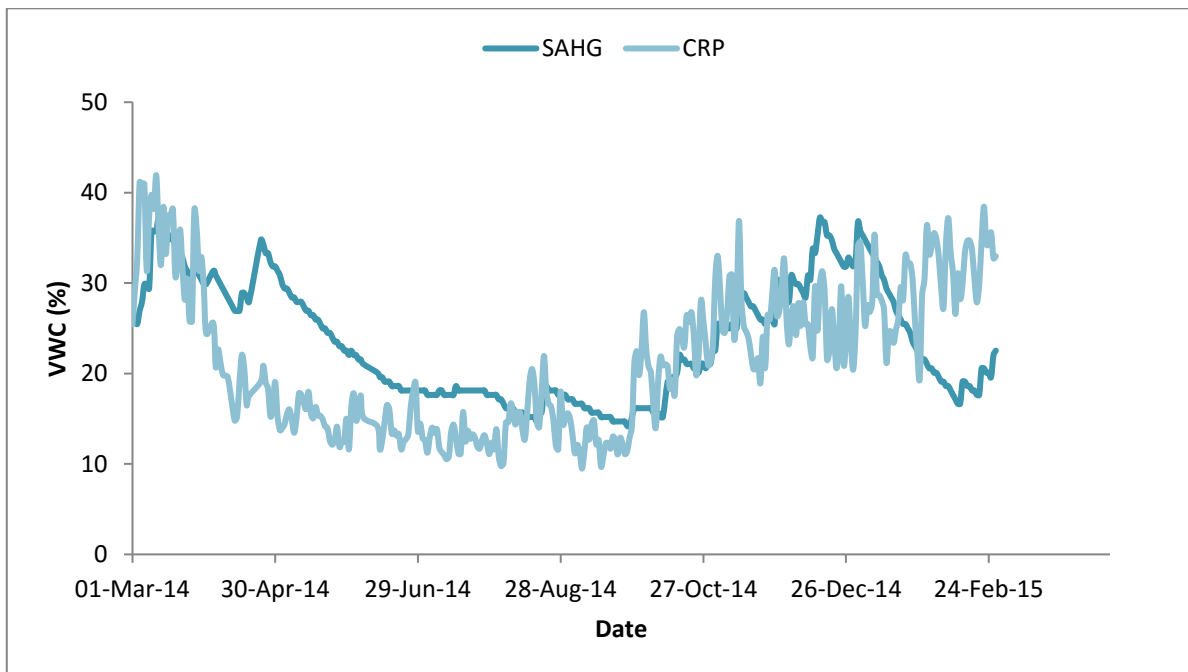
Figure 48: CRP estimates against SAHG estimates

The SAHG soil water product varied less daily than the CRP, which had higher and more frequent fluctuations. The first nine months (March 2014 to November 2014) of the time series analysis showed a close correlation between the CRP and SAHG soil water estimates. The last three months (December 2014 to February 2015) showed a poorer relationship, as the fluctuations of the CRP soil water estimates did not correspond to the fluctuations of the SAHG soil water estimates. This could be due to an error in the PyTOPKAPI model, such as an error in the input data. The differences in soil water estimates can be attributed to the same factors as mentioned before. The SAHG soil water product measures the SSI (%) in the A and B soil horizons. In this case, the SSI was obtained at an average depth of one metre. Therefore, there is a vertical scaling issue. There is also a horizontal scaling issue, as the SAHG product is on a 12.5 × 12.5 km spatial grid, which greatly exceeds the measurement footprint of the CRP. Considering this, it is clear that the SAHG product still provides a useful estimate of the relative soil water conditions, which confirms its suitability for both flood forecasting and drought prediction.

A scatter graph of CRP against SAHG was plotted for the one-year period (Figure 49). The graph has an R^2 value of 0.2644 and an intercept of 14.68. The graph showed that the SAHG product generally estimated higher soil water values than the CRP.
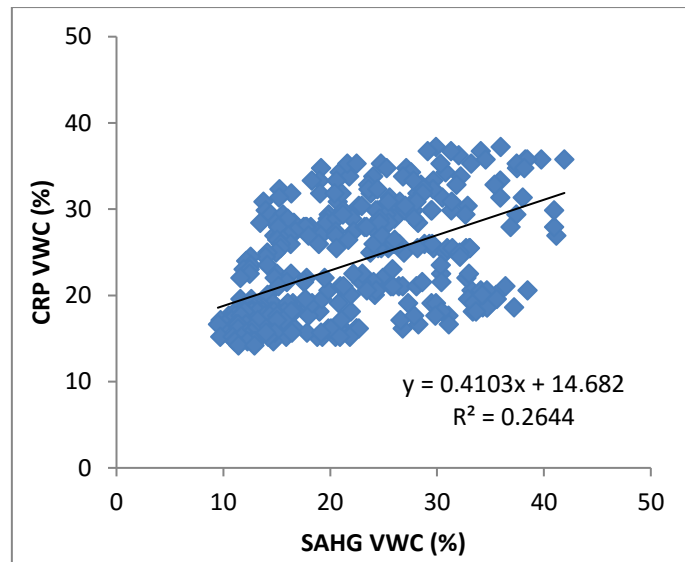
Figure 49: Scatter graph of CRP against SAHG

6.4 Total Evaporation

6.4.1 Energy flux: Summer

Energy fluxes of sensible heat (H), latent energy (LE) and nett radiation (R_n) were measured at the Baynesfield maize site in summer from 10 December 2015 to 24 January 2016. On clear summer days, the nett radiation peaked at 700 W·m⁻² at midday. The diurnal trends followed typical bell-shaped curves following the sun path from about 05:00 to 19:00. Days with rainfall were characterised by low and spiky nett radiation values (for example 7-11 January 2016). The effect of rain on the sensible heat and latent energy is noticeable during this period when the sensible heat dominated before the rain (10 January 2016). Following the rain, the latent energy dominated the fluxes of latent energy and sensible heat. On clear days, maximum fluxes of sensible heat and latent energy were between 200 W·m⁻² and 350 W·m⁻² (Figure 50**Error! Reference source not found.**).
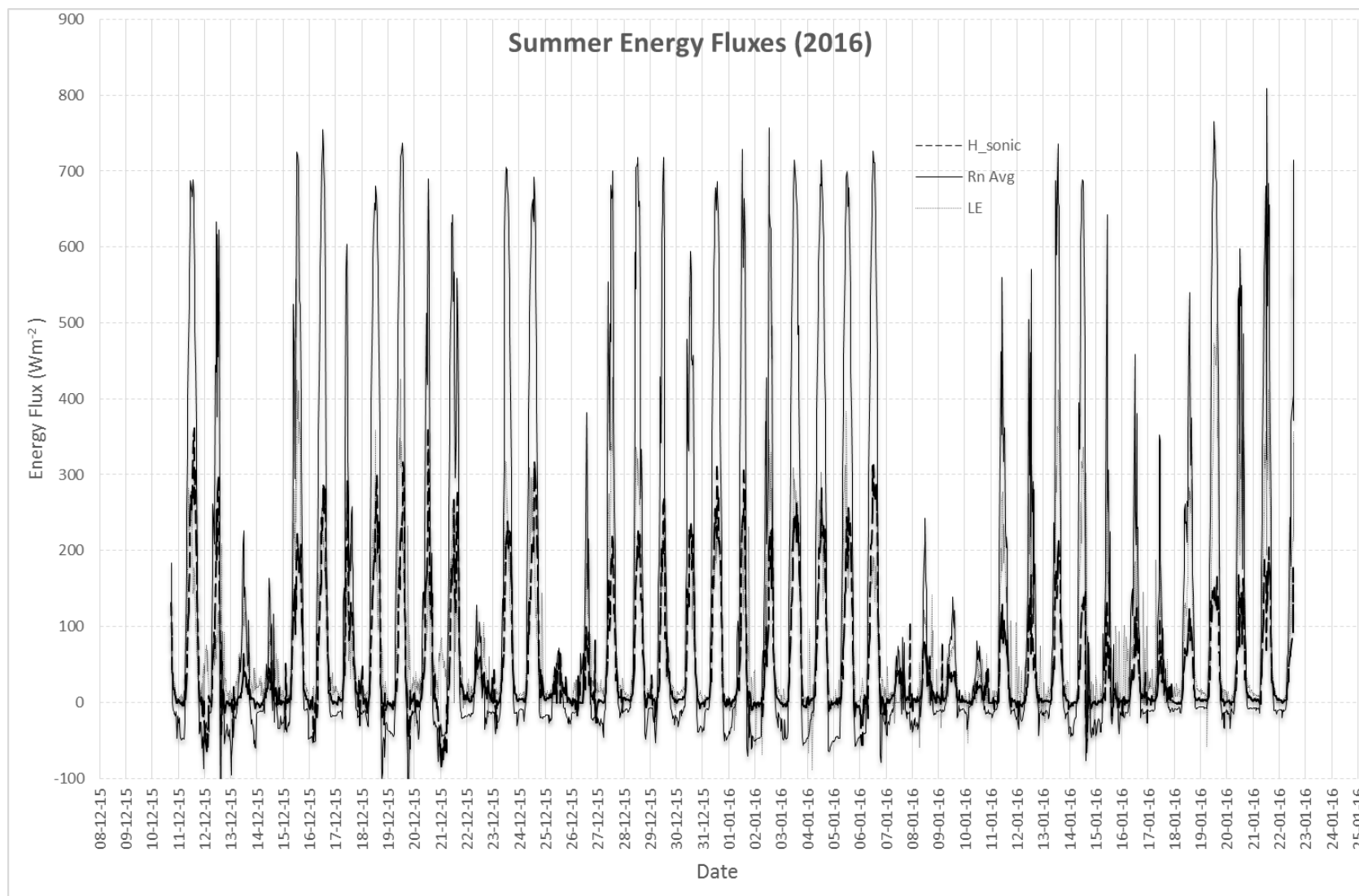
Figure 50: Half-hourly trends in the summer eddy covariance energy flux components (nett radiation, sensible heat and latent energy) for the maize at Baynesfield for Dec 2015 to Jan 2016

Since long-time series data of these fluxes are not easily interpretable, a five-day period of typical summer conditions is shown in Figure 51. On 11 December 2015, conditions were clear and the nett radiation peaked close to 700 W·m⁻². Interestingly, latent energy peaked at 280 W·m⁻² at 09:00 early in the day and then steadily dropped, while heat increased to 360 W·m⁻² at 14:00 (Figure 51) with a resultant maximum temperature of 34°C. This pattern showed that the maize plants were avoiding stress through stomatal closure once conditions got too hot in the day. These hot, dry conditions were indicative of the drought conditions experienced at that time in the KwaZulu-Natal region.

The next day (12 December 2015) was characterised by intermittent clouds (note the spiky nature of the nett radiation data) and then rain in the later afternoon. On this day, latent energy remained low (<110 W·m⁻²) while sensible heat peaked at 300 W·m⁻². The following two days (13 and 14 December 2015) were cold and overcast and the nett radiation peaked at <200 W·m⁻². Rain over these two days totalled 27 mm. From this period onward, latent energy dominated the sensible heat. This was particularly evident on 15 December when the latent energy peaked at 400 W·m⁻² while the sensible hat only reached 200 W·m⁻² at midday. This was despite the nett radiation reaching a maximum of 720 W·m⁻² at 12:00. This data illustrates the importance of climate and soil water in controlling the surface energy balance components during summer months.
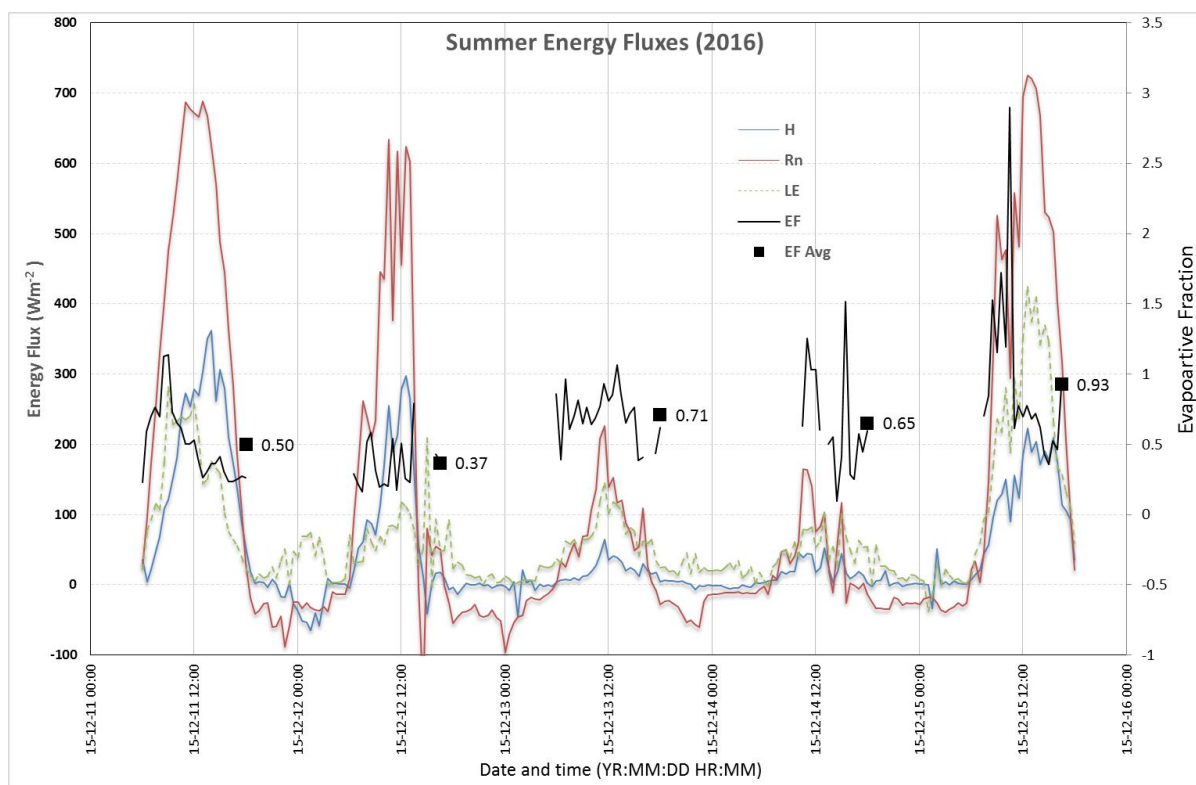
Figure 51: Half-hourly trends in the summer eddy covariance energy flux components (nett radiation, sensible heat and latent energy) for the maize at Baynesfield for a five-day period in December 2015

6.4.2   Energy flux: Winter

A six-week period of winter energy fluxes is presented to contrast with the summer period and to provide data for the second validation period (Figure 52**Error! Reference source not found.**).
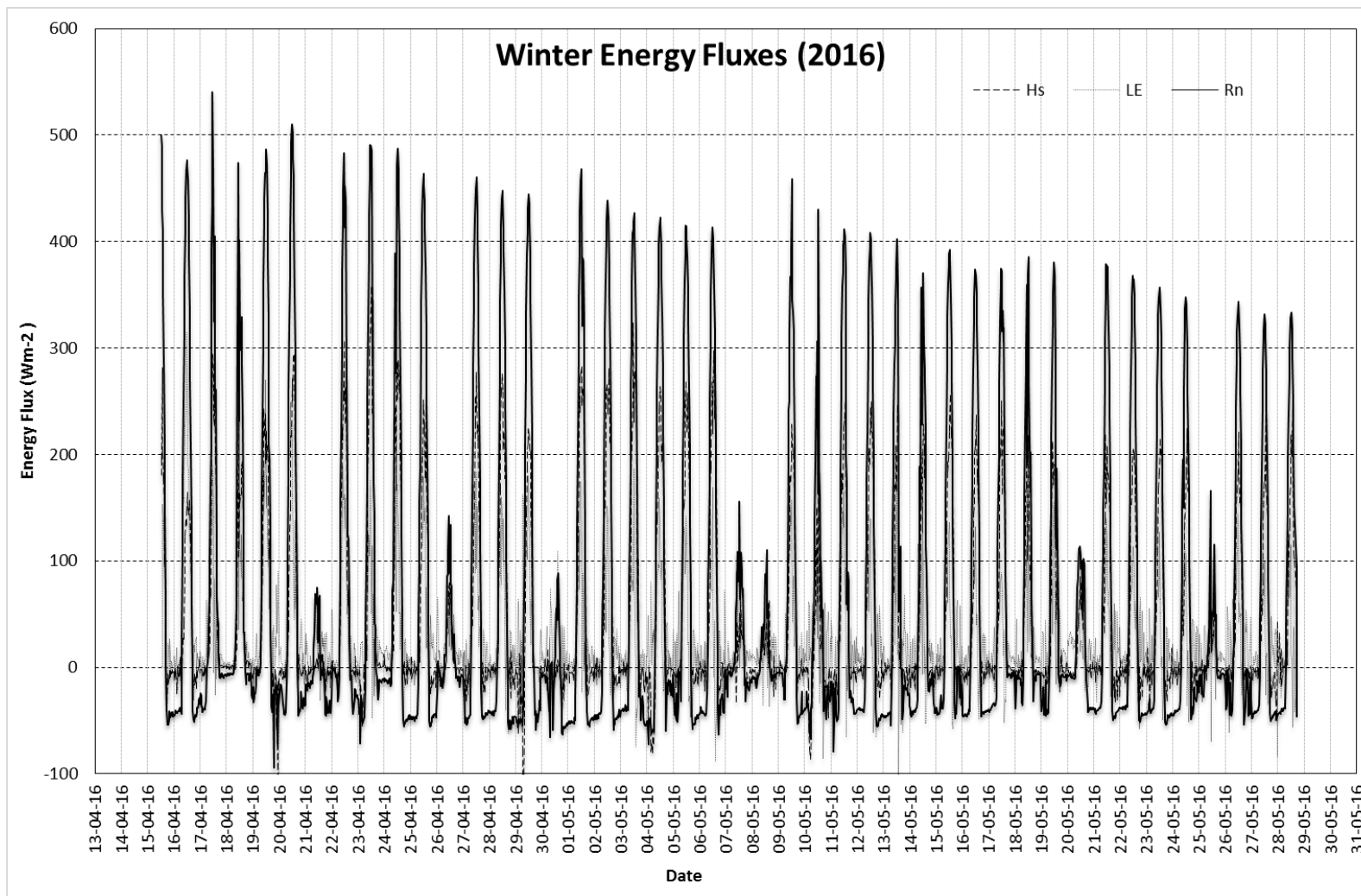
Figure 52: Half-hourly trends in the winter eddy covariance energy flux components (nett radiation, sensible heat and latent energy) for the maize at Baynesfield for April to May 2016

The nett radiation by mid-April had declined by over 200 W·m⁻² with maximum values peaking at approximately 500 W·m⁻². By end of May, the nett radiation had declined steadily to a maximum of only 325 W·m⁻². The winter period in the summer rainfall region is characterised by clear cloudless days and this was reflected in the generally smooth nature of the half-hourly data of the winter energy fluxes. A five-day series of winter data is presented for clarity. 16 April 2016 was characterised by a clear cloudless day (nett radiation maximum = 470 W·m⁻²) and a maximum temperature of 33°C. This resulted in a high spike in the latent energy flux at midday while the sensible heat only reached 160 W·m⁻². The following two days were marked by colder cloudier condition (max temperature only 20°C). This resulted in the sensible heat generally dominating the energy balance for the remaining four-day period. This condition of a hot day followed by several colder days is typical of the arrival of a cold frontal system in KwaZulu-Natal.

6.4.3 Daily total evaporation

Integrating the half-hourly fluxes of the latent heat and converting the W·m⁻² to mm provided a time series of the daily evaporation for Baynesfield for both the summer and winter measurement periods (Figure 53 and Figure 54). During summer (Figure 53), values varied between 0.5 mm on rainy days and a maximum of 4.8 mm at the end of January (Figure 53). Daily total evaporation was generally about 3 mm, which could be considered low for summer maize at this site. However, the drought conditions of the 2015/2016 summer season may have been a contributing factor to these lower than expected values. By comparison, the winter values were much lower than summer and averaged between 1 mm and 2 mm in April, dropping to <1 mm in May (Figure 54).
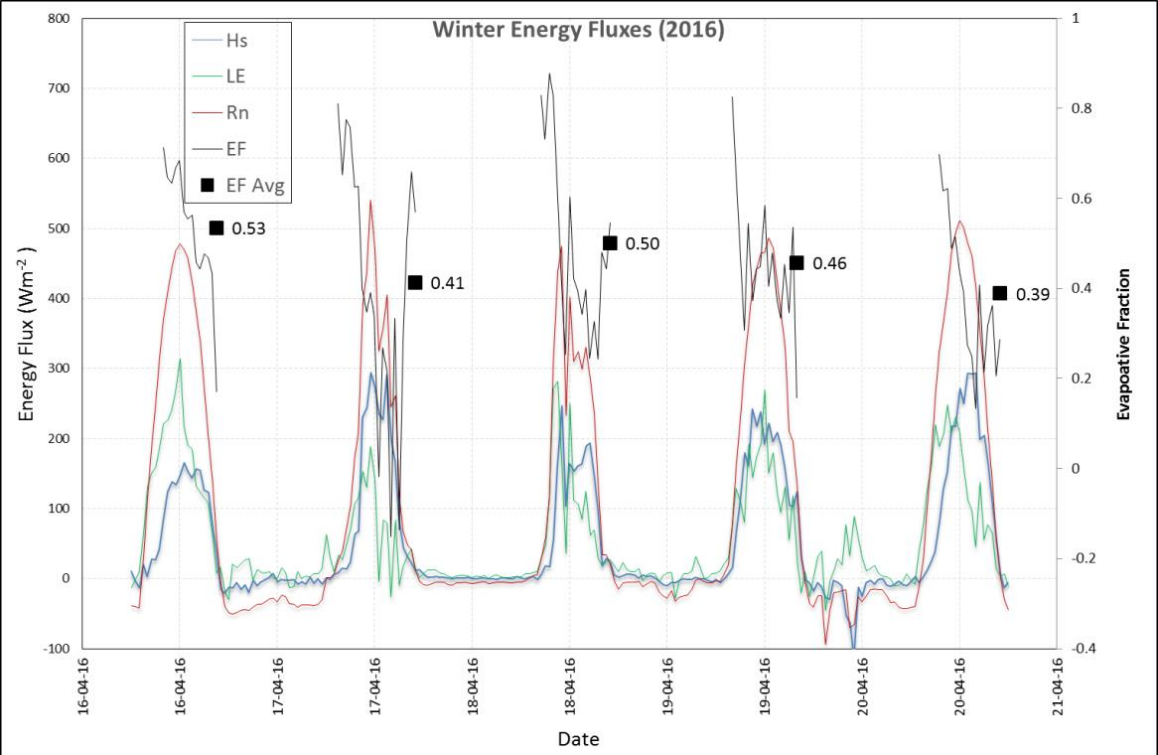
Figure 53: Daily total evaporation in the summer at the maize site at Baynesfield from 2 December to 15 January 2016
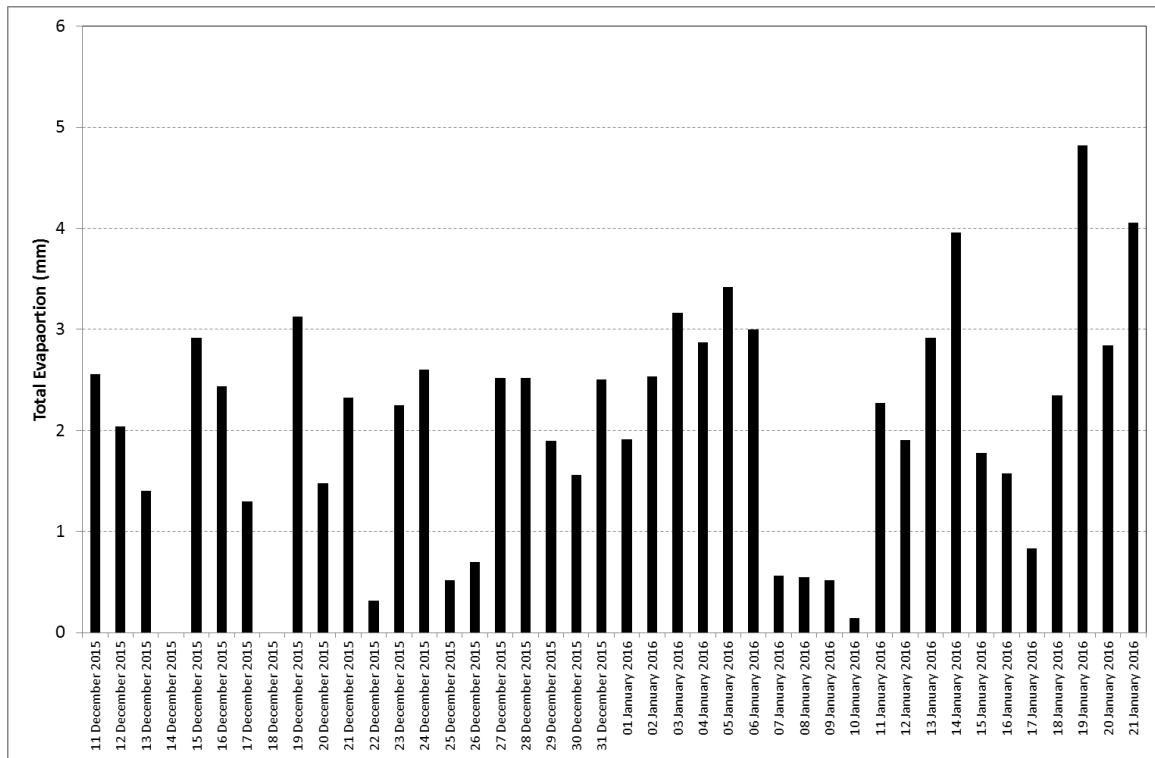
Figure 54: Daily total evaporation in the winter at the maize site at Baynesfield for April to May 2016

6.4.4 Relevance of the Diurnal Energy Balance and Daily Total Evaporation estimates

Actual estimates of both half-hourly and daily total evaporation, as well as other energy balance components derived from the eddy covariance system could be used to validate the SEBS model outputs including some preliminary comparisons of the observed and modelled evaporative fraction estimates used in the derivation of the SEBS soil moisture outputs (Table 6).

The SEBS remote sensing based method solves the energy budget at the land surface using land surface temperature, albedo, NDVI and surface emissivity data. An important assumption in the model for soil water is the diurnal self-preservation of the evaporative fraction. The evaporative fraction is defined as the ratio between the latent heat flux and the available energy at the land surface and is used to facilitate the calculation of soil water in a simplified manner:

$$EF = \frac{LE}{R_n - G} \qquad (41)$$

where *EF* is evaporative fraction; *LE* is latent energy; R_n is nett radiation and *G* is the soil heat flux.

The observation that evaporative fraction is often constant during daytime is based on studies by Crago and Brutsaert (1996), Nichols and Cuenca (1993), and Shuttleworth et al. *(*1989). They used in situ measurements of surface energy balance components to show that evaporative fraction is almost constant during the daytime hours under clear skies. Evaporative fraction supposedly removes the available energy diurnal cycle and isolates surface control (soil and plant resistance to moisture loss) on turbulent heat flux partitioning (Gentine et al., 2007). These controls vary on daily time scales. However, more recent studies by Lhomme and Elguero (1999) have shown that evaporative fraction is not necessarily constant, leading to total evaporation estimation errors, in particular in the morning and late afternoon due to the typical parabolic shape of the diurnal evaporative fraction curve (Gentine et al., 2007).

The half-hourly diurnal trends from using the measured latent and sensible heat fluxes from sunrise to sunset. Daily averages for the evaporative fraction for both winter and summer are shown in Figure 28 and Figure 30 respectively. As discussed above, micrometeorological conditions varied markedly from day to day and seasonally. These changing conditions were reflected in the highly variable diurnal

evaporative fraction values in both seasons. In summer, when the latent energy dominated (despite the drought conditions), the average evaporative fraction values were generally above 0.50. In winter, when the sensible heat dominated the fluxes, they were below 0.50 showing some coherence to the evaporative fraction data (Figure 51 and Figure 52). There was some evidence of evaporative fraction self-preservation in summer (Figure 51) but not in winter (Figure 52). The values were more erratic near sunrise and sunset and on cloudy days. Available energy ($R_n − G$) that appears in the denominator of evaporative fraction is small near these times. Therefore, the inclusion of early morning and late afternoon evaporative fraction values in the estimation of daily evaporative fraction can lead to large errors in evapotranspiration estimation. Since the Landsat 8 overpass time on South Africa is 10:00, this could be an important factor when estimating both total evaporation and SWC from remote sensing. The sensitivity of the models to evaporative fraction is clearly an area that requires further investigation since the evaporative fraction behaviour depends on environmental factors, SWC and canopy cover measured by leaf area index.

The robustness of the self-preservation of evaporative fraction and the range of its applicability under different environmental conditions requires long-term energy flux data, which are both demanding and costly to obtain. Unfortunately, due to the 16-day return time of the Landsat 8 satellite, the breakdown of our eddy covariance system and limited time frame, we were only able to obtain four corresponding days for SEBS and observed evaporative fraction comparisons during the second validation experiment (Table 6). This data discussed further in Chapter 6. This is an area that requires further investigation to improve modelled estimates of soil water using the concept of evaporative fraction self-preservation.

7. SOIL WATER BACK-CALCULATED FROM SEBS

The SEBS model, developed by Su (2002), was run in ILWIS 3.8.5 to estimate relative evaporation and evaporative fraction in Baynesfield. The SEBS model uses remote sensing and meteorological data sets to estimate heat fluxes. Landsat 8 images were used to estimate relative evaporation and evaporative fraction using the SEBS model. The Landsat 8 satellite, as seen in Figure 55, is the latest addition to the Landsat series. It was launched on 11 February 2013 (Markham et al., 2015). Landsat satellites have continuously acquired information of the Earth's land surface since 1972, thus the continuation of data acquisition from the Landsat 8 satellite is essential (USGS, 2013). Landsat 8 orbits the Earth at an altitude of 705 km, which results in 14 full orbits being completed each day, with every point of the Earth being covered once every 16 days. The satellite carries out north to south orbits and has an overpass time of 10:00 (Markham et al., 2015).

Figure 55: Landsat 8 satellite

Landsat 8 images were used in this study due to their spatial resolution. It can estimate relative evaporation and evaporative fraction at a spatial resolution of 30 m; however, it has a temporal resolution of 16 days. The Landsat 8 product consists of several bands (1 to 1), each band with its own spectral characteristics and wavelength range (Table 3).

Table 3: Characteristics of the various Landsat 8 bands (USGS, 2015)

Spectral bands	Wavelength (μm)	Resolution (m)
1 – coastal/aerosol	0.43-0.45	30
2 – blue	0.45-0.51	30
3 – green	0.53-0.59	30
4 – red	0.64-0.67	30
5 – near infrared	0.85-0.88	30
6 – short wave infrared (SWIR) 1	1.57-1.65	30
7 – SWIR 1	2.11-2.29	30
8 – panchromatic	0.50-0.68	15
9 – cirrus	1.36-1.38	30
10 – thermal infrared sensor (TIRS) 1	10.60-11.19	100
11 – TIRS 2	11.50-12.51	100

Landsat 8 satellite imagery was freely acquired from http://earthexplorer.usgs.gov (the Earth Explorer website). The dataset selected was the L8 operational land imager (OLI)/TIRS. The catchment study area fell within one Landsat 8 image. The images acquired were for clear sky conditions. The ILWIS 3.8.5 software was downloaded from http://52north.org/downloads/ilwis/. The images (bands) were imported into ILWIS 3.8.3 as digital numbers. The bands required were 2, 3, 4, 5, 6, 7, 10 and 11. These bands were rescaled to top of atmosphere (TOA) reflectance and/or radiance, using the radiometric rescaling coefficients provided in the metadata file. The procedure followed has been outlined by Allen et al. (2002) and the United States Geological Survey (USGS, 2015). The USGS (2015) provides the necessary equations for the conversion to TOA radiance, conversion to TOA reflectance and conversion to TOA brightness temperature. The equations to obtain the inputs into the SEBS model, such as the albedo, NDVI, surface emissivity and land surface temperature maps, are presented in Allen et al. (2002). Although the equations in Allen et al. (2002) were intended to be used in SEBAL, they can be used in other models such as SEBS.

7.1 Conversion to TOA Radiance

Bands 10 and 11 (TIRS bands) were converted to TOA radiance using the radiance rescaling factors provided in the metadata file (USGS, 2015).

$$ \text{L}\lambda = (M_L \times Q_{cal}) + A_L \tag{42} $$

where, $L\lambda$ is the TOA spectral radiance [Watts/(m^2 × srad × μm)], ML is the band-specific multiplicative rescaling factor (RADIANCE_MULT_BAND_X) from the metadata file (where X is the band number), Q_{cal} is the quantized and calibrated standard product pixel value (digital number), and A_L is the band-specific additive rescaling factor (RADIANCE_ADD_BAND_X) from the metadata (where X is the band number).

7.2 Conversion to TOA Reflectance

Bands 2, 3, 4, 5, 6 and 7 (OLI bands) were converted to TOA planetary reflectance using reflectance rescaling coefficients provided in the metadata file (USGS, 2015).

$$ \text{P}\lambda' = (M_P \times Q_{cal}) + A_P \tag{43} $$

where $P\lambda'$ is the TOA planetary reflectance (without solar angle correction), M_p is the band-specific multiplicative reflectance factor (REFLECTANCE_MULT_BAND_X) from the metadata file (where X is the band number). A_p is the band-specific additive rescaling factor (REFLECTANCE_ADD_BAND_X) from the metadata (where X is the band number).

The TOA reflectance was then corrected for the sun angle (USGS, 2015):

$$ \text{P}\lambda = \frac{\text{P}\lambda'}{\sin(\Theta_{SE})} \tag{44} $$

where $p\lambda$ is the TOA planetary reflectance and Θ_{SE} is the local sun elevation (ESUN), which is obtained from the metadata file.

The ESUN values were determined for bands 2, 3, 4, 5, 6 and 7 using the following equations (Allen et al., 2002):

$$ ESUN = (\pi \times d^2) \times \left(\frac{RAD\_MAX}{REF\_MAX}\right) \tag{45} $$

where d is the Earth-sun distance, RAD_MAX is the maximum radiance and REF_MAX is the maximum reflectance (all of which are found in the metadata file).

The ESUN values (Table 4) are required to create an equation to determine albedo for the TOA (Allen et al., 2002).

$$\alpha_{TOA} = \sum(\omega\lambda \times P\lambda) \qquad (46)$$

$$\omega\lambda = \frac{ESUN\lambda}{\sum ESUN\lambda} \qquad (47)$$

Table 4: Calculated ESUN values

Band	ωλ	Band	ωλ
2	0.300	5	0.143
3	0.277	6	0.036
4	0.233	7	0.012

The ESUN band values change due to changes in the Earth-sun distance (*d*), maximum radiance and maximum reflectance of each data product. However, the $\omega\lambda$ band value was determined to be the same for each image as the ratio remained the same.

Albedo was then calculated by correcting TOA albedo using the following equation (Allen et al., 2002):

$$\propto = \frac{\alpha_{TOA} - \alpha_{Path\_radiance}}{\tau_{sw}^2} \qquad (48)$$

where $\alpha_{Path\_radiance}$ *is* 0.03 and τ_{sw} is 0.774 (Allen et al., 2002).

The generated albedo map is illustrated in Figure 56. Albedo ranges from 0.0 to 1.0 and is a measure of the reflectivity of the Earth's surface. As the reflectivity increases, the albedo value increases. Grasslands generally have an albedo of between 0.15 to 0.25.
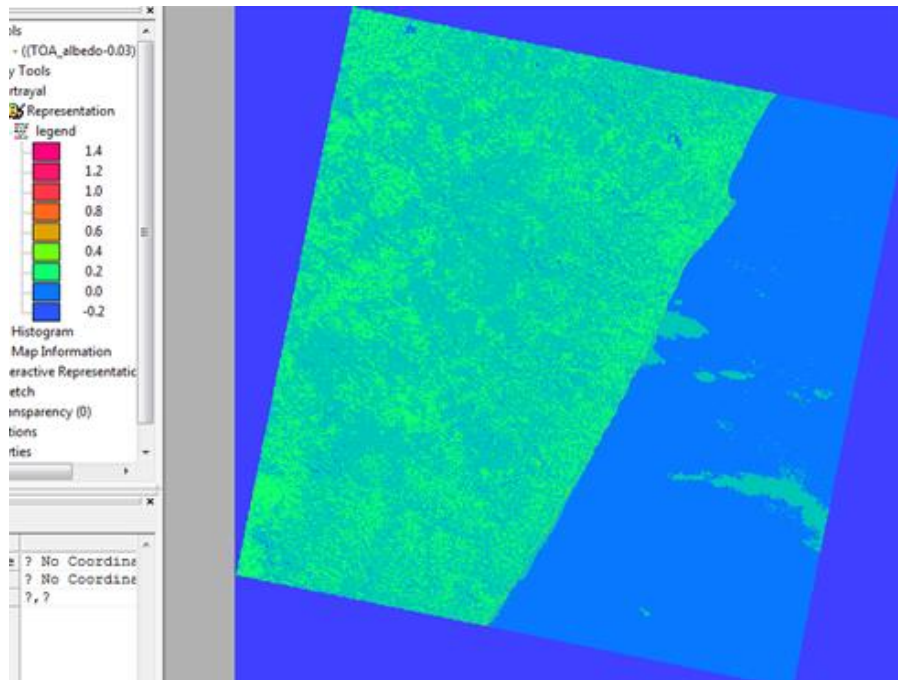
Figure 56: Albedo map generated in ILWIS

The NDVI was determined by Allen et al. (2002):

$$NDVI = \frac{(P5 - P4)}{(P5 + P4)} \qquad (49)$$

where *P5* is the corrected reflectance band five and *P4* is the corrected reflectance band 4.

56

The generated NDVI map is illustrated in Figure 57. The NDVI ranges from −1.0 to 1.0. The more vegetation present, the higher the NDVI value. Water bodies have a negative NDVI value.
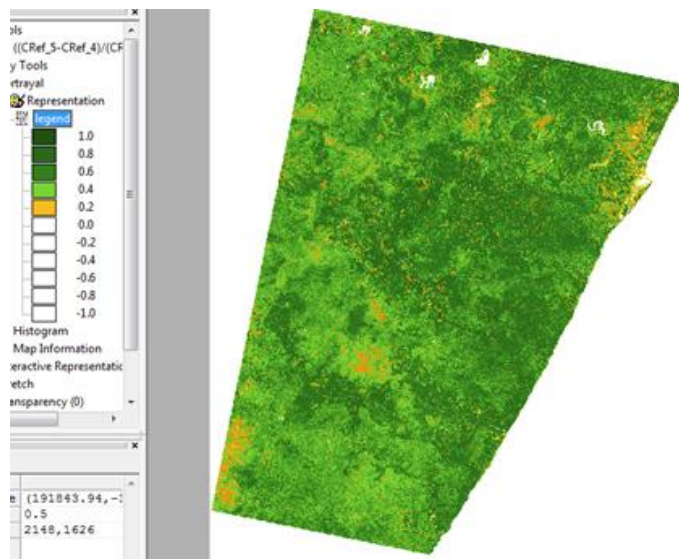
Figure 57: NDVI map generated in ILWIS

The surface emissivity (ε_o) was determined using the following equation (Allen et al., 2002):

$$\varepsilon_o = 1.009 + 0.047 \times \ln(NDVI) \tag{50}$$

The generated surface emissivity map is illustrated in Figure 58. The surface emissivity is 0.999 for NDVI values less than 0.
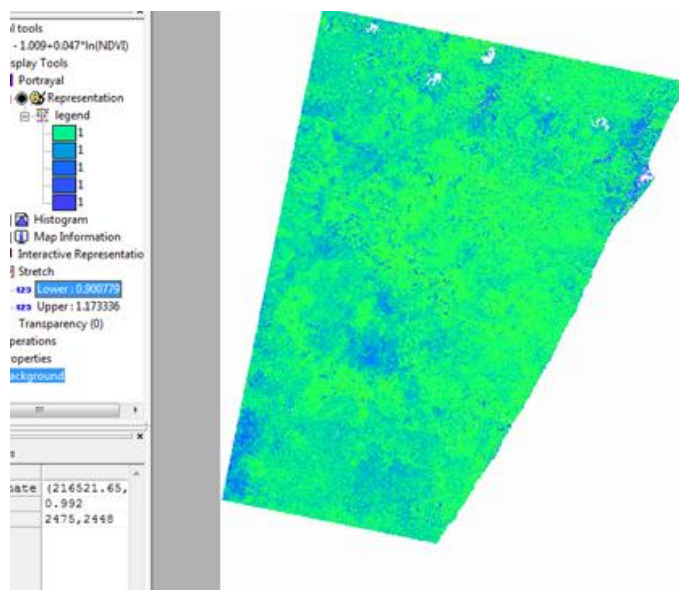
Figure 58: Surface emissivity map generated in ILWIS

The TIRS bands (bands 10 and 11) are converted from spectral radiance to at-satellite brightness temperature, using the following equation (USGS, 2015):

$$Tbb = \frac{K2}{ln\left[\frac{K1}{L\lambda} + 1\right]} \tag{51}$$

Where *K1* and *K2* are constants that are found in the metadata file and *Lλ* is either band 10 or band 11, according to high or low gain conditions. Band 11 was used in this study, as high gain is suited for grassland vegetation.

The land surface temperature can be determined by Allen et al. (2002):

$$LST = \frac{Tbb}{\varepsilon o^{0.25}}$$

(52)

Figure 59 shows the generated land surface temperature map expressed in degrees kelvin.
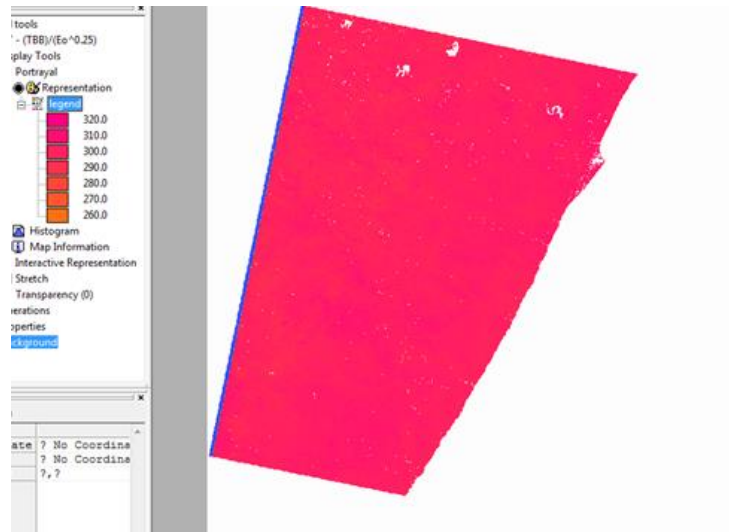
Figure 59: Land surface temperature map generated in ILWIS

The SEBS model was run in ILWIS (Figure 60) after the input maps (albedo, NDVI, surface emissivity, land surface temperature, and digital elevation model) were created. The meteorological data required to run the model was obtained from the eddy covariance weather data, which is located within Baynesfield. On the days where this data was not available, data from the nearby Agricultural Research Council weather station was used. The data required from the weather station were the instantaneous downward solar radiation, wind speed, air temperature, pressure, mean daily air temperature and sunshine hours. The downward solar radiation, wind speed, air temperature and pressure data were at the time of the satellite overpass (10:00).
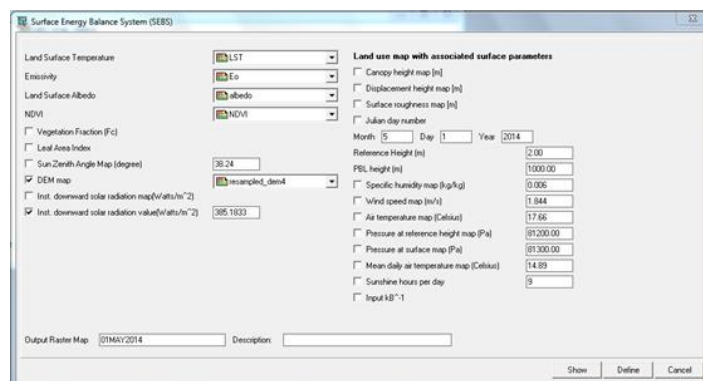
Figure 60: The SEBS model in ILWIS

The SEBS model was run (Figure 60) and many outputs generated. These outputs included daily evaporation, relative evaporation, evaporative fraction, nett radiation, soil heat flux, sensible heat flux dry, sensible heat flux wet, sensible heat flux index and leaf area index. For this research, the evaporative fraction (Figure 61) and relative evaporation (Figure 62) outputs were required.
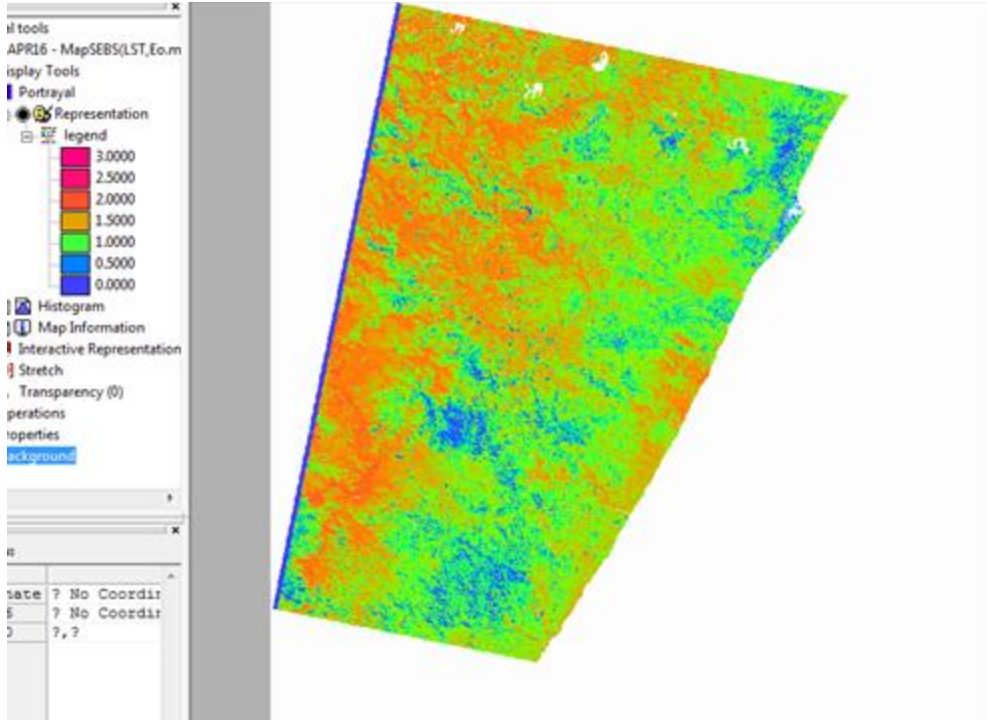
Figure 61: Evaporative fraction map generated as an output of the SEBS model in ILWIS
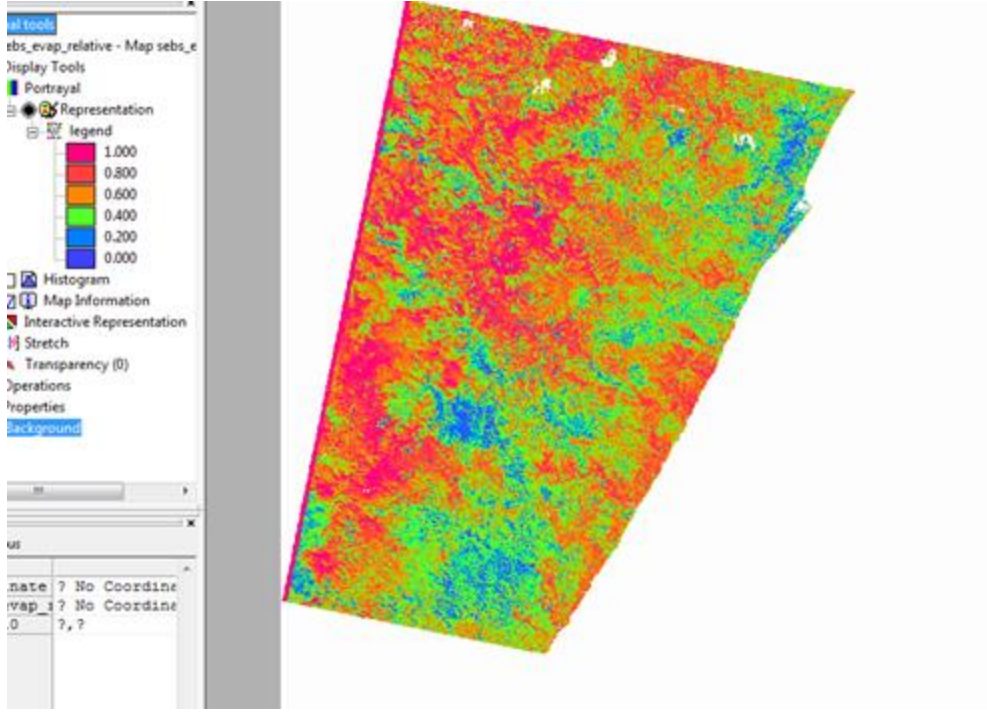
Figure 62: Relative evaporation map generated as an output of the SEBS model in ILWIS

The daily soil water map from the SEBS model in ILWIS 3.8.5 is shown in Figure 63.
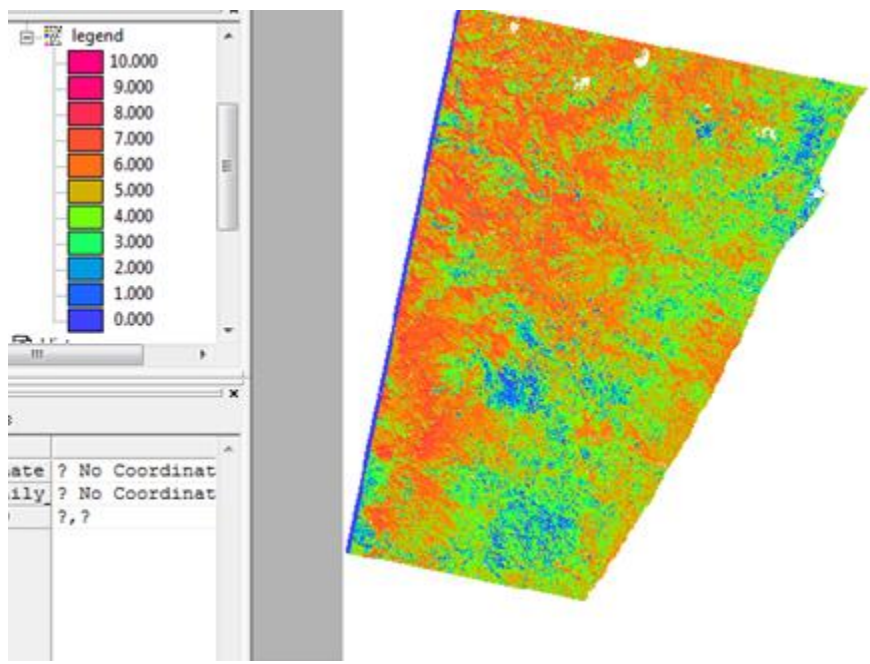
Figure 63: Daily evaporation map generated as an output of the SEBS model in ILWIS

Table 5: Relative evaporation, evaporative fraction and daily total evaporation values determined with SEBS and the eddy covariance data (observed)

Date	Relative total evaporation	Total evaporation fraction (observed)	Total evaporation fraction (SEBS)	Deviation (SEBS – observed)	Daily total evaporation (mm)	Daily SEBS total evaporation (mm)
23-Dec-15	0.87	0.59	0.86	0.27	2.25	4.96
25-Feb-16	0.91	–	0.88	–	–	7.95
28-Mar-16	0.47	–	0.87	–	–	2.63
13-Apr-16	0.73	0.77	0.80	0.03	2.28	3.40
29-Apr-16	0.45	0.45	0.52	0.07	1.40	4.44
15-May-16	0.93	0.27	0.91	0.64	–	2.93

Table 6 shows that the modelled relative evaporation and the evaporative fractions followed a similar trend for this period, in this area. The relative evaporation and the evaporative fraction values were then used in the equations developed by Su (2002) and Scott et al. (2003) to obtain estimates of soil water.

These estimates (based on a 30 m × 30 m spatial grid) are shown in Figure 64. Due to the CRP failing on 16 January 2016, the comparison between CRP estimates and the back-calculated soil water was not possible beyond this period. From the observed and modelled daily total evaporation it can be noted that the SEBS model overestimates the daily total evaporation, when compared to the observed daily total evaporation.
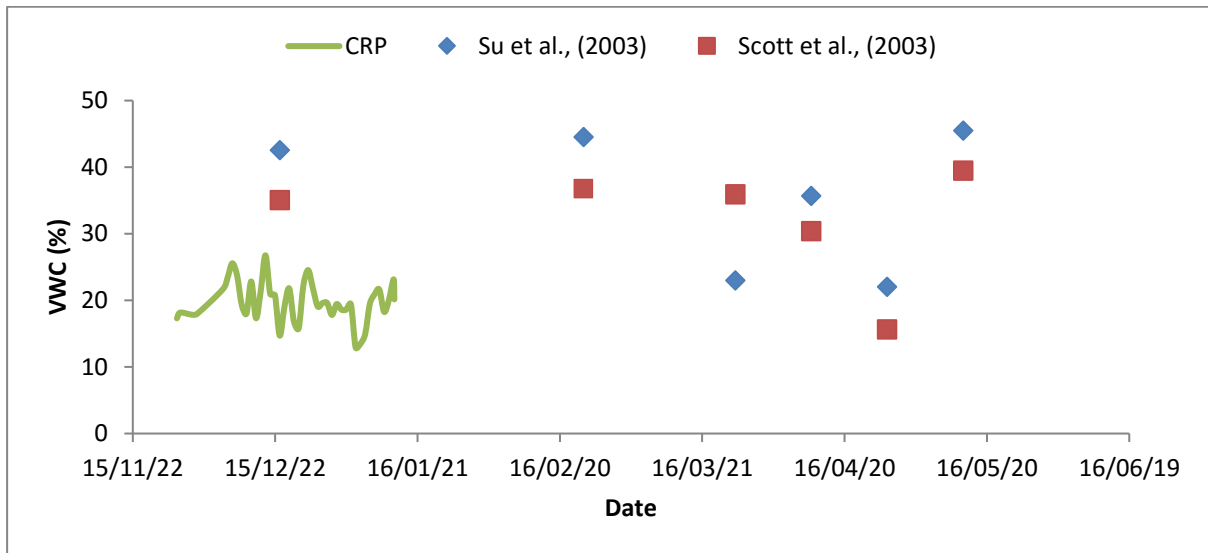
Figure 64: CRP and the back-calculated soil water estimates against time

The daily evaporation estimates from the SEBS model are shown in Figure 65. The graph is plotted on a 16-day interval, such that the gaps indicate when the data from that day could not be used due to cloud cover. The daily evaporation during this period ranged from 2.5 mm/day to 8 mm/day. When these estimates are compared to the daily evaporation values estimated by the eddy covariance system, the SEBS daily soil water estimates are noticeably higher.
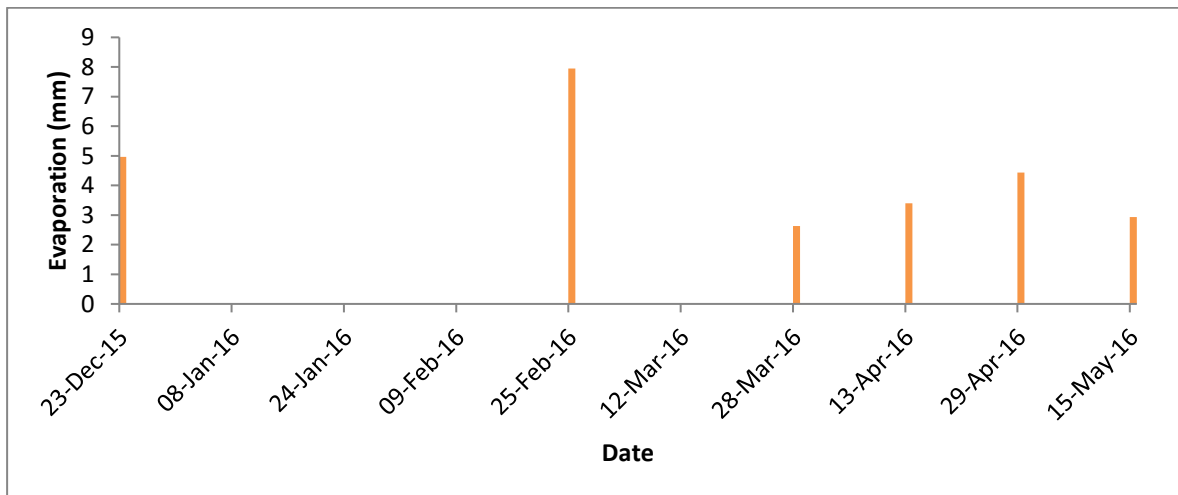
Figure 65: SEBS daily evaporation for the Baynesfield maize site in 2016

For the period from 01 March 2014 to 01 March 2015, the relative evaporation and evaporative fractions were estimated using the SEBS model and used in the two equations to obtain soil water (Table 6). This was done as the previous period was limited by a lack of CRP soil water record. These soil water estimates were then plotted against the CRP estimates from the same period.

Table 6: Relative evaporation and evaporative fraction values

Date	Relative Evaporation	Evaporative Fraction
23-Mar-14	0.88	0.91
24-Apr-14	0.75	0.86
26-May-14	0.85	0.58
11-Jun-14	0.85	0.86
13-Jul-14	0.87	0.85
29-Jul-14	0.21	0.42
14-Aug-14	0.16	0.32
15-Sep-14	0.50	0.78
04-Dec-14	0.59	0.84

From Table 6, the relative evaporation and evaporative fraction values followed a similar seasonal trend, as the values are higher in wetter periods and lower in dry periods. These values were then used in the respective equations to obtain soil water estimates. The relative evaporation and the evaporative fraction was then used in the respective equations to obtain estimates of soil water (Figure 66). The back-calculated soil water using both methods results in the estimates following a general season trend. The back-calculation method proposed by Scott et al. *(2003)* provided slightly better estimates of soil water than the method proposed by Su et al. *(2003)* when compared to the CRP soil water estimates.
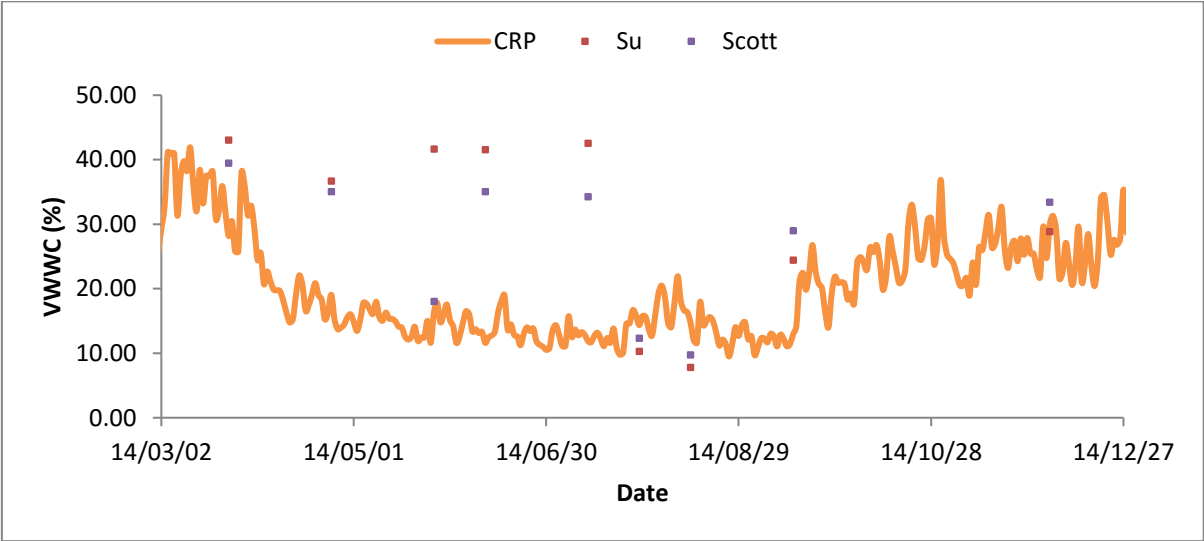
Figure 66: CRP estimates and back-calculated soil water against time

The daily evaporation estimates from the SEBS model was plotted against time (Figure 67). The daily evaporation follows the seasonal trend as the daily evaporation is higher in the wetter periods (March to May and September to December) and lower in the drier periods (July to August) as expected.
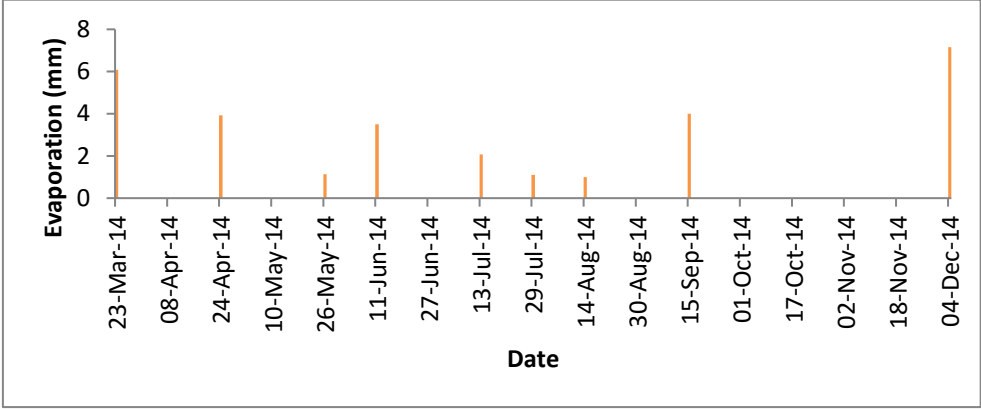
Figure 67: SEBS daily evaporation

8. CONCLUSION

The development of remote sensing technologies is essential; therefore, it is a necessity to obtain reliable and accurate data to calibrate and validate remote sensing products. Currently, using modelling to obtain hydrological parameters has increased and models have become more advanced and continuously improve. This has resulted in finer scaled modelled products, which require inputs at a fine spatial and temporal resolution. Although conventional in situ soil moisture estimation methods have been invaluable to calibrate and validate remote sensing and modelled products, the limitations of point measurement, due to the heterogeneity of soil water, result in discrepancies. This needs to be addressed to adequately calibrate and validate remote sensing and modelled soil moisture products. Up-to-date soil water estimates is of great interest across a wide range of disciplines including numerical weather prediction, agricultural applications and flood modelling.

The CRP, once properly calibrated, provides spatial estimates of soil water at an intermediate scale, which bridges the measurement gap between conventional in situ point estimates and large-scale remote sensing soil water estimates. The CRP calibration procedure is adequate; however, potential errors can be introduced throughout the procedure, which range from selecting the sample points, determining a representative bulk density and determining the average neutron count (N_o) value. Therefore, to minimize potential errors, proper procedures must be adhered to. The CRP estimates were used to validate modelled soil water estimates. These included the SAHG soil water product and the back-calculation of soil water from relative evaporation estimated from the SEBS model.

The SAHG soil water product was validated with the CRP. There was a good correlation between the SAHG and CRP datasets. The SAHG soil water followed the same seasonal trend as the CRP and had a continuous dataset (no missing values). Although the SAHG product performed well, there was still the presence of vertical and horizontal scaling issues due to differences in the measurement depth and footprint of the two datasets. There was also the issue of converting SSI to VWC, which required a representative porosity of the study area to be determined.

The back-calculation of soil water from relative evaporation and evaporative fraction, estimated using the SEBS model, looked like a promising technique. The spatial resolution was less than the catchment area and the measurement depth was representative of the root zone of the vegetation (0.50 m). Therefore, this product would have the least horizontal and vertical scaling issues when validated against the CRP. Although the back-calculation method results in soil water estimates on a 30 m spatial grid, the temporal resolution of the imagery used is 16 days, which is very impractical for continuous soil water monitoring.

There is room for improving the relationship between soil water and total evaporation. The relationship has been researched and expressed in previous studies; however, it is not a simple linear relationship. Therefore, the work of previous studies could be built upon and improved to better understand the relationship between soil water and total evaporation, thus improving our understanding and links between the hydrological processes.

9. FUTURE RESEARCH

The current project has shown the power of the stationary CRP to measure scales of soil water never achieved in South Africa before. Through this project we have provided evidence to show that the HylarsMet model is providing SSI data that can be used with confidence for flood forecasting. However, there is still room for improving these products by "training" these models using actual soil water data collected from a South African COSMOS network of probes. We believe that this technology needs to be adopted by the SAWS who have for some years unsuccessfully attempted to establish a soil water monitoring network. However, we have also demonstrated that other soil water remote sensing products (such as SMOS and SEBS) have limitations in both the vertical and horizontal scales when compared to the 34 ha CRP footprint. Improving these predictions is an area that requires further investigation. This would require improving and better understanding of the model algorithms to model the energy fluxes at the land surface by investigating the sensitivity of the models to the assumption of self-preservation of the evaporative fraction and other environmental factors. This will require sites where long-term carbon and water fluxes are being measured with co-located stationary CRPs. Such research is demanding in terms of both capacity and capital resources. Areas where long-term measurements are being conducted (SAEON at Cathedral Peak and WRC at Two Streams) could provide the platform for this research. These catchments have the potential to provide significant monitoring (including the CRP technology) and research data to enable sophisticated research analysis and modelling pertinent to addressing global change questions.

The RV-01 soil moisture rover uses the cosmic ray method to passively and non-invasively monitor water content in the top 50 cm of soil. The RV-01 system measures naturally occurring cosmic ray neutrons, which are utilised as a proxy for SWC. The RV-01 system records neutron intensity from a sensor located in a weatherproof detector module. The system also records GPS coordinates, barometric pressure, relative humidity and the temperature from a separate control module. The neutron detectors are housed in a rugged aluminium enclosure while the control module (which includes the data logger) is housed in plastic pelican case that can be installed in a motor vehicle to obtain large spatial maps of soil water by surveying the area while driving.

The RV-01 rover yields soil moisture averaged over swaths that have a width equal to the footprint and a length that depends on the speed of the vehicle and the desired precision of the measurement. The team are currently developing a RV-01 rover system as preliminary results obtained with a prototype rover used by our US partners are particularly encouraging. Mobile application allows spatial scale matching of satellite pixels of the average of COSMOS rover values to satellite pixels. This allows for physical upscaling since the rover can match many satellite pixels with varying land cover types. Generating soil moisture maps with a cosmic ray rover at intermediate scales will aid in large-scale hydrologic studies. The project team have recently invested R800 000 in this technology through a USAID NSF PEER project. Support is required to extend the application of the RV-01 rover research to drought and flood forecasting, irrigation scheduling, wetland delineation and climate change impacts (such as bush encroachment) to name just a few of the numerous possibilities of this new technology of which there are only a few worldwide.

The prediction of both above- and below-ground biomass using neutron intensities from the CRP is an area of research that can potentially provide production estimates from food crops. In addition, the effect of the biomass hydrogen pool on the soil water calibration also needs to be fully investigated to improve the calibration equations for soil water estimation.

Recent research in the USA on the RV-01 rover investigated the idea of screening all neutrons except those coming from below. This has resulted in the development of a local-neutron detector, which is like the conventional surface neutron detector, except that it does not have an artificial source of neutrons. There are potentially many applications for this instrument, most importantly will be high-resolution neutron and soil moisture mapping (metre scale), and the new possibility to calibrate COSMOS probes on multiple measurements of neutrons at metre scales within the hectometre scale of COSMOS probe. This may replace, or at least complement, the standard calibration on soil samples and oven-drying.

The stationary probe and CRP rover have provided a 34 ha footprint that we have found useful for remote sensing validation at this larger scale. However, this scale has also presented limitations as it is not always possible to find homogenous areas of crops and natural vegetation of this size. The ability to map soil water at a finer resolution will represent a major advance in our hydrological and agricultural research.

REFERENCES

Albergel, C., De Rosnay, P., Gruhier, C., Mu˜noz-Sabater, J., Hasenauer, S., Isaksen, L., Kerr, Y. and Wagner, W. 2012. Evaluation of remotely sensed and modelled soil moisture products using global ground-based in situ observations. *Remote Sensing of Environment*, 118, 215-226.

Albergel, C., Rudiger, C., Carrer, D., Calvet, J.-C., Fritz, N., Naeimi, V., Bartalis, Z. and Hasenauer, S. 2009. An evaluation of ASCAT surface soil moisture products with in-situ observations in Southwestern France. *Hydrology and Earth System Sciences*, 13, 115-124.

Allen, R., Bastiaanssen, W. and Waters, R. 2002. Personal communication. The University of Idaho and the Idaho Department of Water Resources, Idaho.

Allen, R.G., Tasumi, M. and Trezza, R. 2007. Satellite-based energy balance for mapping evapotranspiration with internalized calibration (METRIC)-Model. *ASCE: Journal of Irrigation and Drainage Engineering*, July/August, 395-406.

Bastiaanssen, W.G.M., Menenti, M., Feddes, R.A. and Holtslang, A.A. 1998. A remote sensing surface energy balance algorithm for land (SEBAL): 1. Formulation. *Journal of Hydrology*, 212, 198-212.

Brocca, L., Hasenauer, S., Lacava, T., Melone, F., Moramarco, T., Wagner, W., Dorigo, W. and Bittelli, M. 2011. Soil moisture estimation through ASCAT and AMSR-E sensors: An intercomparison and validation study across Europe. *Remote Sensing of Environment*, 115, 3390-3408.

Brocca, L., Tarpanelli, A., Moramarco, T, Melone, F., Ratto, SM., Cauduro, M., Ferraris, S., Berni, N., Ponziani, F., Wagner, W. and Melzer, T. 2013. Soil moisture estimation in alpine catchments through modeling and satellite observations. *Soil Science Society of America.*

Carlson, T.N., Dodd, J.K., Benjamin, S.G. and Cooper, J.N. 1981. Satellite estimation of the surface-energy balance, moisture availability and thermal inertia. *Journal of Applied Meteorology*, 20, 1, 67-87.

Chan, C.Y. and Knight, R.J. 1999. Determining water content and saturation from dielectric measurements in layered materials. *Water Resource Research*, 35, 1, 85-93.

Crago, R.D. 1996. Conservation and variability of the evaporative fraction during the daytime. *Journal of Hydrology*, 180, 1, 173-194.

Crow, W. 2007. A novel method for quantifying value in spaceborne soil moisture retrievals, *Journal of Hydrometeorology*, 8, 56-67.

De Bruin, H.A.R., Van den Hurk, B.J.J.M. and Kohsiek, W. 1995. The scintillation method tested over dry vine yard area. *Boundary-Layer Meteorology*, 76, 25-40.

Desilets, D. and Zreda, M. 2013. Footprint diameter for a cosmic-ray soil moisture probe: Theory and Monte Carlo simulations. *Water Resources Research*, 49, 3566-3575.

Desilets, D., Zreda, M. and Ferre, T.P.A. 2010. Nature's neutron probe: Land surface hydrology at an elusive scale with cosmic rays. *Water Resources Research*, 46, 1-7.

Dorigo, W.A., Wagner, W., Hohensinn, R., Hahn, S., Paulik, C., Xaver, A. and Jackson, T. 2011. The International Soil Moisture Network: A data hosting facility for global in situ soil moisture measurements. *Hydrology and Earth System Sciences*, 15 1675-1698.

Draper, C.S., Walker, J.P., Steinhle, P. and Holmes, T.R.H. 2009. An evaluation of AMSR-E derived soil moisture over Australia. Department of Civil and Environmental Engineering, University of Melbourne, Melbourne, Australia.

Drexler, J.Z., Snyder, R.L., Spano, D. and Paw U, K.T. 2004. A review of models and micrometeorological methods used to estimate wetland evapotranspiration. *Hydrological Processes*, 18, 2071-2101.

Dutta, R. and D'este, C. 2013. Virtual calibration of cosmic ray sensor: Using supervised ensemble machine learning. *International Journal of Advanced Computer Science and Applications*, 4, 8.

Everson, C.S. 1985. Ecological effects of fire in the montane grasslands of Natal. PhD thesis, University of Natal, Pietermaritzburg.

Everson C.S., Clulow, A.D., Becker, M., Watson, A., Ngubo, C., Bulcock, H., Mengistu, M., Lorentz, S. and Demlie, M. 2014. The long term impact of Acacia mearnsii trees on evaporation, streamflow, low flows and ground water resources. Phase II: Understanding the controlling environmental variables and soil water processes over a full crop rotation. WRC Project: K5/2022 (Inpress). Water Research Commission, Pretoria.

Everson, C.S., Molefe, G.L. and Everson, T.M. 1998. Monitoring and modelling components of the water balance in a grassland catchment in the summer rainfall area of South Africa. WRC Report, 1998/01/01, Research Report No. 493/1/98. Water Research Commission, Pretoria.

Everson, C.S. and Tainton, N.M. 1984. The effect of thirty years of burning on the Highland Sourveld of Natal. *Journal of the Grassland Society of Southern Africa*, 1, 3, 15-20.

Fang, B. and Lakshmi, V. 2014. Soil moisture at watershed scale: Remote sensing techniques. *Journal of Hydrology*, 516, 258-272.

Finnigan, J.J., Clements, R., Malhi, Y., Leuning, R. and Cleugh, H.A. 2003. A re-evaluation of long term flux measurement techniques: 1. Averaging and coordinate rotation. *Boundary-Layer Meteorology*, 107, 1-48.

Franz, T.E., Zreda, M., Ferre, T.P.A. and Rosolem, R. 2013. An assessment of the effect of horizontal soil moisture heterogeneity on the area-average measurement of cosmic-ray neutrons. *Water Resources Research*, 49, 1-9.

Franz, T.E., Zreda, M., Rosolem, R. and Ferre, T.P.A. 2012. A universal calibration function for determination of soil moisture with cosmic-ray neutrons. *Hydrology and Earth System Sciences Discussions*, 9, 10303-10322.

French, A.N., Jacob, F., Anderson, M.C., Kustas, W.P., Timmermans, W., Gieske, A., Su, Z., Su, H., McCabe, M.F., Li, F., Prueger, J. and Brunsell, N. 2005. Surface energy fluxes with the Advanced Spaceborne Thermal Emission and Reflection radiometer (ASTER) at the Iowa 2002 SMACEX site (USA). *Remote Sensing of Environment,* 99, 55-65.

Friedman, S.P. 1998. A saturation degree-dependent composite spheres model for describing the effective dielectric constant of unsaturated porous media. *Water Resources Research*, 34, 11, 2949-2961.

Fritschen, L.J. and Simpson, J.R. 1989. Surface energy balance and radiation systems: General description and improvements. *Journal of Applied Meteorology*, 28, 680-689.

Gao, W., Shaw, R.H. and Paw U, K.T. 1989. Observation of organized structure in turbulent flow within and above a forest canopy. *Boundary-Layer Meteorology*, 47, 349-377.

Gentine, P., Entekhabi, D., Chehbouni, A., Boulet, G. and Duchemin, B. 2007. Analysis of evaporative fraction diurnal behaviour. *Agricultural and Forest Meteorology*, 143, 1, 13-29.

Gruber, A., Dorigo, W.A., Zwieback, S., Xaver, A. and Wagner, W. 2013. Characterizing coarse-scale representativeness of in situ soil moisture measurements from the International Soil Moisture Network. *Vadose Zone Journal*, 12, 2, 1-16.

Gruhier, C., Albergel, C., De Rosnay, P.H. and Zeiner, B. 2011. Comparison between H-SAF large scale surface soil moisture, H-SAF assimilated soil moisture and SMOS Level 2 soil moisture. *CESBIO, Toulouse,* France 22.

Guillem, M.P. 2010. Multi-scale soil moisture retrievals from microwave remote sensing observations. Unpublished thesis, Remote Sensing Lab, Dept. Teoria del Senyal, Comunicacions Universitat Polit Ecnica de Catalunya.

Gurney, R.J. and Camillo, P.J. 1984. Modelling daily evapotranspiration using remotely sensed data. *Journal of Hydrology*, 69, 305-324.

Hafeez, M., Khan, S., Song, K. and Rabbani, U. 2007. Spatial mapping of actual evapotranspiration and soil moisture in the Murrumbidgee Catchment: Examples from National Airborne Field Experimentation. *MODSIM 2007 International Congress on Modelling and Simulation, Modelling and Simulation Society of Australia and New Zealand,* 74-80.

Hanson, R.L. 1991. Evapotranspiration and Droughts. In: Paulson, R.W., Chase, E.B., Roberts, R.S. and Moody, D.W., Compilers, National Water Summary 1988-89. *Hydrologic Events and Floods and Droughts*: U.S. Geological Survey Water-Supply Paper 2375, 99-104.

Hill, R.J. 1992. Review of optical scintillation methods of measuring the refractive index spectrum, inner scale and surface fluxes. *Waves Random Media*, 2, 179-201.

Hydroinnova Manual. 2013. *Cosmic-Ray Soil Moisture/Snow Sensing System*. Wellesley Drive NE., Albuquerque, NM.

Jackson, T.J., Cosh, M.H., Bindlish, R., Starks, P.J., Bosch, D.D., Seyfried, M., Goodrich, D.C., Moran, M.S. and Du, J. 2010. Validation of advanced microwave scanning radiometer soil moisture products. *IEEE Transactions on Geoscience and Remote Sensing*, 48, 12.

Jackson, R.D., Reginato, R.J. and Idso, S.B. 1977. Wheat canopy temperature: A practical tool for evaluating water requirements. *Water Resources Research,* 13, 651-656.

Jiao, Q., Zhu, Z. and Du, F. 2014. Theory and application of measuring mesoscale soil moisture by cosmic-ray fast neutron probe. *IOP Conference Series: Earth and Environmental Science*, 17.

Jones, S.B., Wraith, J.M. and Or, D. 2002. Time domain reflectometry measurement principles and applications. *Hydrological Processes*, 16, 141-153.

Kerr, Y., Waldteufel, P., Wigneron, J.-P., Martinuzzi, J.-M., Font, J. and Berger, M. 2001. Soil moisture retrieval from space: The soil moisture and ocean salinity mission (SMOS), *IEEE Transactions on Geoscience and Remote Sensing*, 39, 1729-1735.

Kerr, Y.H., Waldteufel, P., Wigneron, J.P., Delwart, S., Cabot, F., Boutin, J., Escorihuela, M.J., Font, J., Reul, N., Gruhier, C., Juglea, S.E., Drinkwater, M.R., Neira, M. and Mecklenburg, S. 2010. The SMOS mission: New tool for monitoring key elements of the global water cycle. *Proceedings of the IEEE*, 98, 5, 666-687.

Kipp & Zonen. 2014. *Instruction Manual-LAS MkII ET System*. (www.kippzonen.com).

Koike, T., Nakamura, Y.K. and Fujii, I. 2004. Development of an advanced microwave scanning radiometer (AMSR-E) algorithm of soil moisture and vegetation water content. *Annual Journal of Hydraulic Engineering*, 48, 2), 217-222.

Kustas, W.P. and Daughtry, C.S.T. 1989. Estimation of the soil heat flux/net radiation ratio from spectral data. *Agricultural and Forest Meteorology*, 49, 205-223.

Lakshmi, V. 2013. Remote sensing of soil moisture. *ISRN Soil Science*, 2013, 33.

Ledieu, J., De Ridder, P., De Clerck, P. and Dautrebande, S. 1986. A method of measuring soil moisture by time-domain reflectometry. *Journal of Hydrology*, 88, 319-328.

Lhomme, J.P. and Elguero, E. 1999. Examination of evaporative fraction diurnal behaviour using a soil-vegetation model coupled with a mixed-layer model. *Hydrology and Earth System Sciences Discussions*, 3, 2, 259-270.

Massman, W.J. 2000. A simple method for estimating frequency response corrections for eddy covariance systems. *Agricultural and Forest Meteorology*, 104, 185-198.

Massman, W.J. and Lee, X. 2002. Eddy covariance flux corrections and uncertainties in long-term studies of carbon and energy exchanges. *Agricultural and Forest Meteorology*, 113, 121-144.

Mecklenburg, S., Drusch, M., Kerr, Y., Font, J. and Roger, O. 2013. ESA's soil moisture and ocean salinity mission: Mission performance and operations. European Space Agency, ESA-ESRIN, Via Galileo Galilei, Frascati, Italy.

Mekkonen, D.F. 2009. Satellite remote sensing for soil moisture estimation: Gumara Catchment, Ethiopia. *ITC*, 2009.

Meyers, T.P. and Baldocchi, D.D. 2005. Current micrometeorological flux methodologies with applications in agriculture. In: Hatfield, J.L., Baker, J.M. (eds). *Micrometeorology in Agricultural Systems Agronomy Monograph*, 47, 381-396.

Moran, M.S., Hymer, D.C., Qi, J. and Kerr, Y. 2002. Comparison of ERS-2 SAR and Landsat TM imagery for monitoring agricultural crop and soil conditions. *Remote Sensing of Environment*, 79, 243-252.

Nichols, W.E. and Cuenca, R.H. 1993. Evaluation of the evaporative fraction for parameterization of the surface energy balance. *Water Resources Research*, 29, 11, 3681-3690.

Njoku, E., Jackson, T., Lakshmi, V., Chan, T. and Nghiem, S. 2003. Soil moisture retrieval from AMSR-E. *IEEE Transactions on Geoscience and Remote Sensing*, 41, 215-229.

Ntelekos, A., Georgakakos, K. and Krajewski, W. 2006. On the uncertainties of flash flood guidance: Toward probabilistic forecasting of flash floods. *Journal of Hydrometeorology*, 7, 271-285.

Paw U, K.T., Brunnet, Y., Collineau, S., Shaw, R.H., Maitani, T., Qui, J. and Hipps, L. 1992. On coherent structure in turbulence within and above agricultural plant canopies. *Agricultural and Forest Meteorology*, 61, 55-68.

Paw U, K.T., Qui, J., Su, H.B., Watanabe, T. and Brunnet, Y. 1995. Surface renewal analysis: A new method to obtain scalar fluxes. *Agricultural and Forest Meteorology*, 74, 119-137.

Paw U, K.T., Snyder, R.L., Spano, D. and Su, H.B. 2005. Surface renewal estimates of scalar exchange. In: Hatfield, J.L., Baker, J.M. (Eds), *Micrometeorology in Agricultural Systems Agronomy Monograph,* 47, 455-483.

Price, J.C. 1982. On the use of satellite data to infer surface fluxes at meteorological scales. *Journal of Applied Meteorology*, 21, 8, 1111-1122.

Qin, J., Yang, K., Chen, Y., Zhao, L. and Han, M. 2013. Spatial up-scaling of in-situ soil moisture measurements based on MODIS-derived apparent thermal inertia. A Laboratory of Tibetan Environment Changes and Land Surface Processes, Institute of Tibetan Plateau Research, Chinese Academy of Sciences.

Raupach, M.R., Finnigan, J.J. and Brunet, Y. 1989. Coherent eddies in vegetation canopies. In: *Proc. 4th Australasian Conf. on Heat and Mass Transfer, Christchurch, New Zealand, May 9-12*. Bergell House, New York, 75-90.

Roth, K., Schulin, R., Fluhler, H. and Attinger, W. 1990. Calibration of time domain reflectometry for water content measurements using a composite dielectric approach. *Water Resources Research,* 26, 10, 2267-2273.

Sabins, F.F. 2007. *Remote Sensing Principles and Interpretation*. Waveland Press, Illinois. 23.

Sahoo, A.K., Houser, P.R., Ferguson, C., Wood, E.F., Dirmeyer, P.A. and Kafatos, M. 2008. Evaluation of AMSR-E soil moisture results using the in-situ data over the Little River Experimental Watershed, Georgia. Center for Research on Environment and Water, IGES, Calverton, MD 20705, United States.

Savage, M.J., Everson, C.S. and Metelerkamp, B.R. 1997. Evaporation measurement above vegetated surfaces using micrometeorological techniques. Water Research Commission Report No. 349/1/97, 248, ISBN 1-86845 363 4.

Savage, M.J., McInnes, K.J. and Heilman, J.L. 1995. Placement height of eddy correlation sensors above short turfgrass surface. *Agricultural and Forest Meteorology,* 74, 195-204.

Scipal, K., Scheffler, C. and Wagner, W. 2005. Soil moisture-runoff relation at the catchment scale as observed with coarse resolution microwave remote sensing, *Hydrology and Earth System Sciences*, 9, 173-183.

Scott, C.A., Bastiaanssen, W.G.M. and Ahmad, M.D. 2003. Mapping spatio-temporal distributions of soil moisture throughout irrigated watersheds using optical and high resolution imagery. *ASCE Journal of Irrigation and Drainage Engineering*, 129, 5, 326.

Scott, D.F. 1994. *The hydrological effects of fire in South African catchments.* Unpublished thesis, Department of Agricultural Engineering, University of Natal, South Africa.

Seguin, B. and Itier, B. 1983. Using midday surface temperature to estimate daily evaporation from satellite thermal IR data. *International Journal of Remote Sensing*, 4, 371-383.

Sellers, P.J., Randall, D.A., Collatz, G.J., Berry, J.A., Field, C.B., Dazlich, D.A. and Zhang, C. 1996. A revised land surface parameterization (SiB2) for atmospheric GCMS. Part 1: Model formulation. *Journal of Climate*, 9, 4, 676-705.

Shuttleworth, W.J., Leuning, R., Black, T.A., Grace, J., Jarvis, P.G., Roberts, J. and Jones, H.G. 1989. Micrometeorology of temperate and tropical forest (and discussion). *Philosophical Transactions of the Royal Society of London B: Biological Sciences*, 324, 1223, 299-334.

Sinclair, S. and Pegram, G.G.S. 2010. A comparison of ASCAT and modeled soil moisture over South Africa, using TOPKAPI in land surface mode. *Hydrology and Earth System Sciences*, 14, 613-626.

Sinclair, S. and Pegram, G.G.S. 2012. PyTOPKAPI: An open-source implementation of the TOPKAPI hydrological model. Pegram and Associates.

Sinclair, S. and Pegram, G.G.S. 2013. A sensitivity assessment of the TOPKAPI model with an added infiltration module. *Journal of Hydrology*, 479, 0, 100-112.

Snyder, R.L., Spano, D. and Paw U, K.T. 1996. Surface renewal analysis for sensible heat and latent heat flux density. *Boundary-Layer Meteorology* 77, 249-266.

Song, C., Jia, L and Menenti, M. 2013. retrieving high-resolution surface soil moisture by downscaling AMSR-E brightness temperature using MODIS LST and NDVI data. *IEEE Journal of Selected Topics in Applied Earth Observations and Remote Sensing*, 2013, 1939-1404.

Spano, D., Duce, P., Snyder, R.L. and Paw U, K.T. 1997. Surface renewal estimates of evapotranspiration: Tall canopies. In *II International Symposium on Irrigation of Horticultural Crops*, 449, 63-68.

Spano, D., Snyder, R.L., Duce, P. and Paw U, K.T. 2000. Estimating sensible and latent heat flux densities from grape vine canopies using surface renewal. *Agricultural and Forest Meteorology*, 104, 171-183.

Su, Z. 2002. The surface energy balance system (SEBS) for estimation of turbulent heat fluxes. *Hydrology and Earth System Sciences*, 6, 85-99.

Su, Z., Li, X., Zhou, Y., Wan, L., Wen, J. and Sintonen, K. 2003a. Estimating areal evaporation from remote sensing. In *International Geoscience and Remote Sensing Symposium, 21-25 July 2003, Toulouse (PID20349.pdf)*.

Su, Z., Pelgrum, H. and Menenti, M. 1999. Aggregation effects of surface heterogeneity in land surface processes. *Hydrology and Earth System Sciences Discussions*, 3, 4, 549-563.

Su, Z., Schmugge, T., Kustas, W.P. and Massman, W.J. 2001. An evaluation of two models for estimation of the roughness height for heat transfer between the land surface and the atmosphere. *Journal of Applied Meteorology*, 40, 11, 1933-1951.

Su, Z., Yacob, A., Wen, J., Roerink, G., He, Y, Gao, B., Boogaard, H. and Van Diepen, C. 2003b. Assessing relative soil moisture with remote sensing data: Theory, experimental validation, and application to drought monitoring over the North China Plain. *Physics and Chemistry of the Earth*, 28, 89-101.

Swinbank, W.C. 1951. Measurement of vertical transfer of heat and water vapour by eddies in the lower atmosphere. *Journal of Meteorology*, 8, 135-145.

Thiermann, V. and Grassl, H. 1992. The measurement of turbulent surface-layer fluxes by use of bichromatic scintillation. *Boundary-Layer Meteorology* 58, 367-389.

Topp, G.C., Davis, J.L. and Annan, A.P. 1980. Electromagnetic determination of soil water content using TDR: I. Applications to wetting fronts and steep gradients. *Soil Science Society of America Journal,* 46, 4, p 672-678.

Topp, G.C., Davis, J.L. and Annan, A.P. 2003. The early development of TDR for Soil measurements. *Soil Science Society of America Journal*, 2, 492-499.

United States Geological Survey (USGS). 2013. Using the USGS Landsat 8 product. [Internet]. Available from: http://landsat.usgs.gov/Landsat8_Using_Product.php. [Accessed: February 2016].

United States Geological Survey (USGS). 2015. *Landsat 8 (L8) data users handbook.* USGS, Reston, Virginia.

Van Atta, C.W. 1977. Effect of coherent structures on structure functions of temperature in the atmospheric boundary layer. *Archives of Mechanics*, 29, 161-171.

Villarreyes, C.A.R., Baroni, G. and Oswald, S.E. 2013. Calibration approaches of cosmic-ray neutron sensing for soil moisture measurement in cropped fields. *Hydrology and Earth System Sciences*, 10, 4237-4274.

Wagner, W. 2008. Remote sensing of soil moisture in support to hydrological and meteorological modelling. METIER Training Course "Remote Sensing of the Hydrosphere" Finish Environment Institute, Helsinki, Finland*.

Wagner, W., Lemoine, G. and Rott, H. 1999. A method for estimating soil moisture from ERS scatterometer and soil data. *Remote Sensing of Environment*, 70, 191-207.

Walker, J.P., Willgoose, G.R. and Kalma, J.D. 2004. In situ measurement of soil moisture: A comparison of techniques. *Journal of Hydrology*, 2963, 85-99.

Wang, L. and Qu, J.J. 2009. Satellite of remote sensing application for surface soil moisture monitoring. A review. *Frontiers of Earth Science in China*, 3, 2, 237-247.

Wieringa, J. 1993. Representative roughness parameters for homogeneous terrain. *Boundary-Layer Meteorology*, 63, 323-363.

Zazueta, F.S. and Xin, J. 1994. *Soil Moisture Sensors.* University of Florida. Cooperative Service*.

Zhang, A., Jia, G., Wang, S., Zhoa, T.B. and Feng, J.M. 2011. Evaluation of AMSR-E derived soil moisture over northern China. *Atmospheric and Oceanic Science Letters*, 4, 4, 223-228.

Zhao, W. and Li, A. 2013. A downscaling method for improving the spatial resolution of AMSR-E derived soil moisture product based on MSG-SEVIRI data. *Remote Sensing of Environment*, 5, 2013, 6790-6811.

Zreda, M., Desilets, D., Ferre, T.P.A and Scott, R.L. 2008. Measuring soil moisture content non-invasively at intermediate spatial scale using cosmic-ray neutrons. *Geophysical Research Letters*, 35.

APPENDIX

1. Capacity Building

Capacity building and technology transfer activities included scientific training of students for postgraduate qualifications, scientific papers delivered at regional and overseas conferences and numerous informal study group sessions by local and international visitors to the trial sites.

Research capacity was built by registering students at the University of Pretoria and the University of KwaZulu-Natal. Table 7 indicates the students who have completed their qualifications.

Table 7: Candidates who have completed postgraduate qualifications

NAME	DEGREE	STATUS
Justin Domleo	BSc (Hons) – UKZN	Complete
Thigesh Vather	MSc – UKZN	Complete

In the past, UKZN has also invested in building capacity on the use of surface energy balance models together with remote sensing for improving the spatial estimates of total evaporation, biomass and water use of different vegetation types. Through this project, these skills were further developed in a member of the project team, namely, Michael Mengistu. The CRP is a new technology to southern Africa. One of the objectives of this project was to increase the research capacity in this domain in South Africa. Siphiwe Mfeka (field assistant) and Kent Lawrence have also received technical training on the project.

Winter school

The Centre for Water Resources Research (CWRR), UKZN, USAID PEER project and SAEON hosted the inaugural Winter Field School on hydrological processes for Hydrology honours students (or students in related disciplines) in the Cathedral Peak Catchments. The school attracted five honours students – two each from UKZN and the University of Zululand (UNIZUL) and one from the University of Venda, all currently enrolled in a BSc Hydrology Honours programme or related BSc Honours programme.

Conference abstracts

Thigesh Vather (PhD student) presented at the 18th SANCIAHS SYMPOSIUM.

Authors:

- Mr T Vather, University of KwaZulu-Natal.
- Ms KT Chetty, University of KwaZulu-Natal.
- Prof CS Everson, South African Earth Observation Network.
- Dr MG Mengistu, South African Weather Services.

Soil water is an important hydrological parameter, which is essential for a variety of applications. The current methods of estimating soil water are ground-based measurements, remote sensing and modelling. In recent years the CRP, which provides area-averaged soil water at an intermediate scale, has been implemented in several countries across the globe. The key objectives of this study were to test the suitability of the CRP to provide spatial estimates of soil water and use these estimates to validate satellite-based soil water estimates. Once set up and calibrated in Cathedral Peak Catchment VI, the CRP was found to provide spatial estimates of soil water, which correlated well with the *in-situ* soil water network dataset and yielded a R^2 value of 0.8445. The calibrated CRP was used to validate satellite-based soil water products, which consisted of remote sensing products (SMOS and AMSR-2) and modelled products (SAHG and surface energy balance system (SEBS) back-calculation).

Keywords: Cosmic ray probe, soil water, SMOS, SEBS, AMSR-2, SAHG

5th International COSMOS Workshop

August 22nd-24th, 2016 in Copenhagen (Denmark)

COSMOS is the COsmic-ray Soil Moisture Observing System

Objectives

The cosmic-ray neutron method is an emerging and promising technology for non-destructive moisture measurements of the top 10-50 cm of the subsurface within a hectometre footprint. The fifth international COSMOS workshop focused on the latest progress and current challenges of cosmic-ray neutron monitoring and modelling. Special focus was on improvements of calibration, better understanding of neutron response to moisture changes, and new applications of the technique (e.g. snow depth studies, biomass estimation, irrigation strategies). The workshop consisted of invited and contributed oral presentations. Prof. Everson and Mr Vather attended the workshop.

Everson C.S. Cosmic ray probe to aid Mapungubwe's threatened endemic forest. Platform presentation.

Steyn, M.T., Smit, C. Everson & J. Annandale. Potential of the CRP as an irrigation management tool for potatoes under centre pivot irrigation.

Journal abstracts

Thesis and honours abstracts

The following section comprises the abstracts and summaries from the theses of the PhD and MSc candidates:

1.1   JM Domleo

JM Domleo

211513256

Submitted in partial fulfilment of the requirements for the degree BSc Hons

Discipline of Environmental Hydrology

University of KwaZulu-Natal

Pietermaritzburg

September 2014

ABSTRACT

The determination of soil water content on different spatial scales is problematic due to environmental inconsistencies and soil heterogeneity. This study considers different soil water content measuring techniques. It specifically looks at the use of the cosmic ray probe and how it may overcome these spatial scale difficulties, particularly on an intermediate scale. The Cosmic Ray Probe was set up at Baynesfield Estate, KwaZulu-Natal, South Africa. The results showed that, in order to accurately measure soil water content, further calibration data is required. Furthermore, a two point calibration (as done in this study) is not sufficient enough to apply confidence in the Cosmic Ray Probe. It was also found that the timing of the calibration periods played a role in the accuracy of the Cosmic Ray Probe calibration.

1.2 T Vather

COMPARISON BETWEEN SATELLITE-BASED AND COSMIC RAY PROBE SOIL MOISTURE ESTIMATES: A CASE STUDY IN THE CATHEDRAL PEAK CATCHMENT

THIGESH VATHER

Submitted in partial fulfilment of the requirements for the degree of MSc in Hydrology,

School of Agriculture, Earth and Environmental Sciences, University of KwaZulu-Natal,

Pietermaritzburg, November 2015.

ABSTRACT

Soil moisture is an important hydrological parameter, which is essential for a variety of applications, extending to numerous disciplines. Currently, there are three methods of estimating soil moisture. These include: (a) ground-based (*in-situ*) measurements, which are carried out using field instruments; (b) remote sensing based methods, which use specialized sensors on satellites and aircrafts and (c) land surface models, which use meteorological data as inputs, at a predefined spatial resolution (Albergel et al. (2012); Mecklenburg et al., 2013). In recent years the CRP, which is an *in-situ* technique, has been implemented in several countries across the globe. The CRP provides area-averaged soil moisture at an intermediate scale and thus bridges the gap between *in-situ* point measurements and satellite-based soil moisture estimates (Zreda et al., 2012). The aim of this study was to first evaluate the current techniques for soil moisture estimation, in order to identify the research gaps and limitations. The key objectives of this study were to test the suitability of the CRP to provide spatial estimates of soil moisture and use these estimates to validate satellite-based (remote sensing and modelled) soil moisture estimates in the Cathedral Peak Catchment VI. The CRP was set up and calibrated in Cathedral Peak Catchment VI. An *in-situ* soil moisture network was created in Catchment VI, which was used to validate the calibrated CRP soil moisture estimates. Once calibrated, the CRP was found to provide spatial estimates of soil moisture, which correlated well with the *in-situ* soil moisture network dataset and yielded a R^2 value of 0.8445. The calibrated CRP was used to validate satellite-based soil moisture products. The remote sensing products used were the Level Three AMSR2 and SMOS products. The AMSR2 and SMOS products generally underestimated soil moisture throughout, but followed the general trend of the CRP, with AMSR obtaining a R^2 of 0.505 and SMOS obtaining a R^2 of 0.4853, when compared against the CRP estimates. The CRP was used to validate modelled soil moisture products, which consisted of the SAHG product and the back-calculation of soil moisture, using equations by Su et al. (2003) and Scott et al. (2003), and products derived from the SEBS Model. The SAHG model performed well, as it provided estimates that correlated well with the CRP dataset and yielded a R^2 value of 0.624 compared to the CRP estimates. The SEBS back-calculation technique performed very poorly, as it overestimated in the wet periods and underestimated in the dry periods.

2. Data Storage

All processed data have been stored on the Cloud 10 shared drive at UKZN:

Contact: Colin Everson

Email: eversonc@ukzn.ac.za

Enquiries: Tel: 0332605427

Centre for Water Resources Research

University of KwaZulu-Natal

Carbis Road

Scottsville

Pietermaritzburg

3209

South Africa